

LIBRARY
Michigan State
University

This is to certify that the

dissertation entitled

SOL-GEL DERIVED METAL OXIDE THIN FILMS
DESIGN OF NEW MATERIALS FOR CHEMICAL SENSING

presented by

Kathryn G. Severin

has been accepted towards fulfillment
of the requirements for

Ph.D. degree in Chemistry


Major professor

Date 10/30/96

**PLACE IN RETURN BOX to remove this checkout from your record.
TO AVOID FINES return on or before date due.**

DATE DUE DATE DUE DATE DUE		
MAR 28 2008 120814	_____	_____
_____	_____	_____
_____	_____	_____
_____	_____	_____
_____	_____	_____
_____	_____	_____
_____	_____	_____

MSU is An Affirmative Action/Equal Opportunity Institution

c:\crl\dtdatdue.pm3-p.

**SOL-GEL DERIVED METAL OXIDE THIN FILMS
DESIGN OF NEW MATERIALS FOR CHEMICAL SENSING**

By

Kathryn Graessley Severin

A DISSERTATION

**Submitted to
Michigan State University
in partial fulfillment of the requirements
for the degree of**

DOCTOR OF PHILOSOPHY

Department of Chemistry

1996

CO. H.

polycry

analytic

metal o

these se

alkoxid

oxide m

more c

understa

prepared

which a

Solution

combina

ABSTRACT

SOL-GEL DERIVED METAL OXIDE THIN FILMS DESIGN OF NEW MATERIALS FOR CHEMICAL SENSING

By

Kathryn Graessley Severin

Semiconductor gas sensors are used for the detection of reducing gases such as CO, H₂, hydrocarbons, and alcohols. When these sensors are constructed from pure polycrystalline metal oxide semiconductors, they do not have adequate selectivity for analytical applications in complex gas streams. This research is devoted to the design of metal oxide thin film materials that will improve the sensitivity, selectivity, and stability of these sensors.

The materials chosen for this research are thin films synthesized from metal alkoxides using sol-gel techniques. This molecular level approach allows the creation of oxide materials, such as amorphous and mixed metal oxides, which are not accessible by more conventional fabrication methods. The initial phase of this research focuses on understanding the relationship between solution chemistry and the characteristics of films prepared from these solutions. The second phase focuses on modification of films in ways which are relevant to gas sensing.

Films are made from tin, titanium, or zirconium alkoxides and valeric acid. Solution reactions are studied with Fourier transform infrared spectroscopy (FTIR) and a combination of FTIR and X-ray photoelectron spectroscopy (XPS) is used to elucidate

film str

calcina

charac

Lattice

XPS a

homog

tempe

quartz

coord

are si

at ten

to the

that

SnO

hom

ruti

film structure and composition. Oxide films are prepared by either H_2O_2 treatment or by calcination of as cast (or “valerate”) films at temperatures up to $1000\text{ }^\circ\text{C}$. These are characterized with XPS, X-ray diffraction (XRD), UV-Vis spectroscopy, and ellipsometry. Lattice oxygen reactivity, which may be correlated to sensor selectivity, is evaluated with XPS after *in situ* H_2 reduction. XRD and angle resolved XPS are used to evaluate the homogeneity of mixed $\text{TiO}_2\text{-SnO}_2$ films as a function of composition and calcination temperature.

Valerate and oxide films are transparent, stable, and exhibit uniform adhesion to quartz substrates. Valerate films are comprised of an amorphous metal-oxygen network coordinated with valerate ligands. The compositions of tin oxide and titanium oxide films are similar to those of polycrystalline SnO_2 and TiO_2 but are largely amorphous if calcined at temperatures $<600\text{ }^\circ\text{C}$. Lattice oxygen reactivity of tin oxide films is inversely related to the temperature used to oxidize the films. Results of redox cycling experiments suggest that films undergo very little irreversible restructuring upon H_2 reduction. As cast $\text{TiO}_2\text{-SnO}_2$ films and those calcined at temperatures $\leq 400\text{ }^\circ\text{C}$ are amorphous and homogeneously mixed. Calcination at higher temperatures leads to the formation of mixed rutile phases and to a surface segregation of titanium oxide.

To Blaine and my wonderful boys Geoff and Greg.

ACKNOWLEDGMENTS

This work was made possible only through the help and support of many people. I would like express my appreciation to Dr. Jeff Ledford for giving me the opportunity to learn about surface science, sol-gel chemistry, and sensors; for providing the ideas which were the foundation of this research project; and for giving the encouragement and guidance necessary for its completion. Thanks also to Professor John McCracken for taking on the role of advisor upon the departure of Ledford and to my committee: Professors Berglund, Pinnavaia, and Harrison for their direction.

Additionally, I would like to thank Ron Haas for his patience in the never-ending-battle to keep the VG surface science instrument running; Russ Geyer for building a multitude of excellent sample holders, manipulators, bellows, etc. for the VG; and the glass shop for providing what must have seemed like an infinite supply of quartz slides.

Successful completion of my research is owed in large part to the other Ledford group members, especially the other "orphans": Paul Park, Greg Noonan, and Per Askeland. They provided not only moral support, but a sounding board for ideas and insights for data interpretation. Additionally, Ed Townsend (and Maria and Sara), Mike Thelen, and honorary member Dana Spence contributed greatly to the enjoyment of being a Ledford group member.

under

Frey v

Heien

maint

Resea

suppo

Natur

Sanity was provided by family and friends. Not only were Blaine, Geoff and Greg understanding and encouraging, but weekends at the lake with Laurie, Steve and Jason Frey were great escapes from the world. The encouragement and support of my parents, Helen and Bill Graessley, was invaluable. Thanks to Cindy Dauphin for helping me to maintain a sense of humor and for providing perspective on my doctorin' work.

Funding for this research was provided by the Center for Fundamental Materials Research at Michigan State University and is gratefully acknowledged. Additional support was provided by an August F. and Ernest J. Frey Reseach Award and a College of Natural Sciences Fellowship.

LIST C

LIST C

CHAP

CHAPT

2
2
2
2
2

CHAPT

3
3
3
3
3

TABLE OF CONTENTS

LIST OF TABLES	ix
LIST OF FIGURES.....	x
CHAPTER 1 DESIGN OF NEW MATERIALS FOR CHEMICAL SENSING	1
1.1 Overview.....	1
1.1.1 Sol-gel Chemistry of Metal Alkoxides	2
1.1.2 Materials for Semiconductor Gas Sensors	4
1.2 Semiconductor Gas Sensors.....	9
1.3 X-ray Photoelectron Spectroscopy (XPS).....	11
1.3.1 Angle Resolved XPS (AR-XPS).....	15
1.4 References.....	21
CHAPTER 2 CHARACTERIZATION OF TITANIUM AND ZIRCONIUM VALERATE SOL-GEL FILMS	23
2.1 Abstract.....	23
2.2 Introduction.....	23
2.3 Experimental	27
2.4 Results and Discussion.....	30
2.5 References.....	56
CHAPTER 3 SYNTHESIS AND CHARACTERIZATION OF TIN VALERATE AND TIN OXIDE THIN FILMS	60
3.1 Abstract.....	60
3.2 Introduction.....	61
3.3 Experimental	63
3.4 Results and Discussion.....	66
3.5 References.....	88

CHA

CHA

CHA

CHAPTER 4	SYNTHESIS AND CHARACTERIZATION OF SOL-GEL DERIVED TITANIUM-TIN OXIDE FILMS.....	91
4.1	Abstract.....	91
4.2	Introduction.....	92
4.3	Experimental	95
4.4	Results and Discussion.....	100
4.4.1	Effect of Preparation on Film Homogeneity.....	100
4.4.2	Effect of Calcination Temperature on Titanium Valerate Films.....	106
4.4.3	Effect of Calcination Temperature on Tin Valerate Films.....	112
4.4.4	Effect of Mixing and Calcination at 400 °C on Film Properties	116
4.4.5	Effect of Mixing and Calcination at 600 °C to 1000 °C.....	120
4.5	Concluding Remarks.....	134
4.6	References.....	136
CHAPTER 5	EFFECT OF PREPARATION TEMPERATURE ON THE REACTIVITY OF TIN OXIDE FILMS	139
5.1	Abstract.....	139
5.2	Introduction.....	140
5.3	Experimental	143
5.4	Results and Discussion.....	146
5.4.1	H ₂ Reduction of Polycrystalline Tin Oxide.....	146
5.4.2	H ₂ Reduction of Tin Oxide Films.....	153
5.5	Concluding Remarks.....	165
5.6	References.....	169
CHAPTER 6	CONCLUSIONS.....	171
6.1	Project Summary	171
6.2	Future Work.....	174

LIST OF TABLES

Table 2.1	Atomic Ratios of Carbon and Oxygen Species Calculated from XPS Intensity Ratios.....	52
Table 3.1	Composition of Films: Ratios ^a of Ligands and Backbone Oxygen to Tin and Estimated Average Tin Oxidation State as Determined by Quantitative XPS Analysis.....	77
Table 4.1	Thickness “d” (nm) and <i>refractive index</i> “n” of films as a function of composition and calcination temperature. Standard deviations are < 5% for thicknesses and < 3% for refractive indices.....	110
Table 4.2	Composition of Valerate Films: Ratios of Ligands and Backbone Oxygen to Metal and Estimated Average Metal Oxidation State as Determined by Quantitative XPS Analysis.....	117
Table 4.3	Band Gap Energies for Films as a Function of Calcination Temperature and Composition.....	119

Figure

Figure

Figure

Figure

Figure

Figure

Figure

Figure

Figure

LIST OF FIGURES

Figure 1.1	Reactions between reducing gases (RH) and metal oxide surfaces which lead to a response in a semiconductor gas sensor 5
Figure 1.2	Band structure of a metal oxide material showing both bulk and surface states. Both the non-equilibrium flat band picture and equilibrium picture with band bending are shown. Occupied bands and surface states are indicated with hatch marks 10
Figure 1.3	Top: XPS spectrum of a Ti/Sn oxide film prepared from an equimolar mixture of Sn and Ti isopropoxides. Bottom: C 1s and O 1s spectra of a tin valerate film. 13
Figure 1.4	The sampling depth in XPS is $3\lambda\cos\theta$, where λ is the mean free path of the photoelectrons in the material and θ is the angle between the surface normal and the analyzer. In AR-XPS the sample is rotated with respect to the analyzer to obtain different sampling depths. 16
Figure 1.5	Trends in concentration measured with AR-XPS for several possible scenarios. These scenarios give rise to enhanced measured concentrations of one component in a binary mixture of A and B. 17
Figure 2.1	FTIR spectra of (a) valeric acid; (b) $\text{Ti}(\text{OPr}^i)_4$; (c) isopropanol; (d) $\text{Zr}(\text{OPr}^n)_4$ in n-propanol; and (e) n-propanol. 31
Figure 2.2	FTIR spectra of (a) $\text{Ti}(\text{OPr}^i)_4$; (b) 1:1 mixture and (c) 1:1.5 mixture of $\text{Ti}(\text{OPr}^i)_4$ and valeric acid; (d) 1:1.5:1.5 mixture of $\text{Ti}(\text{OPr}^i)_4$, valeric acid, and water. 34
Figure 2.3	FTIR spectra of (a) $\text{Zr}(\text{OPr}^n)_4$ in n-propanol; (b) 1:1 mixture and (c) 1:2 mixture of $\text{Zr}(\text{OPr}^n)_4$ and valeric acid; (d) 1:2:1.5 mixture of $\text{Zr}(\text{OPr}^n)_4$, valeric acid, and water. 38
Figure 2.4	FTIR spectra of (a) Ti00, (b) Ti24, and (c) Zr00 films..... 44

Fig

Fig

Fig

Figure

Figure

Figure

Figure

Figure

Figure

Figure 4

Figure 4

Figure 4.3

Figure 2.5	FTIR spectra of hydroxyl region: <i>in situ</i> heating of ZrO ₂ film (a) before heating; (b) heated to 50°C; (c) heated to 100°C; (d) cooled to room temperature in dry nitrogen; (e) exposed to ambient air for 30 minutes.	48
Figure 2.6	Oxygen 1s photoelectron spectra measured for (a) TiO ₂ , (b) Ti ₂ O ₃ , and (c) ZrO ₂ films.	51
Figure 3.1	FTIR spectra of (a) valeric acid and (b) Sn(OPr ⁱ) ₄ in isopropanol and spectra of solutions containing different concentrations of valeric acid and water. Sn(OPr ⁱ) ₄ : valeric acid : water ratios are: (c) 1 : 0.5 : 0, (d) 1 : 1 : 0, and (e) 1 : 1 : 2. Spectra are normalized to the isopropanol band 1769 cm ⁻¹	67
Figure 3.2	FTIR spectra of (a) SnV and (b) SnC films.	70
Figure 3.3	FTIR spectra of sequential treatments of an SnV film: (a) initial spectrum collected at 25°C; heated in nitrogen to: (b) 50°C, (c) 75 °C, and (d) 100°C; (e) cooled to 25°C in nitrogen, and (f) exposed to ambient air at 25°C.	74
Figure 3.4	Valence band photoelectron spectra of SnV film (a) initially and (b) after 12h of X-ray exposure.	80
Figure 3.5	Valence band photoelectron spectra of (a) tin(IV) oxide, (b) SnC film, and (c) SnP film.	83
Figure 3.6	FTIR spectra of SnV film on Si crystal (a) before and (b) after hydrogen peroxide treatment (SnP), and (c) the uncoated Si crystal.	84
Figure 3.7	FTIR spectra of tin valerate gel (a) before and (b) after hydrogen peroxide treatment.	86
Figure 4.1	FTIR spectra of valerate films: (a) SnVal, (b) STVal, (c) EMVal, (d) TSVal, and (e) TiVal.	101
Figure 4.2	AR-XPS analysis of 50%Ti 50% Sn valerate films prepared using Methods 1 and 2 ■ and using Method 3 ●. The curves represent the best fit to the model.	104
Figure 4.3	XRD patterns of calcined TiVal films: (a) TiC250, (b) TiC400, (c) TiC600, (d) TiC800, and (e) TiC1000.	107

Figur

Figure 4.4	XRD patterns of films calcined at 1000 °C: (a) SnC1000, (b) STC1000, (c) EMC1000, (d) TSC1000, and (e) TiC1000.....	109
Figure 4.5	XRD patterns of calcined SnVal films: (a) SnC250, (b) SnC400, (c) SnC600, (d) SnC800, and (e) SnC1000.	114
Figure 4.6	UV-Vis spectra of films calcined at 400 °C: (a) SnC400, (b) STC400, (c) EMC400, (d) TSC400, and (e) TiC400.....	119
Figure 4.7	XRD patterns of calcined STVal films: (a) STC400, (b) STC600, (c) STC800, and (d) STC1000.....	126
Figure 4.8	AR-XPS analysis of ■STVal, ●STC400, ▲STC600, ◆STC800, and ○STC1000 films.....	127
Figure 4.9	XRD patterns of calcined EMVal films: (a) EMC400, (b) EMC600, (c) EMC800, and (d) EMC1000.	129
Figure 4.10	AR-XPS analysis of ■EMVal, ●EMC400, ▲EMC600, ◆EMC800, and ○EMC1000 films.	130
Figure 4.11	XRD patterns of calcined TSVal films: (a) TSC400, (b) TSC600, (c) TSC800, and (d) TSC1000.....	132
Figure 4.12	AR-XPS analysis of ■TSVal, ●TSC400, ▲TSC600, ◆TSC800, and ○TSC1000 films.....	133
Figure 5.1	XPS valence band spectra of polycrystalline tin oxide pellet (a) initially; after sequential H ₂ reductions for 1 h. each at (b) 200 °C, (c) 250 °C, and (d) 300 °C; and (e) after reoxidation in 20% O ₂ (He) for 1 h. at 200 °C.....	147
Figure 5.2	XRD pattern of polycrystalline SnO ₂ (a) initially, with most intense cassiterite peaks labelled, and (b) after H ₂ reduction at 350 °C for 0.5 h. Peaks due to β-tin are designated with a dot (•) and major β-tin peaks are identified.....	148
Figure 5.3	XPS valence band spectra of (a) SnP, (b) SnC200, (c) SnC250, (d) SnC400, and (e) SnC600 films.....	155
Figure 5.4	Changes in oxide concentration with reduction temperature as determined with XPS for ■SnP, ○SnC200, ●SnC400, and ◆SnC600 films.	156

Figure

Figure

Figure

Figure

Figure

Figure

Figure

Figure 5.5	XPS valence band spectra of tin oxide materials after H ₂ reduction at 300 °C: (a) SnP, (b) SnC200, (c) SnC250, (d) SnC400, and (e) SnC600 films.	157
Figure 5.6	Oxidation - reduction cycling of SnP film: □initial film; ■200 °C, ●250 °C, and ◆300 °C H ₂ reduction; and ○200 °C 20% O ₂ (He) oxidation. Oxide/tin atomic ratio is determined with XPS analysis after each sequential <i>in situ</i> treatment.	159
Figure 5.7	Oxidation - reduction cycling of SnC200 film: □initial film; ■200 °C, ●250 °C, and ◆300 °C H ₂ reduction; and ○200 °C 20% O ₂ (He) oxidation. (a) Oxide concentration and (b) tin oxidation state as calculated using charge balance from XPS determined oxide and hydroxyl concentrations after sequential treatments.	161
Figure 5.8	Oxidation - reduction cycling of SnC400 film. □initial film; ■200 °C, ●250 °C, and ◆300 °C H ₂ reduction; and ○200 °C 20% O ₂ (He) oxidation. Oxide/tin atomic ratio is determined with XPS analysis after each sequential <i>in situ</i> treatment. Scale is adjusted to that of Figure 5.7a to avoid an artificial over emphasis of differences.	164
Figure 5.9	AR-XPS analysis of the formation of metal in an SnC400 film after H ₂ reduction for 4h at 350 °C.	167
Figure 5.10	Chemical shift between Sn 3d _{5/2} metal and oxide peaks and the oxide/tin oxide atomic ratio as a function of sampling depth for SnC400 film after H ₂ reduction for 4h at 350 °C.	168
Figure 6.1	Oxide concentration as a function of reduction temperature for ○TiC400, □SnC400, ●TSC400, ■EMC400, and ◆STC400 films. The standard deviation in the reported atomic ratios is ±0.05.	176

1.1

sensing

alkoxi

prepar

impor

allow

recog

suita

sensi

sensi

form

the

way

sem

sen

che

Chapter 1

Design of New Materials for Chemical Sensing

1.1 Overview

This research is part of a larger study to develop new materials for chemical sensing. The materials that are central to this research effort are made from metal alkoxides using sol-gel techniques. Sol-gel chemistry is very versatile and materials can be prepared which are stable, transparent, porous and conductive, properties which are important for chemical sensing. The synthesis can be carried out at room temperature allowing the incorporation of sophisticated organic and organometallic molecular recognition sites. Additionally, the rheological properties of the precursor solutions are suitable for the formation of thin films. Films can be coated onto optical fibers for optical sensing, surface acoustic wave devices for mass sensing, and arrays for conductimetric sensing.

This study is separated into two parts. First, the basic chemistry involved in formation of these films is explored and its relationship to the composition and structure of the resultant films is established. Then, the study focuses on modification of the films in ways which may improve their sensitivity, selectivity and stability when used as semiconductor gas sensor substrates. While the desire to make new materials for chemical sensing is the motivation behind this study, these films have a wide range of physical and chemical properties which are potentially useful for a variety of applications. Among

other

cataly

involv

conde

forme

materi

reactiv

and ox

hydroly

ligands

these m

material

The first

Next, t

alkoxid

The par

step co

others, these films can be used as membranes, optical and protective coatings, and catalysts.

1.1.1 Sol-gel Chemistry of Metal Alkoxides. Traditionally, sol-gel chemistry involves the reaction of silicon alkoxides with water [1]. The hydrolysis and condensation reactions which result are slow, and amorphous silicon oxide glasses are formed. Extension of this chemistry to metal alkoxides opens up the possibility of creating materials with a wide range of properties. However, transition metal alkoxides are more reactive than silicon alkoxides and, unless some control is exerted, polycrystalline oxide and oxohydroxide precipitates are formed when they are exposed to moisture [2]. Their hydrolysis rates can be slowed down by replacing reactive alkoxide groups with strong ligands such as carboxylates or β -diketonates. Gels and films can then be prepared from these modified metal alkoxides [3 - 5].

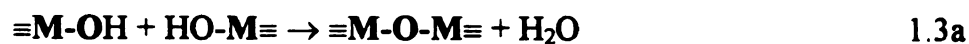
It is generally acknowledged that there are three steps in the formation of sol-gel materials from metal alkoxides ($M(OR)_4$) and carboxylic acids ($R'COOH$) [1-3, 5, 6]. The first is nucleophilic substitution of alkoxide ligands by carboxylate ligands.



Next, the addition of water causes hydrolysis of the carboxylated metal alkoxides and alkoxide ligands are replaced with hydroxyl groups.



The parent alcohol is a byproduct of both of these reactions. Hydrolysis initiates the third step: condensation.



Hydrox

product

solution

mixture

hydroxy

substrat

I

free film

hydrolyz

(Ti(OPr

Ti(OPr)

T

knowled

formed

by analy

infrared

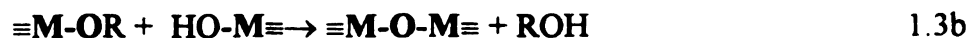
mechani

A

the struc

better co

tailor-ma



Hydroxyl groups react with either hydroxyl or alkoxy groups on other metal centers producing M-O-M bonds and water or the parent alcohol, respectively. The resultant solution consists of a metal oxide network dissolved in an alcohol - carboxylic acid mixture. The metal centers may be coordinated with carboxylate, alkoxide, and/or hydroxyl ligands. Films can be formed by spin casting, dip coating, or spray coating substrates with these solutions.

Berglund *et al.* [7, 8] found that high quality thin films (stable, transparent, crack-free films which exhibit uniform adhesion to glass substrates) could be spin cast from hydrolyzed mixtures of valeric acid ($\text{C}_4\text{H}_9\text{COOH}$) and titanium(IV) isopropoxide ($\text{Ti}(\text{OPr}^i)_4$). Optimum reactant molar ratios were found to be 9 valeric acid : 1.5 water : 1 $\text{Ti}(\text{OPr}^i)_4$.

The research presented in Chapter 2 is undertaken to achieve a more detailed knowledge of the chemistry involved in the production of these films, as well as films formed from zirconium(IV) n-propoxide ($\text{Zr}(\text{OPr}^n)_4$) and valeric acid. This is accomplished by analyzing the solutions at various stages in the synthetic process with Fourier transform infrared spectroscopy (FTIR). Information obtained is related to the rate, extent, and mechanism of the reactions in these systems.

Also established in Chapter 2 are relationships between the solution chemistry and the structure and composition of the films produced. This knowledge should lead to better control of the sol-gel process and ideally, to the ability to produce films which are tailor-made for particular applications. The composition, including the nature and

conce

films

Chapt

releva

functio

functio

semico

to char

These

ethanol

WO₃ a

exhaust

Nb₂O₅ s

[9]

F

between

illustrate

oxide (M

ionosorbe

concentration of ligands, and the structure of titanium valerate and zirconium valerate films are elucidated using FTIR and X-ray photoelectron spectroscopy (XPS).

1.1.2 Materials for Semiconductor Gas Sensors. The research presented in Chapters 3, 4, and 5 is guided by the desire to design materials which have properties relevant to semiconductor gas sensing. In general gas sensors must perform two functions: a receptor function allowing recognition of a particular gas and a transduction function in which the gas concentration is converted to signal output. In the case of semiconductor gas sensors, reactions on the surface of a metal oxide semiconductor lead to changes in surface conductivity.

Currently, there are three types of semiconductor gas sensors in use commercially. These include sensors for the detection of reducing gases (i.e. H₂, CO, hydrocarbons, ethanol) which are based upon SnO₂, In₂O₃, or Fe₂O₃; H₂S sensors based upon SnO₂ and WO₃; and humidity sensors. Additionally, though air/fuel ratio (A/F) is automobile exhaust is now monitored with ZrO₂:Y₂O₃ solid electrolyte sensors, TiO₂, CeO₂, and Nb₂O₅ semiconductor gas sensors are currently under development for this application [9].

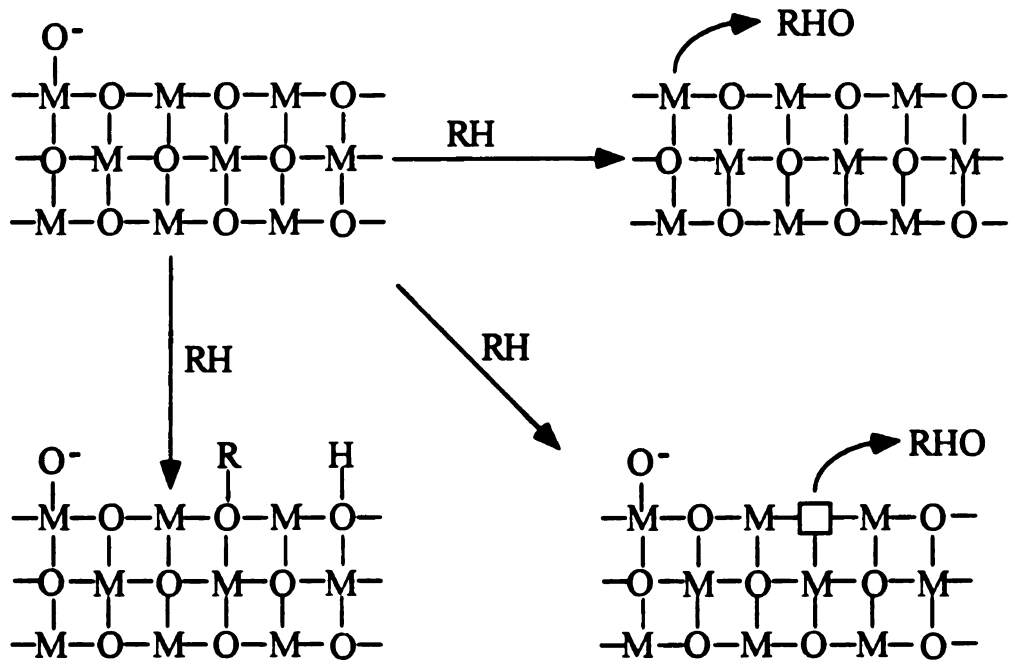
For the detection of reducing gases an n-type semiconductor is used. Reactions between reducing gases and metal oxide surfaces which lead to sensor response are illustrated in Figure 1.2 [9]. Reducing gases (RH) can dissociatively chemisorb on metal oxide (M-O) surfaces and act as electron donors. Alternatively, they can react with either ionosorbed oxygen or lattice oxygen and when the products desorb, inject electrons into

Mecha

Rea

Fig

Mechanism



Reactions

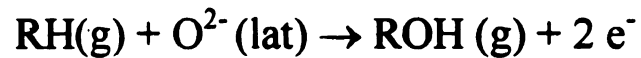
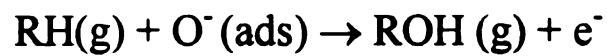
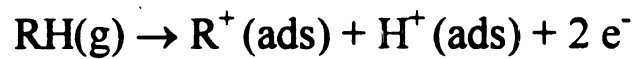


Figure 1.1 Reactions between reducing gases (RH) and metal oxide surfaces which lead to a response in a semiconductor gas sensor.

the surface

Section 1

T

oxide (S

high ten

polycrys

are con

because

than th

prepar

valera

films t

in air

colliap

most

appli

and n

activ

of c

inves

the surface. The effect of these reactions on the surface conductivity is discussed in Section 1.2.

The semiconductor used most commonly for the detection of reducing gases is tin oxide (SnO_2). SnO_2 is chemically inert and therefore stable when sensors are operated at high temperatures in air. SnO_2 sensing elements are in the form of compressed polycrystalline powders or thin films [10]. The use of films is advantageous because they are compatible with the fabrication of microsensors, have rapid response rates, and, because these sensors function at elevated temperatures, they have lower operating costs than their pressed powder counterparts [11, 12].

Chapter 3 focuses on the preparation of tin oxide films. First, tin valerate films are prepared and characterized using the same methods described for titanium and zirconium valerate films. Then, two methods are used to remove the organic components of the films to produce the tin oxide films needed for gas sensing. The first method is calcination in air at 400 °C. This is a conventional method but calcination commonly leads to the collapse of sol-gel materials which lowers their surface area [1]. This is an advantage for most coating applications but a disadvantage for both sensor and heterogeneous catalyst applications. A high surface area maximizes interaction between the substrate and the gas and means improved response for sensors (both in time and sensitivity) [13] and a more active catalyst. In an attempt to remove the organic components while limiting the extent of collapse, a room temperature chemical oxidation with hydrogen peroxide is investigated.

This i

for se

titanu

the co

ambie

produ

[15 .1

oxide

separ

oxide

the m

heate

prepa

(AR-

event

identr

(XRD

ability

selectr

catay

Chapter 4 explores the preparation of mixed metal oxides using sol-gel techniques. This is a promising approach for tailoring the physical and chemical properties of materials for semiconductor gas sensing. The system chosen for this study is tin oxide mixed with titanium oxide. These oxides were chosen because Takahashi and Wada [14] found that the conductivity of $\text{TiO}_2\text{-SnO}_2$ films was strongly dependent upon the components of the ambient gas, making them ideal candidates for gas sensing materials. Indeed, gas sensors produced from mixed $\text{TiO}_2\text{-SnO}_2$ materials have been shown to have better sensitivity [15, 16] and response times [16, 17] than the single metal oxide materials. Second, both oxides have rutile structures and may crystallize in mixed phases rather than crystallize separately. This improves the chances of maintaining a homogeneous mixture of the oxides even after calcination at elevated temperatures.

Important questions addressed in Chapter 4 are: how homogeneously mixed are the metal oxides and how does the homogeneity and crystallinity change as the films are heated in air? Films with Ti:Sn atomic ratios of 100:0, 75:25, 50:50, 25:75, and 0:100 are prepared and their homogeneity is evaluated with XPS, FTIR, and angle resolved XPS (AR-XPS). AR-XPS is used to detect the surface segregation of one of the oxides, an event which commonly occurs in heterogeneous mixed materials [18]. The presence, identity, and particle sizes of crystalline phases are determined with X-ray diffraction (XRD).

One of the most important features of any chemical sensor is its selectivity or its ability to detect a particular molecule in the presence of others [19]. Commonly the selectivity of semiconductor gas sensors is improved by the addition of noble metal catalysts and metal oxide promoters [20]. Other potentially useful strategies for

improvi

semicon

occurin

the mos

an impo

lattice c

coordin

polycry

are obt

reactivi

200 °C

used to

reductio

oxide fi

are tw

significa

selectiv

reductio

stable su

improving sensor selectivity can be found by analogy to selective oxidation catalysis. Like semiconductor gas sensors, catalyst performance depends upon the selectivity of reactions occurring on metal oxide surfaces [9]. It is known that lattice oxygen reactivity is one of the most important factors in the selectivity of catalysts [21 - 23]. It may therefore play an important role in the selectivity of semiconductor gas sensors and films with a range of lattice oxygen reactivities may be selective for different gases.

Since the reactivity of oxygen in defect sites is greater than that of fully coordinated bulk sites [21], amorphous materials may be more reactive than polycrystalline materials. In Chapter 5 tin oxide films with varying degrees of crystallinity are obtained through oxidation of amorphous films at temperatures up to 600 °C. The reactivities of these materials are evaluated using H₂ reduction at temperatures between 200 °C and 400 °C in a reactor attached to the surface science instrument. XPS analysis is used to determine the stoichiometry and the oxidation state of tin before and after H₂ reduction. The effect of calcination temperature on the structure and reactivity of tin oxide films is evaluated and compared to that of a polycrystalline tin oxide powder. There are two important issues. First, do films prepared at different temperatures have significantly different oxide reactivities? If not, this is not a promising approach to making selective sensor materials. Second, do films undergo irreversible restructuring upon reduction? Film stability is evaluated through oxidation-reduction cycling. Potentially stable substrates are those whose reactivity is unchanged by repeated treatments.

1.2 Sem

Sem

reactions c

surfaces ar

reactions c

oxide sem

Th

oxide sem

bonding

energy g

with ban

as an n-t

with en

lattice o

room te

middle

band

can be

remov

these

Surfa

1.2 Semiconductor Gas Sensors

Semiconductor gas sensors respond to changes in conductivity which result from reactions on their surface [9, 24]. Reactions between reducing gases and metal oxide surfaces are shown in Figure 1.1. The increase in conductivity which results from these reactions can be understood by examining the band structure and surface states of a metal oxide semiconductor (Figure 1.2).

The right hand side of the top figure illustrates the bulk band structure of a metal oxide semiconductor. For tin oxide, the top of the valence band is comprised of non-bonding O 2p orbitals and the bottom of the conduction band of Sn 5s orbitals. The energy gap between these two bands (band gap) is approximately 3.6 eV. While materials with band gaps of this magnitude are generally classified as insulators, tin oxide behaves as an n-type semiconductor because it naturally has a high concentration of defect states with energies <0.1 eV below the conduction band [25]. These defects are primarily lattice oxygen vacancies. Electrons from these states can populate the conduction band at room temperature. In the absence of defects, the Fermi level would be located in the middle of the band gap. Their presence moves the Fermi energy closer to the conduction band.

The left side of the top figure shows the energies of the surface states. The surface can be thought of as a defect in the crystal in which the top layer of atoms has been removed. Even though restructuring occurs to lower the surface energy, energy levels in these coordinatively unsaturated surface sites will be different than those in the bulk. Surface metal atoms can be viewed as electron donor sites, lattice oxygen as acceptor

Flat

D

Band

E

Figure 1

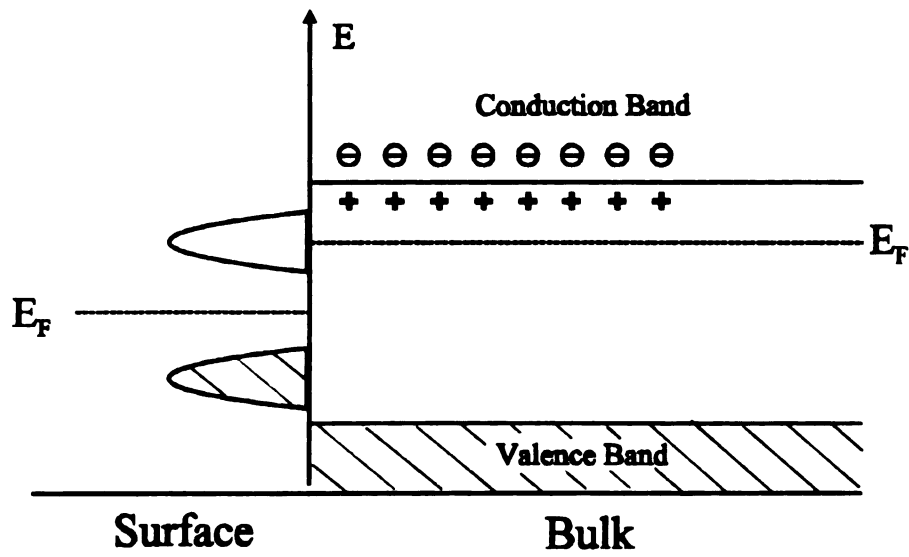
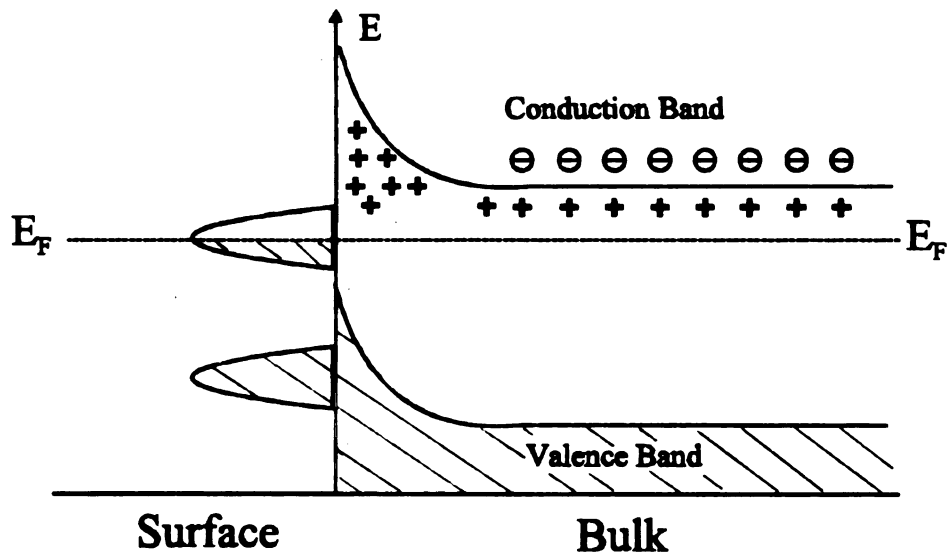
Flat Bands*Band Bending*

Figure 1.2 Band structure of a metal oxide material showing both bulk and surface states. Both the non-equilibrium flat band picture and equilibrium picture with band bending are shown. Occupied bands and surface states are indicated with hatch marks.

sites Sur

chemisorb

gases act a

and the low

since the F

levels, elect

causes band

at the surfac

semiconduct

the adsorbed

operating tem

When

causes the in

at the surfac

adsorbed ox

products des

lower the pot

1.3 X-ray

In th

photoelectron

Photoelectron

have a mean

sites. Surface states are also created by the presence of adsorbed species. Oxygen chemisorbed from ambient air acts as an acceptor at the surface. Chemisorbed reducing gases act as donors. At the surface, the Fermi level is between the highest occupied state and the lowest unoccupied state. As drawn, this is obviously not an equilibrium situation since the Fermi level at the surface is below that of the bulk. In order to equalize the two levels, electrons flow from the near surface region to acceptor states on the surface. This causes band bending, as shown in the bottom illustration, and a potential barrier is created at the surface which decreases the surface conductivity. This is the situation for an n-type semiconductor gas sensor when ambient oxygen is adsorbed on its surface. The nature of the adsorbed oxygen species is temperature dependent but is predominantly O^- at normal operating temperatures ($\sim 300\text{ }^\circ\text{C}$) [26].

When a reducing gas chemisorbs on the surface, it acts an electron donor. This causes the injection of electrons into the near surface region, lowering the potential barrier at the surface. This in turn, increases the surface conductivity. Both lattice oxygen and adsorbed oxygen are acceptor sites. When they react with a reducing gas and the products desorb, electrons from those sites remain. They enter the near surface region, lower the potential barrier, and increase the surface conductivity.

1.3 X-ray Photoelectron Spectroscopy (XPS).

In this technique, a sample is irradiated with X-rays causing the emission of photoelectrons. The kinetic energy of these electrons is measured by the analyzer. Photoelectrons are exponentially attenuated by the material from which they emerge and have a mean free path (λ) which is strongly dependent upon their kinetic energy. Ninety

five per cent

of the sur

100 Å

(KE), the

The bindi

originated

relaxation

unique set

can be de

photoemis

photoelect

Sig

(η_i) in the

where I_s

emission

the mean

$D(\epsilon_j)$ the

X

and $D(\epsilon_j)$

five percent of the photoelectrons which reach the detector have emerged from within 3λ of the surface. Typically, this limits the sampling depth of XPS to a maximum of 50 - 100 Å.

Binding energies (BE) can be determined from photoelectron kinetic energies (KE), the energy of the X-rays ($h\nu$), and the spectrometer work function (ϕ_{sp}):

$$BE = h\nu - \phi_{sp} - KE \quad 1.4$$

The binding energy is characteristic of the atomic orbital from which the electron originated. Binding energies differ from ionization energies by final state effects because relaxation processes occur simultaneously with photoemission. Since each element has a unique set of binding energies associated with it, the elemental composition of a surface can be determined from its XPS spectrum. Shown at the top of Figure 1.3 is a photoemission spectrum of a mixed TiO_2-SnO_2 film. Peaks shown are due to photoelectrons from O 1s, Sn 3d, and Ti 2p orbitals.

Signal intensities (I_i) in XPS spectra can be related to the number density of atoms (η_i) in the surface of a sample by the following relationship [27]:

$$I_i = I_o \eta_i \lambda_T(\epsilon_i) D(\epsilon_i) \quad 1.5$$

where I_o is the X-ray flux, σ_i is the photoionization cross section (probability that a emission will occur from this orbital; this is dependent upon the excitation energy), $\lambda_T(\epsilon_i)$ the mean free path of the photoelectron (this is a function of its kinetic energy (ϵ_i)), and $D(\epsilon_i)$ the transmission function of the instrument.

XPS is seldom used to measure absolute concentrations of elements because the I_o and $D(\epsilon_i)$ are difficult to determine. Of these only the kinetic energy dependence of $D(\epsilon_i)$

Intensity

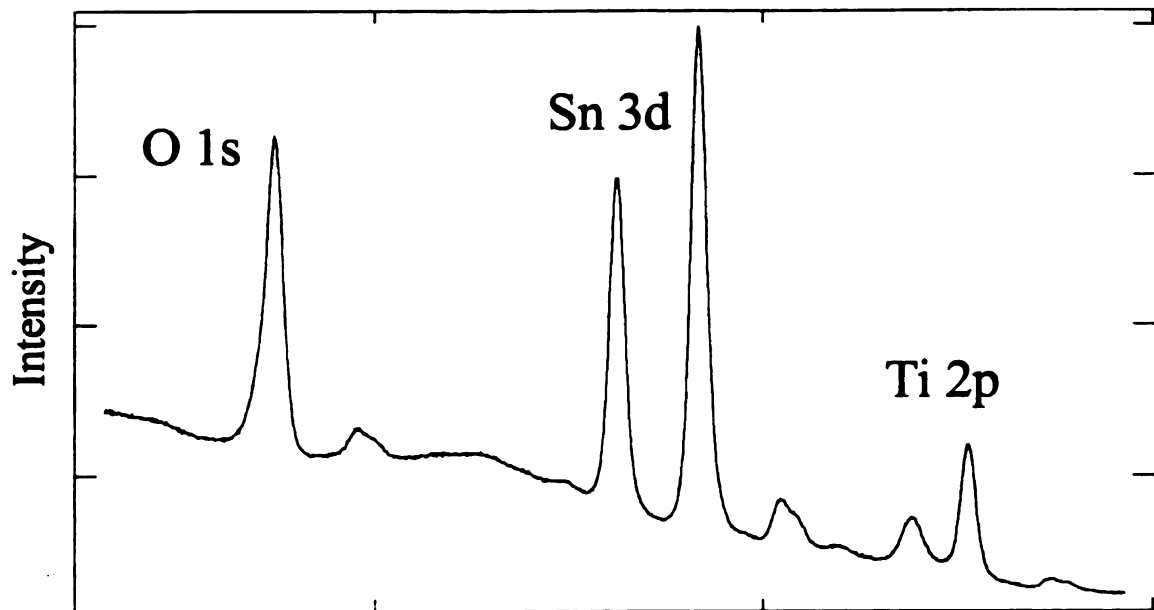
Intensity

Car

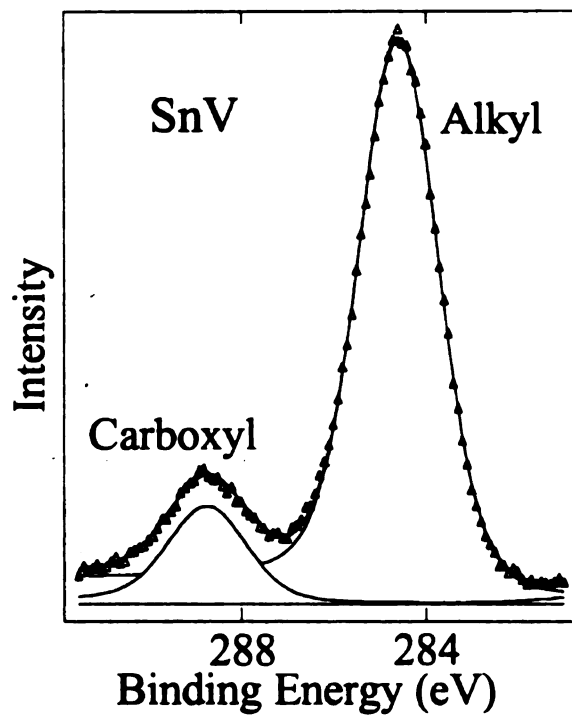
Bi

Figure 1.3

XPS Spectrum of Ti/Sn Oxide Film



Carbon 1s



Oxygen 1s

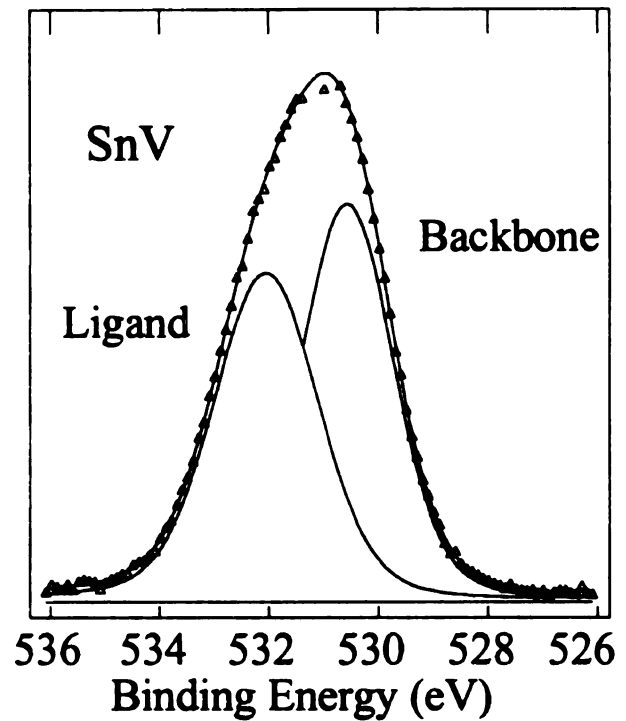


Figure 1.3 Top: XPS spectrum of a Ti/Sn oxide film prepared from an equimolar mixture of Sn and Ti isopropoxides. Bottom: C 1s and O 1s spectra of a tin valerate film.

remains if

The inter

the brack

theoretic

universal

though in

with kin

factors

compos

empiric

the rela

These v

equimo

environ

spectra

carbon

such a

result.

higher

remains if the relative concentrations (C) of two elements A and B are calculated:

$$\left(\frac{C_A}{C_B} \right) = \frac{I_A}{I_B} \left(\frac{\sigma_B \lambda_B \epsilon_B^{-0.5}}{\sigma_A \lambda_A \epsilon_A^{-0.5}} \right) \quad 1.6$$

The intensity of a peak is taken to be its area after background subtraction. The term in the bracket on the right is the sensitivity factor. Sensitivity factors can be determined theoretically using cross sections determined by Scofield [28] and mean free paths from a universal curve [29]. Unfortunately, mean free paths can be material dependent and though it is commonly assumed that $D(\epsilon_i)$ is proportional to $\epsilon_i^{-0.5}$, its relationship changes with kinetic energy and varies differently for different instruments [30]. Better sensitivity factors can be determined empirically by the analysis of standard materials of known composition. For example, from the spectrum in Figure 1.3 it was determined, using empirical sensitivity factors based on the analysis of polycrystalline SnO_2 and TiO_2 , that the relative concentrations of the elements in the surface of this film are 1 Ti : 1 Sn : 4 O. These were the relative concentrations expected since this oxide film was made from an equimolar mixture of $\text{Ti}(\text{OPr}^i)_4$ and $\text{Sn}(\text{OPr}^i)_4$.

Even more specific chemical information can be obtained because chemical environment influences binding energies. Also shown in Figure 1.3 are the C 1s and O 1s spectra of a tin valerate film. In the C 1s spectrum two peaks are present, one due to alkyl carbon and the other to carboxyl carbon. Carbon bonded to an electronegative element such as oxygen has less electron density around it than carbon bonded to C or H. As a result, the electrons are more tightly bound. For this reason, the carboxyl C 1s peak has a higher binding energy than the alkyl C 1s peak. Similarly, when oxygen is bonded to Sn

(backbone
charge and
relative con
their relativ

1.3

varied by
way depth

Co

sputter av
by XPS
difficult
because

over spu
maximum

surface
(compo

A/B rat
the actu

dividing
with no

Ratios

(backbone oxygen) as opposed to C or H (ligand oxygen), it has a higher net negative charge and therefore, the O 1s peak for backbone oxygen has a lower binding energy. The relative concentrations of the different types of carbon or oxygen can be determined from their relative peak areas.

1.3.1 Angle Resolved XPS (AR-XPS). The sampling depth of XPS can be varied by rotating the sample with respect to the analyzer as shown in Figure 1.4. In this way depth profiling can be done in the near surface region of the sample [31].

Commonly depth profiling is done by bombarding a surface with ions which sputter away the sample. Relative concentrations of sample components are determined by XPS analysis as the layers are removed. Unfortunately, with sputter profiling it is difficult to distinguish between ion induced damage and actual sample composition because lighter atoms are preferentially sputtered. AR-XPS analysis has an advantage over sputter depth profiling because it is non-destructive. It is limited, however, to the maximum sampling depth of XPS, which is typically 50 - 100 Å.

AR-XPS can be used to qualitatively assess the distribution of species in the near surface region of the sample. A few of the many possible scenarios for a binary mixture (components A and B) are illustrated in Figure 1.5 along with the trends expected in the A/B ratios measured with sampling depth. (Trends are shown as linear functions but the actual dependence is more complex (*vide infra*)). The ratios are normalized by dividing by the relative concentrations in the bulk mixture. In a homogeneous mixture with no surface segregation, the normalized ratio should be 1 for all sampling depths. Ratios other than 1 can be the result of one component migrating to the surface

hv

Figure 1 4

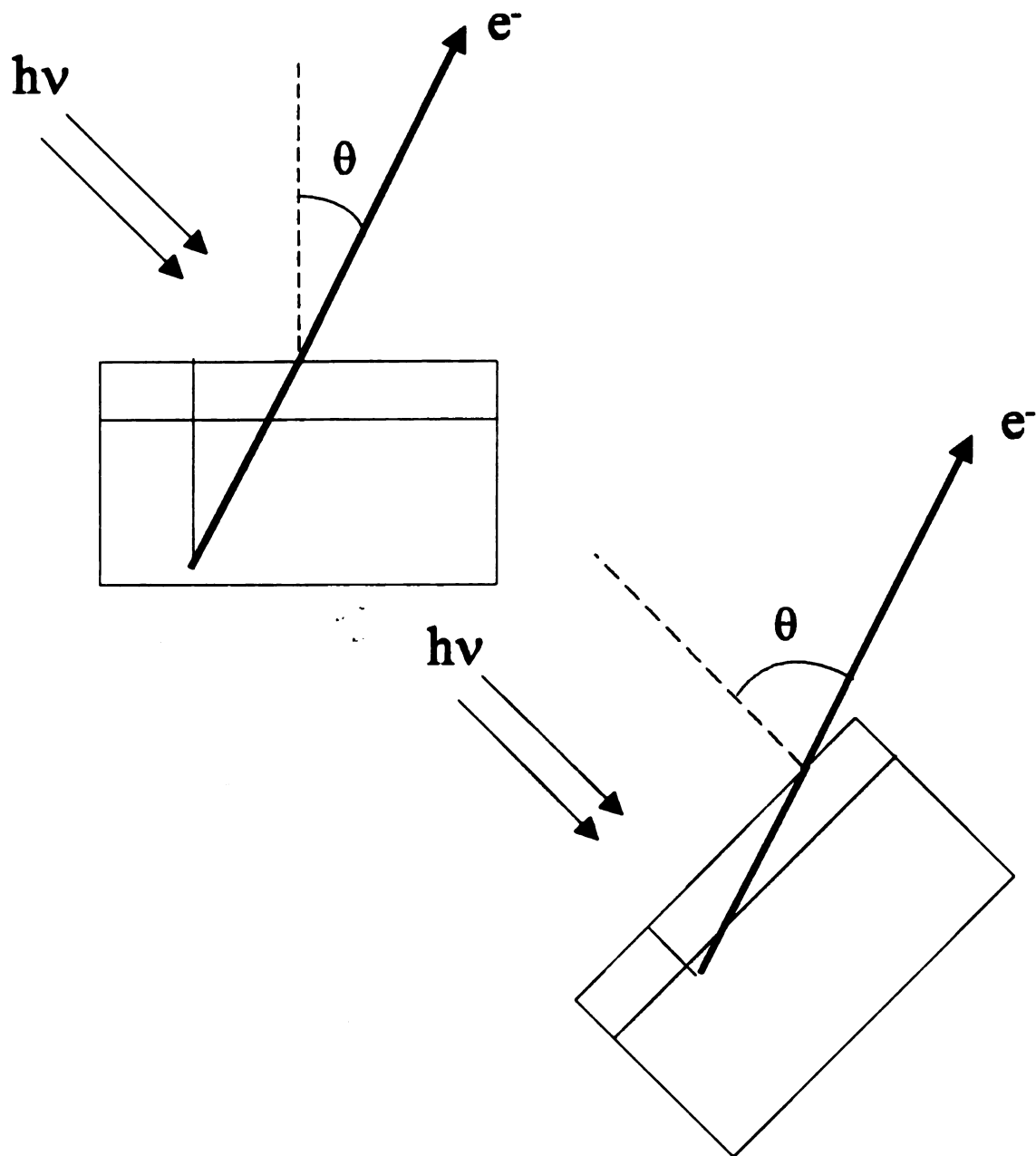
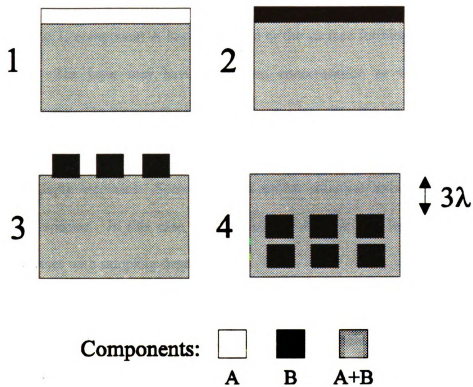


Figure 1.4 The sampling depth in XPS is $3\lambda\cos\theta$, where λ is the mean free path of the photoelectrons in the material and θ is the angle between the surface normal and the analyzer. In AR-XPS the sample is rotated with respect to the analyzer to obtain different sampling depths.

Some Possible Scenarios



Trends

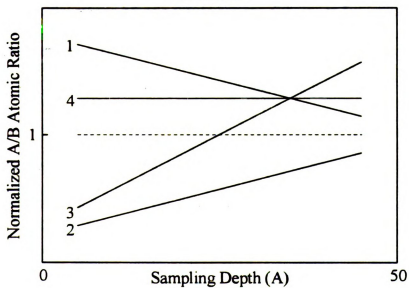


Figure 1.5 Trends in concentration measured with AR-XPS for several possible scenarios. These scenarios give rise to enhanced measured concentrations of one component in a binary mixture of A and B.

(con

form

enha

conce

depth

as the

surfac

surfac

Scena

ratio

surfac

1 Th

have

the su

defici

which

sampli

is grea

(conversely, the other component migrating away from the surface) or due to the formation of crystallites which have a different A/B ratio than in the original bulk mixture.

In Scenario 1, component A has segregated at the surface forming a surface layer enriched in A. The layer may have a uniform concentration or there may be a concentration gradient. As long as the layer thickness is less than the maximum sampling depth (3λ), the measured A/B ratio would be greater than 1 at the surface and approach 1 as the sampling depth increases. Scenario 2 is a similar situation, except that B is the surface enriched species. In this case, the normalized A/B ratio is less than 1 at the surface and increases with sampling depth.

Crystallites which are enriched in component B have formed at the surface in Scenario 3. As a result of the crystallization, the bulk of the sample is enriched in A. The ratio measured for shallow angles will be less than 1 because the crystallites are at the surface. It is possible that as the sampling depth increases the ratio becomes greater than 1. This inversion of the measured ratio would happen if there are few crystallites and they have diameters much greater than 3λ . In this case for the greater sampling depths, only the surface of the crystallites is sampled and the majority of the signal is from the B-deficient amorphous bulk of the sample.

In Scenario 4, crystallites enriched in B have formed again resulting in a bulk which is enriched in A. In this case, the crystallites have formed below the maximum XPS sampling depth. In this case, the measured ratio is independent of the sampling depth but is greater than 1.

surface

concent

different

An equa

from the

a materi

where I

λ is the

expressi

ratio (R_1

peaks us

replaced

R_1 is e

concentra

of R_1 and

Quantitative information can be obtained if a simple model is used to describe the surface segregation of one component of a binary mixture (Scenarios 1 and 2 with no concentration gradient). In this model, a single surface layer of thickness “d” has a different relative concentration of the two components (R_s) than found in the bulk (R_b). An equation was derived, as follows, to get an estimate of the thickness of a surface layer from the relative concentrations measured as a function of analysis angle with AR-XPS.

It is commonly acknowledged that photoelectrons are exponentially attenuated by a material [31]:

$$I_i = \frac{I_i^o}{\lambda_i} \int_0^{\infty} X_i(z) e^{-\frac{z}{\lambda_i}} dz \quad 1.7$$

where I_i is the peak intensity of element i , I_i^o is its intensity in an elemental bulk standard, λ_i is the effective escape depth, and $X_i(z)$ is the mole fraction of i at depth z . This expression can be written in terms of ratios of intensities (R_i and R_i^o) and mole fraction ratio ($R_x(z)$) for a binary mixture when λ_i is the same for both species. This is valid if the peaks used for quantitation have similar binding (kinetic) energies. Additionally, λ_i can be replaced with $\lambda^o \cos\theta$ to indicate its angular dependence:

$$R_i = \frac{R_i^o}{\lambda^o \cos\theta} \int_0^{\infty} R_x(z) e^{-\frac{z}{\lambda^o \cos\theta}} dz \quad 1.8$$

R_i^o is essentially a sensitivity factor so R_i/R_i^o can be replaced with R , the relative concentrations. Assuming the surface layer has a thickness d and a relative concentration of R_s and the bulk has a relative concentration R_b , then this expression becomes:

$$R = \frac{1}{\lambda^o \cos\theta} \left[R_s \int_0^d e^{-\frac{z}{\lambda^o \cos\theta}} dz + R_b \int_d^{\infty} e^{-\frac{z}{\lambda^o \cos\theta}} dz \right] \quad 1.9$$

Solving th

Estimates

between m

W

particular

compositio

Solving the integrals results in the following equation:

$$R = R_s \left(1 - e^{-\frac{d}{\lambda^o \cos \theta}} \right) + R_b \left(e^{-\frac{d}{\lambda^o \cos \theta}} \right) \quad 1.10$$

Estimates of R_s , d , and R_b can be obtained by minimizing the sum of the differences between measured relative concentrations and those generated using this equation.

Whether it is valid to use this equation to estimate a surface layer thickness for a particular sample should be judged based upon the trends in the AR-XPS data and the composition and size of any crystallites present in the sample.

14 R

1 B
P

2 E
V

3 I

4

5

6

7

8

9

10

11

12

13

14

15

16

C
V

1.4 References

1. Brinker, C.J.; Scherrer, G. *Sol-Gel Science, the Physics and Chemistry of Sol-Gel Processing*, Academic Press: San Diego, 1990.
2. Bradley, D.C., Mehrotra, R.C.; Gaur, D.P. *Metal Alkoxides*; Academic Press: London, 1978.
3. Livage, J.; Henry, M.; Sanchez, C. *Prog. Solid St. Chem.*, **1988**, *18*, 259.
4. Mehrotra, R.C.; Gaur, D.P.; Bohra, R. *Metal β -diketonates and Allied Derivatives*, Academic Press, London, 1978.
5. Mehrotra, R.C.; Bohra, R. *Metal Carboxylates*, Academic Press, London, 1983.
6. Sanchez, C.; Livage, J. *New J. Chem.*, **1990**, *14*, 513.
7. Gagliardi, C.D.; Berglund, K.A. in *Processing Science of Advanced Ceramics*, Aksay, I.A.; McVay, G.L.; Ulrich, D.R., Eds.; Mater. Res. Soc. Proc. 155: Pittsburgh, PA, 1986; 127.
8. Gagliardi, C.D.; Dunuwila, D.; Berglund, K.A. in *Better Ceramics Through Chemistry IV*, Zelinsky, B.J.J.; Brinker, C.J.; Clark, D.E.; Ulrich, D.R., Eds.; Mater. Res. Soc. Proc. 180: Pittsburgh, PA, 1990; 801.
9. Madou, M.J.; Morrison, S.R. *Chemical Sensing with Solid State Devices*; Academic Press, Inc.: San Diego, CA, 1989.
10. McAleer, J. F.; Moseley, P. T.; Norris, J. O. W.; Williams, D. E. *J. Chem. Soc., Faraday Trans. 1* **1987**, *83*, 1323.
11. Flietner, B.; Eisele, I. *Thin Solid Films* **1994**, *250*, 258.
12. Stoev, I.; Kohl, D. *Sens. Actuators B* **1990**, *2*, 233.
13. Pink, H.; Treitinger, L. Vite, L. *Japan. J. Appl. Phys.* **1980**, *19(3)*, 513.
14. Takahashi, Y.; Wada, Y. *Yogyo-Kyokai-Shi* **1987**, *95(9)*, 864.
15. Yoshimura, N.; Sato, S.; Itoi, M.; Taguchi, H. *Sozai Busseigaku Zasshi* **1990**, *3*, 47.
16. Chung, W.-Y.; Lee, D.-D.; Sohn, B.-K. *Thin Solid Films* **1992**, *221*, 304. Chung, W.-Y.; Lee, D.-D.; Choi, D.-H. *Sens. Actuators B* **1993**, *13-14*, 517.

17 Na
18 Sea
Joh
19 Jan
20 Yan
R.
Ma
198
Sen
M.
21 Kur
Am
22 Aso
23 Fatt
24 Win
25 Mai
26 Cha
27 Per
28 Sco
29 Sea
30 Sea
Joh
31 Ho
Joh

- 17 . Nakajima, A. *J. Mater. Sci. Lett.* **1993**, *12*, 1778.
- 18 . Seah, M. P. in *Practical Surface Analysis, Vol. 1*, Briggs, D.; Seah, M.P., Eds.; John Wiley & Sons, Inc.: New York, 1990, p.311.
- 19 . Janata, J. *Principles of Chemical Sensors*; Plenum Press: New York, 1989.
- 20 . Yamazoe, N.; Kurokawa, Y.; Seiyama, T. *Sens. Actuators* **1983**, *4*, 283. Huck, R.; Bottger, U.; Kohl, D.; Heiland, G. *Sens. Actuators* **1989**, *17*, 355. Matsushima, S.; Maekawa, T.; Tamaki, J.; Miura, N.; Yamazoe, N. *Chem. Lett.* **1989**, 845. Maekawa, T.; Tamaki, J.; Miura, N.; Yamazoe, N.; Matsushima, S. *Sens. Actuators B* **1992**, *9*, 63. Cheong, H.-W.; Choi, J.-J.; Kim, H. P.; Kim, J.-M.; Churn, G.-S. *Sens. Actuators B* **1992**, *9*, 227.
- 21 . Kung, H.H. *Transition Metal Oxides: Surface Chemistry and Catalysis*; Elsevier: Amsterdam, 1989.
- 22 . Aso, I.; Nakao, M.; Yamazoe, N.; Seiyama, T. *J. Catal.* **1979**, *57*, 287.
- 23 . Fattore, V.; Fuhrman, Z.A.; Manara, G.; Notari, B. *J. Catal.* **1975**, *37*, 215.
- 24 . Windischmann, H.; Mark, P. *J. Electrochem. Soc.* **1979**, *126(4)*, 627.
- 25 . Maier, J.; Gopel, W. *J. Solid State Chem.* **1988**, *72*, 293.
- 26 . Chang, S. C. *J. Vac. Sci. Technol.* **1980**, *17(1)*, 366.
- 27 . Penn, D.R. *J. Electron Spectrosc. Relat. Phenom.* **1976**, *9*, 29.
- 28 . Scofield, J. H. *J. Electron Spectrosc. Relat. Phenom.* **1979**, *8*, 129.
- 29 . Seah, M. P.; Dench, W. A. *Surf. Interface Anal.* **1979**, *1*, 2.
- 30 . Seah, M. P. in *Practical Surface Analysis, Vol. 1*, Briggs, D.; Seah, M.P., Eds.; John Wiley & Sons, Inc.: New York, 1990, p.231.
- 31 . Hofmann, S. in *Practical Surface Analysis, Vol. 1*, Briggs, D.; Seah, M.P., Eds.; John Wiley & Sons, Inc.: New York, 1990, p.151.

Chara

2.1 Ab

FTI

films prep

titanium(IV

temperatur

FTIR The

solutions w

metal-oxyg

for the pres

in all cast

structure d

are higher

solutions c

are more h

2.2 Int

The

and organi

arise from

Chapter 2

Characterization of Titanium and Zirconium Valerate Sol-Gel Films

2.1 Abstract

FTIR and XPS have been used to characterize titanium and zirconium valerate thin films prepared using sol-gel techniques. Films were prepared by hydrolysis of titanium(IV) isopropoxide or zirconium(IV) n-propoxide in excess valeric acid at room temperature. Film solution chemistry, from precursors to cast films, was followed with FTIR. The structure and chemical composition of films spin cast from fresh and day old solutions were determined. Results of these studies suggest that all films consist of a metal-oxygen polymer backbone coordinated with bidentate valerate ligands. No evidence for the presence of alkoxide ligands has been found. A small amount of water is adsorbed in all cast films. While solution aging experiments indicate that the zirconium film structure does not change with solution reaction time, carboxylate ligand concentrations are higher in titanium films made from aged solutions. Titanium films made from aged solutions contain slightly less than 1.5 valerate ligands per titanium atom. Zirconium films are more highly carboxylated with almost two valerate groups per metal center.

2.2 Introduction

The sol-gel process is an attractive approach for the synthesis of glasses, ceramics, and organic-inorganic composite materials [1 - 4]. The advantages of sol-gel techniques arise from the high purity of the metal alkoxide precursors, the molecular homogeneity of

the interm

In addition

preparation

effort has

techniques

control of

tailor-made

Hyd

studied and

structure is

transition m

chemistry

coordinatio

ability to in

result in al

greater tha

employed.

of transiti

Ch

reactions i

diketones

species are

decoupling

the intermediate sols, and the low processing temperatures necessary to prepare materials. In addition, the rheological properties of many sols and gels make them suitable for film preparation using methods such as spin casting and dip coating [4-7]. Thus considerable effort has been devoted to the development of new thin film materials using sol-gel techniques. Understanding the chemistry involved in film synthesis will lead to better control of the sol-gel process and, ultimately, to the ability to produce films which are tailor-made for particular applications.

Hydrolysis and condensation reactions of silicon alkoxides have been extensively studied and, consequently, the relationship between sol-gel chemistry and polysilicate structure is reasonably well understood [8 -12]. In comparison, the sol-gel chemistry of transition metal alkoxides has been less completely characterized. Transition metal sol-gel chemistry differs from that of silicon because transition metals have a variety of coordination states available and lower electronegativities than silicon [13 -16]. Both the ability to increase coordination number and the electropositive nature of transition metals result in alkoxide hydrolysis and condensation rates which are usually orders of magnitude greater than that of silicon alkoxides. Therefore, unless some form of chemical control is employed, hydroxide and/or oxhydroxide species precipitate immediately upon hydrolysis of transition metal alkoxides.

Chemical control of transition metal alkoxide hydrolysis and condensation reactions is often achieved by adding complexing reagents such as organic acids or β -diketones [17 -33]. When these ligands react with metal alkoxides, new molecular species are produced with altered structures and reactivities. Complexation promotes decoupling between hydrolysis and condensation [34] and facilitates the preparation of

uniform.

hydrolysis

Thus, the

backbone

The

and zircon

reported th

from mixtu

However, t

film prop

Films prod

also hydro

those prep

carboxylic

acid and v

A

involved

zirconium

there are

metal alk

substitut

uniform, transparent coatings [35]. Strong complexing ligands are more stable toward hydrolysis than alkoxide ligands due to chelate, electronic, and steric hindrance effects. Thus, the organic ligands become anchored to the transition metal oxo-polymeric backbone and form organic-inorganic networks.

The role of acetic acid as a complexing agent in the sol-gel chemistry of titanium and zirconium alkoxides has been examined in some detail [22-32]. We have previously reported that optically transparent, porous films can be produced at ambient temperatures from mixtures of acetic acid, water, and titanium, zirconium, or hafnium alkoxides [32]. However, these films tend to be of poor quality and are soluble in water. We found that film properties could be improved by complexing with longer chain carboxylic acids. Films produced using valeric acid ($n\text{-C}_4\text{H}_9\text{COOH}$) are not only transparent and porous but also hydrophobic and show greater integrity and better adhesion to glass substrates than those prepared with acetic, propanoic, or butyric acid [33]. Our previous work with carboxylic acid/transition metal alkoxide sol-gel chemistry also focused on the effect of acid and water concentration on the structure of solutions, monoliths, and films [32,33].

A major goal of this work is to gain a more detailed understanding of the chemistry involved in the production of films from titanium(IV) isopropoxide ($\text{Ti}(\text{OPr}^i)_4$) or zirconium(IV) n-propoxide ($\text{Zr}(\text{OPr}^n)_4$) and valeric acid. It is generally acknowledged that there are three principal reaction steps in the synthesis of sol-gel materials from transition metal alkoxides and carboxylic acids [5,13,15,18,34,36]. The first is a nucleophilic substitution of an alkoxide ligand by a carboxylate ligand:



Alcohol is

the remain

Carboxyla

initiates c

groups c

respectiv

acetic

carbo

hydr

chen

briv

as

us

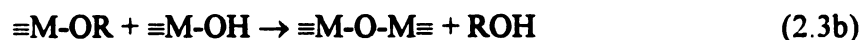
ti

e

Alcohol is a by-product of this reaction. The second is the hydrolysis of one or more of the remaining alkoxide groups:



Carboxylate ligands can also be hydrolyzed but this occurs less readily. Hydrolysis initiates condensation. In condensation, hydroxyl groups react with hydroxyl or alkoxide groups on other metal centers producing M-O-M bonds and water or alcohol, respectively:



Esterification reactions also play a fundamental role in the solution chemistry of acetic acid modified alkoxides [27-29, 36]. Esters can be formed by the reaction of a carboxylic acid with either an alcohol molecule or an alkoxide ligand producing water or a hydroxyl ligand, respectively [29]. The importance of esterification reactions in the chemistry of valeric acid modified alkoxides is not known.

Carboxylate ligands can adopt a variety of coordination modes and as bidentate bridging ligands, can act as network formers. The separation ($\Delta\nu$) between the asymmetric ($\nu_{as}(\text{COO})$) and symmetric ($\nu_s(\text{COO})$) carboxyl stretch frequencies can be used as an indicator of carboxylate coordination mode [37]. Separations much greater than that of the ionic form of the ligand tend to indicate monodentate coordination, otherwise bidentate coordination is implied. It has also been suggested that bidentate bridging ligands typically exhibit $\Delta\nu$ values similar to ionic species, while bidentate chelating ligands show smaller splittings [37]. This reasoning has been applied to

determine

coordinat

band in th

bond angl

with coord

bands of c

suggest th

Th

(FTIR) s

and Zr(C

mechan

involves

chemic

elucida

2.3

propo

Aldr

chem

vale

Cor

determine coordination mode of acetate ligands in sols and gels [22,28,32]. Carboxylate coordination mode can also be inferred from the frequency of the $\nu_{\text{as}}(\text{COO})$ absorbance band in the infrared spectrum of a material. Grigor'ev found that the greater the OCO bond angle, the higher the $\nu_{\text{as}}(\text{COO})$ frequency [38]. Since bond angle tends to decrease with coordination mode: monodentate > bidentate bridging > bidentate chelating, $\nu_{\text{as}}(\text{COO})$ bands of considerably higher frequency than in the spectrum of the ionic form of the ligand suggest the presence of monodentate ligands.

The first half of this paper is devoted to a Fourier transform infrared spectroscopy (FTIR) study of the sol-gel solution chemistry specific to valeric acid modified $\text{Ti}(\text{OPr}^i)_4$ and $\text{Zr}(\text{OPr}^n)_4$. Information is obtained which can be related to the rate, extent, and mechanism of the sol-gel reactions in these systems. The second part of the paper involves the characterization of titanium and zirconium valerate films. The structure and chemical composition of these films, including the nature and concentration of ligands, are elucidated using a combination of FTIR and X-ray photoelectron spectroscopy (XPS).

2.3 Experimental

Materials. Titanium(IV) isopropoxide, zirconium(IV) n-propoxide 70% in n-propanol, isopropanol (99.5%, HPLC grade), and valeric acid (99+%) were obtained from Aldrich Chemical Company and used without further purification. All syntheses used chemicals obtained from freshly opened bottles and distilled, deionized water. Sodium valerate was prepared by mixing valeric acid with sodium carbonate (Aldrich Chemical Company).

Sol
techniques
carboxylat
vials. Mol
the films
vortex mix
The reacti
titanium so
yellow

Tw
to titanium
was the sam
of titanium
of both se
identical w
solutions a

Fil
or KBr) a
dessicator
complete a
in triplicate

Solution Preparation. The methods used to synthesize films were based on techniques developed in these laboratories for the preparation of transition metal carboxylate thin films [33]. Reactions were carried out at room temperature in capped vials. Molar ratios of metal alkoxide : valeric acid : water of 1:9:1.5 were used to prepare the films. Valeric acid was added to the alkoxide, immediately followed by water. A vortex mixer was used to vigorously stir solutions following the addition of each reactant. The reaction between valeric acid and both metal alkoxides was exothermic. The resulting titanium solutions were clear and colorless; zirconium solutions were clear and slightly yellow.

Two sets of titanium solutions were prepared. In the first, isopropanol was added to titanium isopropoxide before the addition of valeric acid. The alcohol concentration was the same as in the 70% $Zr(OPr^i)_4$ solution (2.3 alcohol : 1 alkoxide). The second set of titanium solutions was prepared without the addition of alcohol. Results of the analysis of both sets of titanium solutions and the films prepared from these solutions were identical within experimental error. Results presented in this paper are for titanium solutions and films prepared without added isopropanol.

Film Preparation. Solutions were deposited onto the desired substrate (quartz or KBr) and spun for five minutes. Films were air-dried overnight and stored in a dessicator. All films prepared in this study were transparent, colorless, and exhibited complete and uniform coverage of quartz substrates. Each solution and film was prepared in triplicate. In order to simplify discussion, titanium and zirconium films cast immediately

after solut

solutions a

For

obtained

spectromet

software p

2 cm⁻¹ Fil

solution pl

reactions

features w

performed

holder ec

Omega C

X

analyzed

precision

using a

kV and

each fil

energies

with a p

quantita

after solution preparation are denoted Ti00 and Zr00, respectively. Films prepared from solutions aged for 24 h before casting are denoted Ti24 and Zr24.

Fourier Transform Infrared Spectroscopy (FTIR). FTIR spectra were obtained using a Mattson Instruments Galaxy 3020 Fourier transform infrared spectrometer. Data acquisition and processing were performed using an Enhanced First software package. The mid-IR region ($4000\text{--}400\text{ cm}^{-1}$) was examined with a resolution of 2 cm^{-1} . Films were cast on KBr windows; solution spectra were obtained from a drop of solution placed between two KBr windows. To identify artifacts which could be due to reactions with KBr, several films were cast on Ge and analyzed with FTIR. Spectral features were the same for films cast on both substrates. *In situ* heating experiments were performed under nitrogen purge (99.5%, AGA Gas Co.) using a stainless-steel sample holder equipped with cartridge heaters (Omega). The temperature was fixed using an Omega CN 1200 controller.

X-ray Photoelectron Spectroscopy (XPS). Films cast on quartz slides were analyzed with a Perkin-Elmer surface science instrument equipped with a model 10-360 precision energy analyzer and an omnifocus small spot lens. All spectra were collected using a non-monochromatized Mg anode (1253.6 eV) operated at a power of 300 W (15 kV and 20 mA) with an analyzer pass energy of 50 eV . Three regions were scanned in each film: C 1s, O 1s and the most intense metal core band (Ti 2p or Zr 3d). Binding energies were referenced to adventitious carbon (C 1s = 284.6 eV) and were measured with a precision of $\pm 0.1\text{ eV}$. Empirically derived sensitivity factors [39] were used for quantitative XPS calculations involving the C1s and O1s. For the Ti 2p and Zr 3d,

2

1

2

i:

b

m

st

o

ar

Si

fo

[4

85

bu

fo

alk

sensitivity factors were derived from the analysis of TiO_2 and ZrO_2 (Aldrich Chemical Company, 99.99+%). XPS peaks were fitted with 20% Lorentzian-Gaussian mix Voigt functions using a non-linear least squares curve fitting program [40]. Each reported result is based on the analysis of at least three films. It must be noted that the use of XPS to evaluate film composition assumes that the films are homogeneous.

2.4 Results and Discussion

FTIR Spectra of Reactants. The FTIR spectra of reactants, as well as those of isopropanol and n-propanol, are shown in Figure 2.1. The assignment of FTIR absorption bands for valeric acid (Figure 2.1a) is straightforward [41,42]. Three methyl and methylene C-H stretching absorbances are observed at 2962, 2935, and 2876 cm^{-1} superimposed on an O-H absorbance centered near 3000 cm^{-1} . The strong absorbance observed at 1711 cm^{-1} is due to a dimeric carboxylic COO asymmetric stretch. Bending and stretching vibrations of C-O-H groups are observed at 1414, 1280, and 940 cm^{-1} . Skeletal vibrations are evident at 1382, 1109, and 752 cm^{-1} .

In the FTIR spectrum of $\text{Ti}(\text{OPr}^i)_4$ (Figure 2.1b) absorbance bands are assigned as follows: the band at 1126 cm^{-1} is due to a combination of skeletal and C-O stretches [43] that observed at 1002 cm^{-1} is a $\nu(\text{C-O})\text{Ti}$ vibration [44], a skeletal vibration band is at 852 cm^{-1} [44], and a $\nu(\text{Ti-O})$ band appears at 621 cm^{-1} [43]. Due to steric hindrance by bulky isopropoxide groups, $\text{Ti}(\text{OPr}^i)_4$ is monomeric with a coordination number of four, [30,45]. Isopropanol (Figure 2.1c) can be most easily distinguished from the alkoxide by the sharp bands at 953 and 818 cm^{-1} .

Absorbance

Figure 2

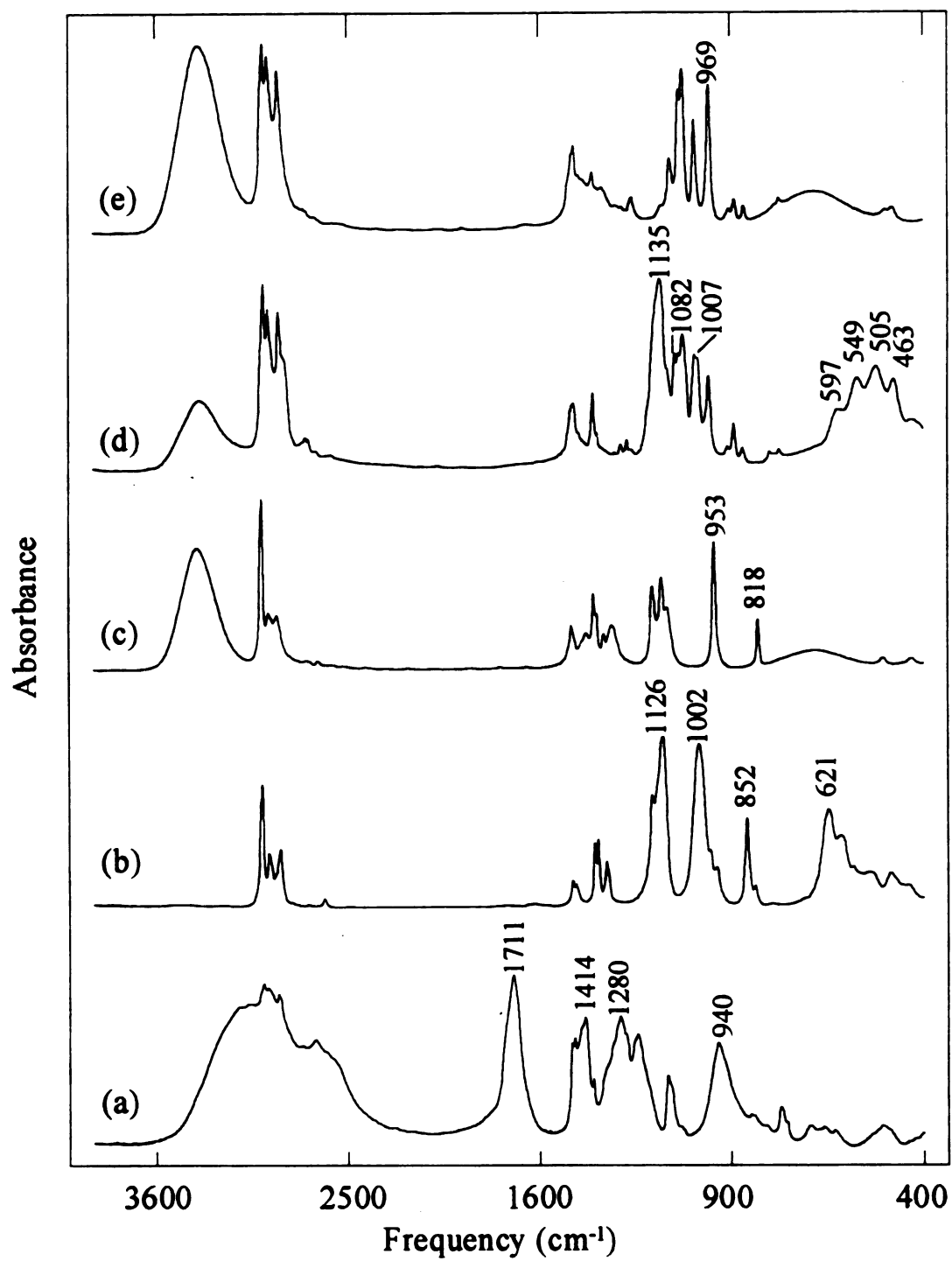


Figure 2.1 FTIR spectra of (a) valeric acid; (b) Ti(OPr)₄; (c) isopropanol; (d) Zr(OPr)₄ in n-propanol; and (e) n-propanol.

At
assigned to
 cm^{-1} is attributed
1082 and
vibrations.
Alcohol at
based upon
consistent
indicate that
The zircon
propanol [
solvents]

Sol
alkoxide-a
spectra of
reaction m
The conce
readily co
concentrat
solutions a
that conde
excess val

Absorption bands in the spectrum of $Zr(OPr^n)_4$ in n-propanol (Figure 2.1d) are assigned based upon the analysis of similar alkoxides [13,43]. The strong band at 1135 cm^{-1} is attributed to a combination of $\nu(C-O)Zr$ and skeletal stretches, bands observed at 1082 and 1007 cm^{-1} are also associated with the alkoxide and may be due to $\nu(C-O)Zr$ vibrations, and those observed at 597 , 549 , 505 , and 463 cm^{-1} are attributed to $\nu(Zr-O)$. Alcohol absorbances between 1100 and 900 cm^{-1} make it difficult to determine structure based upon $\nu(C-O)Zr$ bands, however, multiple bands in the low frequency region are consistent with an oligomeric structure. Ebulliometric studies by Bradley and Carter [46] indicate that $Zr(OPr^n)_4$ is oligomeric in n-propanol with a molecular complexity of 2.44. The zirconium coordination sphere is also thought to be increased by solvation in n-propanol [47]. This limits the extent of oligomerization compared to that in non-polar solvents. N-propanol (Figure 2.1e) can be identified by a sharp band at 969 cm^{-1} .

Solution Reactions. Solution reactions were investigated by preparing a series of alkoxide-acid mixtures with increasing valeric acid concentrations. In addition to the spectra of 1:1 (alkoxide : acid) mixtures of each alkoxide and valeric acid, spectra of reaction mixtures with the lowest detectable level of unreacted valeric acid are shown. The concentration of these solutions indicates the number of valerate ligands which can be readily coordinated to each alkoxide. To the latter solution, water was added at a molar concentration of 1.5 water per metal alkoxide. This is the concentration of water in film solutions and is sufficient water to completely hydrolyze carboxylated alkoxides provided that condensation also occurs. Analysis of these solutions avoids interference due to excess valeric acid present in the 1:9 film mixtures. It is recognized that the presence of

excess

about

acid co

films. s

valerat

Absort

respec

11 an

respec

mixtur

(1575

forme

bands

to bid

$\nu_{\text{as}}(\text{CO})$

lower

cm^{-1}) i

Interes

split in

there a

excess valeric acid may alter the solution chemistry, however, fundamental information about the interaction of solution species can be obtained by analyzing mixtures with lower acid concentration.

In order to evaluate the coordination mode of valerate ligands in solutions and films, sodium valerate was prepared and analyzed with FTIR. The absorbances for sodium valerate can be assigned by analogy to those of sodium acetate reported by Spinner [48]. Absorbances at 1562 and 1421 cm^{-1} ($\Delta\nu = 141 \text{ cm}^{-1}$) are $\nu_{\text{as}}(\text{COO})$ and $\nu_{\text{s}}(\text{COO})$ bands, respectively, of the ionic valerate groups.

Titanium Solutions. Figure 2.2 shows the FTIR spectra of $\text{Ti}(\text{OPr}^i)_4$ (Figure 2.2a), 1:1 and 1:1.5 mixtures of this alkoxide and valeric acid (Figures 2.2b and 2.2c, respectively), and the latter mixture after the addition of water (Figure 2.2d). For a 1:1 mixture (Figure 2.2b), no free valeric acid is observed (1711 cm^{-1}) and $\nu_{\text{as}}(\text{COO})$ bands (1575 and 1529 cm^{-1}) are present. This means that all of the valeric acid has reacted and formed valerate ligands which are bonded to titanium. The frequency of the $\nu_{\text{as}}(\text{COO})$ bands are close to that of ionic valerate (1562 cm^{-1}) and, therefore, are assumed to be due to bidentate valerate ligands. Based upon its frequency, the stronger, higher energy $\nu_{\text{as}}(\text{COO})$ band (1575 cm^{-1}) is probably due to bridging valerate ligands. Whether the lower energy band is due to bridging or chelating ligands cannot be determined.

The appearance of absorption bands characteristic of isopropanol (953 and 818 cm^{-1}) indicates that valerate ligands have displaced alkoxide ligands producing alcohol. Interestingly, the alkoxide absorbance at 1002 cm^{-1} in titanium(IV) isopropoxide is now split into two distinct bands at 1014 and 993 cm^{-1} . This suggests that in the 1:1 solution, there are two types of alkoxide ligands present, probably terminal and bridging alkoxides,

Absorbance

Figure 2

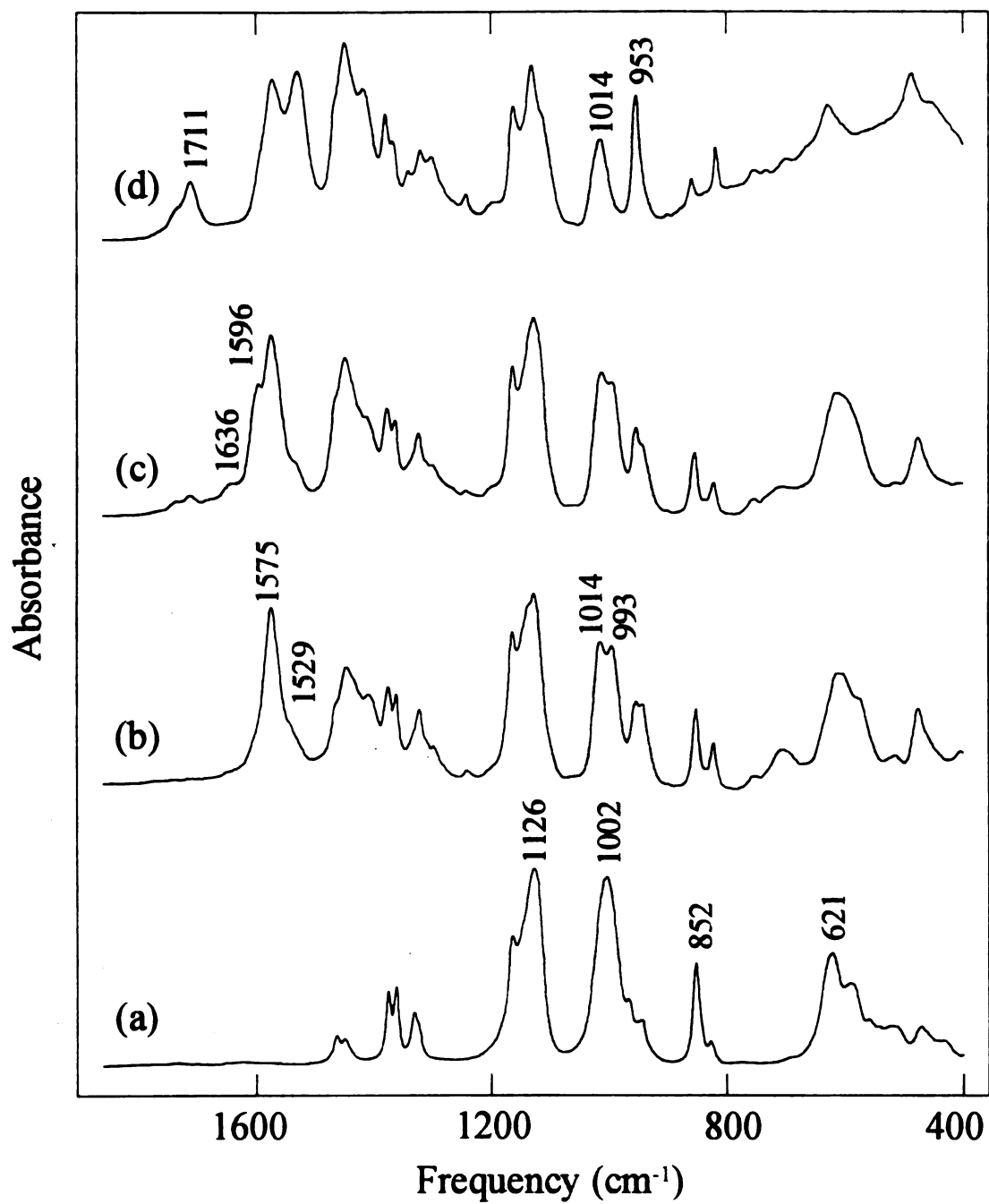


Figure 2.2 FTIR spectra of (a) $\text{Ti}(\text{OPr}^i)_4$; (b) 1:1 mixture and (c) 1:1.5 mixture of $\text{Ti}(\text{OPr}^i)_4$ and valeric acid; (d) 1:1.5:1.5 mixture of $\text{Ti}(\text{OPr}^i)_4$, valeric acid, and water.

respec

have h

bulky

but the

to six

monom

acid me

valeric

readily

per titan

$\nu_{\text{max}}(\text{COO})$

band at

is consi

coordin

observe

band at

this paper

F

There is

band at 9

readily hy

respectively. The assignment is based upon other alkoxides: typically terminal alkoxides have higher vibrational frequencies than bridging alkoxides [13]. The replacement of a bulky isopropyl group with a valerate ligand not only increases the coordination to five, but the decrease in steric hindrance also allows a further increase in coordination number to six with the formation of alkoxide bridges. The transformation of $\text{Ti}(\text{OPr}^i)_4$ from a monomeric to an oligomeric structure was also reported by Sanchez *et al.* [49] for acetic acid modification of this alkoxide.

The spectrum of the 1:1.5 solution contains a band at 1711 cm^{-1} due to dimeric valeric acid. Apparently, titanium centers do not accommodate a second valerate ligand as readily as they accept the first. On average, there are between 1 and 1.5 valerate ligands per titanium atom in this solution. There are two new bands (1636 and 1596 cm^{-1}) due to $\nu_{\text{as}}(\text{COO})$ absorbances. While the latter may be ascribed to bidentate bridging ligands, the band at 1636 cm^{-1} probably indicates the formation of monodentate valerate ligands. This is consistent with steric hindrance at the titanium center which would make bidentate coordination more difficult. Alcohol and alkoxide bands are very similar to those observed in the 1:1 solution spectrum. It should be noted that there is a small absorbance band at 1734 cm^{-1} . The assignment of this band will be discussed in some detail later in this paper.

Figure 2.2d shows the spectrum of the 1:1.5 mixture after the addition of water. There is still a substantial terminal alkoxide band at 1014 cm^{-1} but the bridging alkoxide band at 993 cm^{-1} is no longer evident. Apparently, bridging alkoxide groups are more readily hydrolyzed than terminal alkoxides. Condensation is occurring as evidenced by the

presence of a rising background in the low energy portion of the spectrum that is commonly attributed to phonon bands in a titanium oxygen network [50]. The increase in valeric acid concentration indicates that valerate ligands are also displaced by the addition of water. Sanchez *et al.* [30] also observed that free acid was formed when greater than 1 mole of water per metal alkoxide was added to acetate modified titanium alkoxides. The high frequency $\nu_{\text{as}}(\text{COO})$ bands present in the solution spectra before the addition of water (1636 and 1596 cm^{-1}) are no longer present. Either these carboxylates are preferentially hydrolyzed or the decrease in steric hindrance which occurs when isopropyl groups are hydrolyzed allows conversion from monodentate to bidentate coordination. Two $\nu_{\text{as}}(\text{COO})$ bands of about equal intensity are present and of the same frequency as that in the 1:1 solution spectrum (Figure 2.2b). As stated previously, the higher energy band is probably due to bidentate bridging ligands and the lower may be due to either bridging or chelating ligands.

It should be noted that small absorbance bands due to alkoxide ligands are present in the freshly prepared titanium film solution (1 $\text{Ti}(\text{OPr}^i)_4$: 9 valeric acid : 1.5 water) spectra (not shown). The FTIR spectrum of a solution which has been aged for 24 h does not contain bands characteristic of alkoxide ligands.

Zirconium Solutions. Figure 2.3a shows the FTIR spectrum of $\text{Zr}(\text{OPr}^n)_4$ in n-propanol. When a stoichiometric amount of valeric acid is added to the alkoxide (Figure 2.3b), it reacts completely (no band at 1711 cm^{-1}) and forms valerate ligands ($\nu_{\text{as}}(\text{COO})$ bands at 1562 and 1535 cm^{-1} with a 1600 cm^{-1} shoulder). As in the titanium solutions, the higher frequency bands are probably due to bidentate bridging ligands and the lower may

be due to either bridging or chelating valerates. The relative intensity of alcohol bands between 1200 and 800 cm^{-1} also increases with respect to the alkoxide bands in this region of the spectrum. This is consistent with the displacement of alkoxide ligands and formation of alcohol. Unlike titanium, none of the alkoxide (C-O)Zr features split and their relative intensities do not appear to change with the addition of valerate ligands. This implies that alkoxide ligand coordination and oligomerization is unchanged by carboxylation. However, absorbance bands due to n-propanol also occur in this region of the spectrum making it difficult to say this unequivocally. The maximum intensity of the bands between 700 and 500 cm^{-1} is shifted to a slightly higher frequency than in the alkoxide spectrum. This may be due to coordination with valerate ligands [13].

The spectrum of the 1:2 mixture is shown in Figure 2.3c. Small bands at 1711 cm^{-1} (unreacted valeric acid) and 1734 cm^{-1} (*vide infra*) are present. These bands are not present in the spectrum of a 1:1.5 mixture (not shown). Nearly two valerate ligands are readily coordinated to zirconium atoms in this solution. A broad band due to $\nu_{\text{as}}(\text{COO})$ occurs between 1589 and 1535 cm^{-1} indicating valerate ligands with bidentate coordination only. In comparison to the 1:1 solution spectrum, the relative intensities of the alkoxide bands are decreased and the alcohol bands increased. This is most clearly seen by comparing the intensity of the alkoxide band at 1135 cm^{-1} with the alcohol bands in this region.

Figure 2.3d shows the spectrum of this solution after the addition of water. Unlike the titanium solutions, addition of water completely removes all alkoxide ligands from zirconium. Alkoxide bands at 1139, 1082, and 1007 cm^{-1} are not evident. Indeed, this portion of the spectrum resembles that of n-propanol (Figure 2.1e). The alkoxide bands

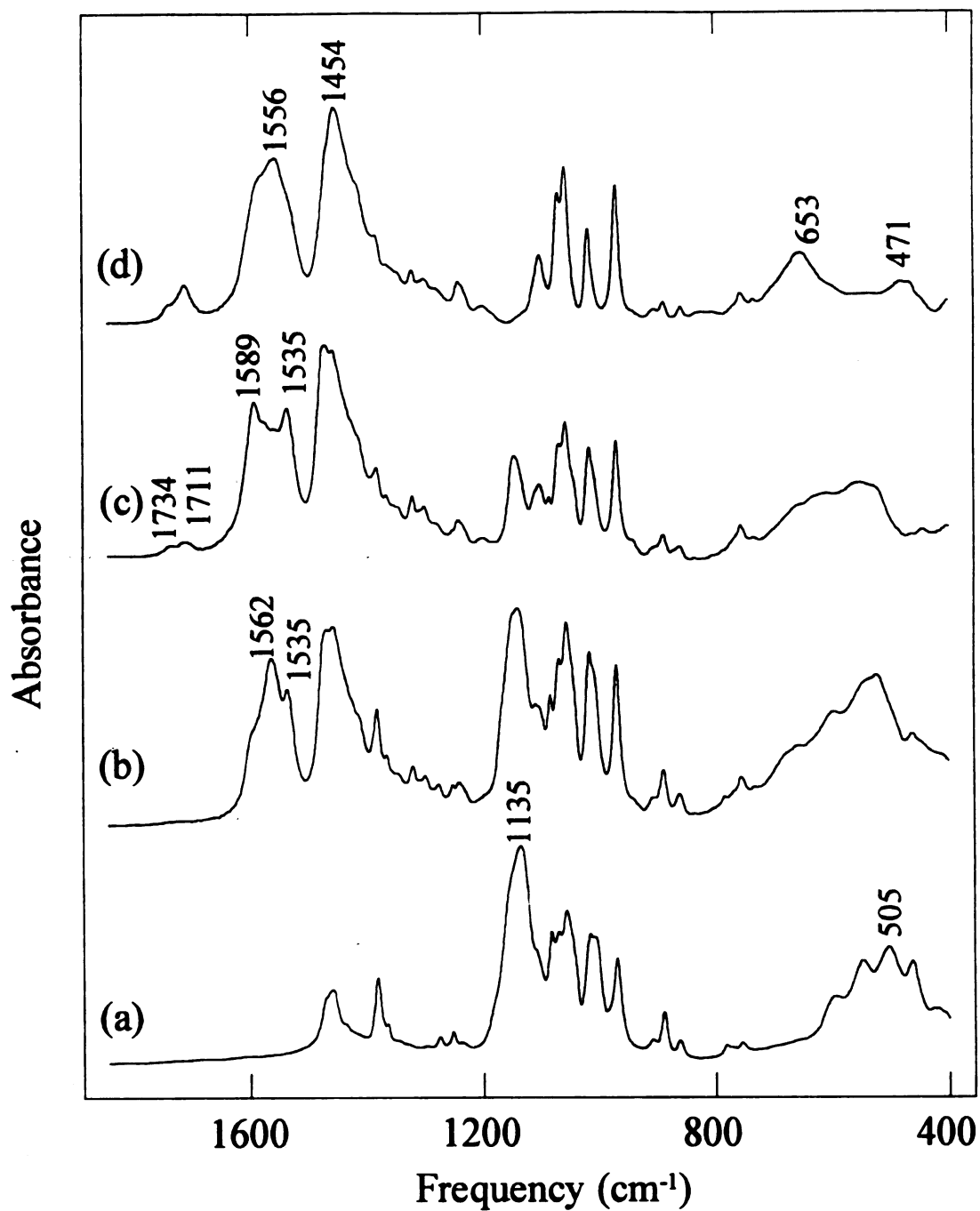


Figure 2.3 FTIR spectra of (a) $Zr(OPr^n)_4$ in n-propanol; (b) 1:1 mixture and (c) 1:2 mixture of $Zr(OPr^n)_4$ and valeric acid; (d) 1:2:1.5 mixture of $Zr(OPr^n)_4$, valeric acid, and water.

between 600 and 450 cm^{-1} are also absent. Absorption bands at 635 and 471 cm^{-1} are probably due $\nu(\text{Zr-O})$ vibrations of oxy bridges formed upon condensation. As in titanium solutions, some of the valerate groups are hydrolyzed as well, as seen by the increase in the intensity of the band at 1711 cm^{-1} . $\nu_{\text{as}}(\text{COO})$ bands are present in the same range as before the addition of water, indicating only bidentate coordination.

Comparison of Titanium and Zirconium Solution Reactions. The results of the FTIR analysis of $\text{Ti}(\text{OPr}^i)_4$ -valeric acid and $\text{Zr}(\text{OPr}^n)_4$ -valeric acid solution spectra are consistent with the three step reaction scheme presented in the introduction. However, our study has revealed that there are differences in the reactivity of the two alkoxides. In particular, $\text{Zr}(\text{OPr}^n)_4$ readily accepts a higher level of carboxylate ligands than $\text{Ti}(\text{OPr}^i)_4$ and $\text{Zr}(\text{OPr}^n)_4$ alkoxide ligands are more rapidly hydrolyzed than those on $\text{Ti}(\text{OPr}^i)_4$. These differences can be related to both the chemical nature of the metal atoms and to steric factors associated with their ligands.

As stated in the introduction, transition metal alkoxides are more reactive toward nucleophilic substitution reactions than silicon alkoxides due to the more electropositive nature of transition metals and the ability to expand their coordination sphere. For analogous reasons, in general, zirconium alkoxides would be expected to be more reactive than titanium alkoxides. Zirconium is less electronegative than titanium, and zirconium is able to accommodate a larger coordination sphere than titanium. Coordination numbers of up to 8 are possible for zirconium, whereas the optimum coordination number for titanium is 6 [51].

The nature of the ligands on the metal center also affects the reactivity of a particular alkoxide. The reactivity of alkoxy ligands with respect to nucleophilic substitution decreases in the order: tertiary>secondary>primary [15]. This is related to the ability of the alkoxide to form a good leaving group. Therefore, isopropyl ligands would be expected to be more reactive than n-propyl ligands in nucleophilic substitution reactions. The reactivity of alkoxy ligands is also influenced by the structure of the alkoxide compound. Monomeric alkoxides are more reactive than oligomeric alkoxides. For these reasons, $\text{Ti}(\text{OPr}^i)_4$ is expected to be very reactive in nucleophilic substitution reactions. Indeed, 1:1 mixture of this alkoxide with valeric acid undergoes a strongly exothermic reaction producing a dimeric complex in which titanium has a coordination number of six.

Addition of a second valerate ligand apparently occurs more readily for the zirconium valerate alkoxide complex than for its titanium counterpart. Not only is zirconium larger than titanium, but it is coordinated with less bulky primary alkoxide ligands. It is also possible that the oligomeric nature of $\text{Zr}(\text{OPr}^n)_4$ is unchanged by reaction with valeric acid. Relatively labile solvate molecules, as well as alkoxide ligands, could be displaced in the substitution reaction to accommodate bidentate valerate ligands without a change in the oligomeric nature or coordination number. However, stable dimeric titanium complexes would need to be broken in order to accommodate the addition of a second bidentate valerate ligand. Evidence of the inability of titanium to accommodate further carboxylate ligands is the presence of monodentate coordination in

the 1:1.5 Ti(OPr)ⁱ₄ valeric acid solution. No monodentate valerate ligands are apparent in the zirconium solution spectra.

Alkoxide ligands are evident in the titanium solution spectra after the addition of water. Aging of the film solutions for 24 h leads to the removal of the alkoxide ligands. In contrast, addition of water to the zirconium solutions results in the complete and immediate removal of all alkoxide ligands. This difference may be related the hydrolysis and/or condensation rate of the materials. Since carboxylates are more electronegative ligands than alkoxides there will be a higher partial charge on the highly carboxylated zirconium center than on titanium. Consequently, it would be expected to be more reactive in nucleophilic substitution reactions such as hydrolysis. The hydrolysis rate also depends upon the concentration of water. Sufficient water for complete hydrolysis is present only if condensation occurs as well. Therefore, if condensation is slow, it will in turn limit the hydrolysis rate.

The spectra of solutions containing unreacted valeric acid (Figures 2.2c, 2.2d, 2.3c, and 2.3d) show an absorbance band at 1734 cm⁻¹. Bands of this frequency are commonly attributed to the presence of esters. Esterification is important in acetic acid transition metal alkoxide sol-gel chemistry. However, higher order carboxylic acids (i.e.: valeric acid) are known to form esters less readily than acetic acid [52]. Esterification is typically a slow reaction at room temperature and in the absence of an acid catalyst [52]. Though our solutions are warmed briefly by the exothermic reaction of the alkoxides with valeric acid, our solutions are not externally heated or allowed to stand for more than 24 h before casting.

To see how readily esters could be prepared and to identify absorbance due to esters, mixtures of valeric acid and the alcohols were prepared with concentrations similar to that in the solutions used to cast films (for purposes of this calculation only, it was assumed that all alkoxide groups react to form alcohol in solution). The alcohol - valeric acid mixtures were heated at 40°C for 1/2 h with and without concentrated sulfuric acid catalyst. No changes were observed in the spectra of uncatalyzed mixtures. Spectra of the catalyzed mixtures contained new bands which could be attributed to the presence of esters. The most prominent new bands in the spectrum of the n-propanol mixture are at 1739 and 1180 cm^{-1} and are typical of $\nu(\text{C}=\text{O})$ and $\nu(\text{C}-\text{O})$ vibrations, respectively, in ester molecules [41]. Similarly, bands are observed at 1734 and 1183 cm^{-1} in the spectrum of the acid catalyzed isopropanol-valeric acid mixture.

The presence of an absorption band at 1734 cm^{-1} does not necessarily indicate the presence of esters in a solution. Very dilute solutions of valeric acid in both isopropanol and n-propanol were prepared and analyzed with FTIR. In the spectra of these solutions, a shoulder at 1734 cm^{-1} is evident on the C-O stretch band of dimeric valeric acid (1711 cm^{-1}). The shoulder is not present in the spectrum of a dilute solution of valeric acid in CCl_4 . Heating and aging the valeric acid/alcohol mixtures did not change the relative intensity of the two bands. Based upon these results, the band at 1734 cm^{-1} in these dilute solutions is not attributed to esters but to valeric acid which is involved in carbonyl-alcohol H-bonds [41].

We believe that the bands at 1734 cm^{-1} in the solution spectra (Figures 2.2 and 2.3) are also due to the presence H-bonded valeric acid-alcohol species. First, in these spectra

and in all film solution spectra there was no evidence of corresponding $\nu(\text{C-O})$ bands. Second, esters proved to be difficult to produce from valeric acid and these alcohols in the absence of an acid catalyst. Therefore, we do not believe that esterification plays a significant role in the chemistry of valeric acid-alkoxide solutions used to prepare the films.

FTIR Characterization of Valerate Films. The infrared spectra of titanium (Ti00 and Ti24) and zirconium (Zr00) valerate films are presented in Figure 2.4. All FTIR absorbance bands in film spectra can be assigned to valerate ligands, hydroxyl groups (either hydroxyl ligands or water), or to the metal-oxygen backbone. No film spectrum contains bands that can be attributed to alkoxide groups, valeric acid, or alcohols.

Valerate Ligands. The three bands observed at 2959, 2933, and 2873 cm^{-1} are identical in all titanium and zirconium films. The relative intensity and position of these peaks are similar to those observed for valeric acid (Figure 2.1a) and, therefore, are attributed to valerate ligands. Less intense bands observed in all film spectra at 1319, 1302, 1109, and 752 cm^{-1} are also due to valerate ligands.

The most intense absorbances in the film FTIR spectra are $\nu(\text{COO})$ bands associated with valerate ligands (1650 - 1200 cm^{-1}). In the spectrum obtained for the Ti00 film (Figure 4a), $\nu_{\text{as}}(\text{COO})$ and $\nu_{\text{s}}(\text{COO})$ frequencies of comparable intensity are observed at 1530 cm^{-1} and 1448 cm^{-1} , respectively ($\Delta\nu = 82 \text{ cm}^{-1}$). For the Ti24 film (Figure 2.4b), the $\nu_{\text{as}}(\text{COO})$ band is less intense than the $\nu_{\text{s}}(\text{COO})$ band. In addition, the $\nu_{\text{as}}(\text{COO})$ band in the spectrum of the Ti24 film consists of two distinct bands at 1559 and 1528 cm^{-1} with a shoulder at 1577 cm^{-1} ($\Delta\nu = 111, 80, \text{ and } 129 \text{ cm}^{-1}$, respectively) [53]. The frequency range spanned by the $\nu_{\text{as}}(\text{COO})$ bands and $\nu_{\text{s}}(\text{COO})$ bands are unchanged by solution

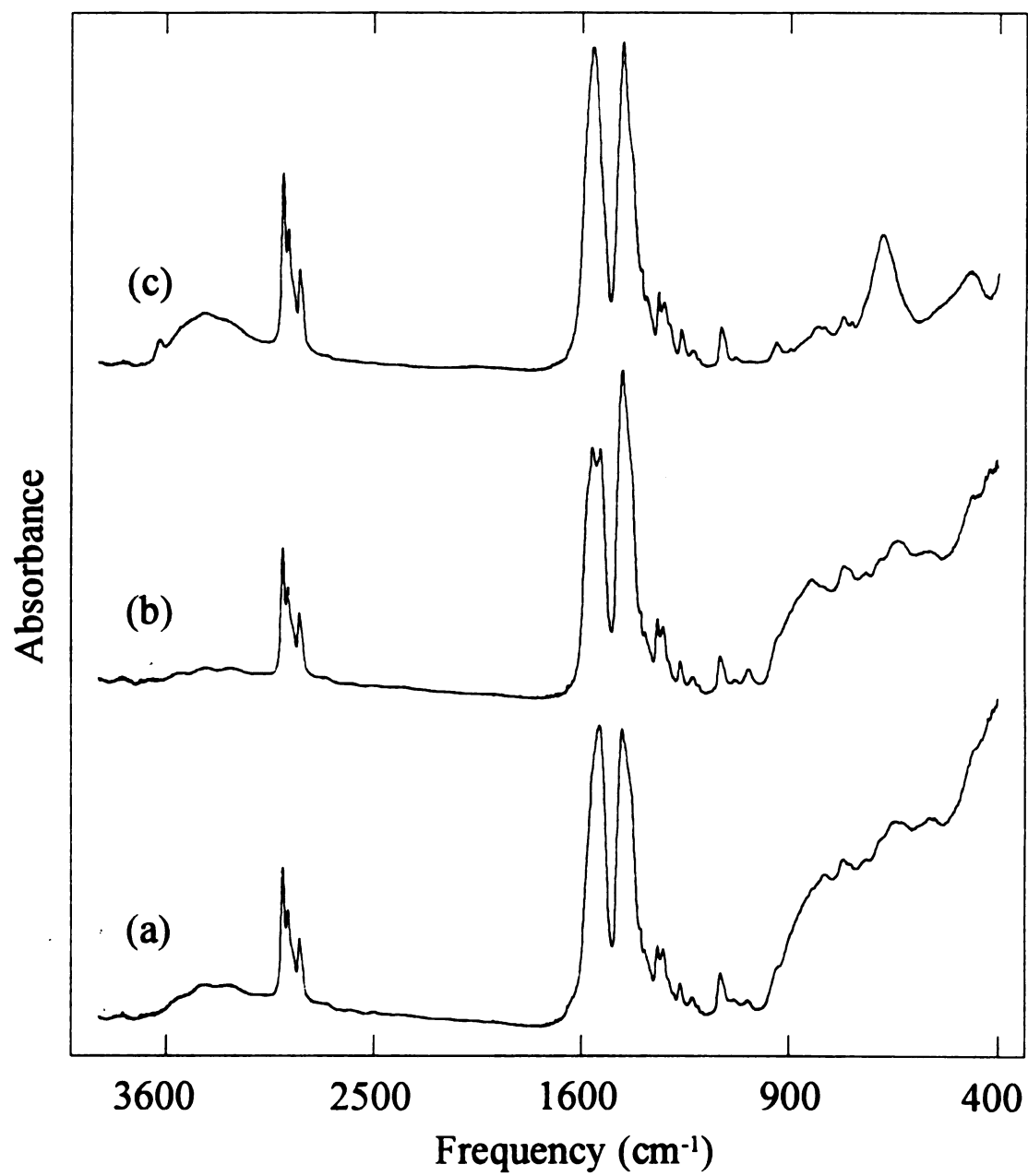


Figure 2.4 FTIR spectra of (a) TiO₂, (b) Ti₂₄, and (c) ZrO₂ films.

aging. Thus we believe that solution aging does not necessarily lead to new valerate coordination configurations but rather to a redistribution of ligands amongst configurations. Comparing these $\Delta\nu$ values with that in sodium valerate (141 cm^{-1}) suggests that titanium films contain only bidentate ligands. While the presence of chelating ligands cannot be ruled out, we believe it is possible that our films contain only bidentate bridging ligands which vary slightly in bond angle giving rise to several distinct maxima. Doeuff *et al.* [36] reported three distinct $\nu_{\text{as}}(\text{COO})$ bands present in a crystalline acetate alkoxy titanium complex known to contain only bridging acetates of varying bond angle.

In the spectrum obtained for the Zr00 film (Figure 2.4c), the $\nu_{\text{as}}(\text{COO})$ band at 1554 cm^{-1} and $\nu_{\text{s}}(\text{COO})$ band at 1447 cm^{-1} are of similar intensity. Solution aging has little effect on the carboxylate stretch region of the FTIR spectra of the zirconium films. The spectrum obtained for the Zr24 film shows $\nu_{\text{as}}(\text{COO})$ and $\nu_{\text{s}}(\text{COO})$ bands at 1559 and 1445 cm^{-1} , respectively. $\Delta\nu$ values are 107 and 114 cm^{-1} and indicate that the zirconium films contain only bidentate valerate ligands. Paul *et al.* [54] report values of 1540 and 1420 cm^{-1} for the asymmetric and symmetric COO stretches of zirconium(IV) propionate ($\Delta\nu = 120\text{ cm}^{-1}$) and ascribed these bands to the presence of bidentate ligands.

Spectra of solutions used to prepare these films (not shown) were also collected but, due to the presence of excess valeric acid and alcohol, they are of limited value in providing information about the polymer structure in solution. However, asymmetric carboxylate stretches can be readily seen in the solution spectra. Comparing this region of

the solution spectra with that in the film spectra, suggests that carboxylate coordination modes are similar before and after spin casting.

Hydroxyl Groups. Broad bands due to H-bonded hydroxyl groups are observed near 3400 cm^{-1} in the spectra of all films. The intensity of the hydroxyl stretch observed in the zirconium film spectra is essentially unchanged by solution aging and greater than that observed in the titanium film spectra. In zirconium films, the sharp band observed at 3639 cm^{-1} is typical of "free" or non-H-bonded hydroxyl groups [41]. Water has a characteristic absorbance near 1600 cm^{-1} [41]. Unfortunately, the strong carboxylate absorbances in this region make it impossible to use this band to distinguish between hydroxyl ligands and water.

In order to determine whether these absorbances are associated with water or hydroxyl ligands, changes in the hydroxyl stretch absorbances were observed while heating titanium and zirconium films in dry nitrogen. Heating titanium films at 50°C essentially removed the hydroxyl stretch band centered at 3400 cm^{-1} . This band is partially restored by exposure to ambient air after cooling. Hydroxyl groups should not be removed at such low temperatures and, therefore, we ascribe the hydroxyl bands observed in the FTIR spectra of titanium films to sorbed water.

Figure 2.5 shows the effect of heating on the hydroxyl region of the ZrO_2 film spectrum. The intensity of the hydroxyl absorbances decreased upon heating slowly to 50°C (Figure 2.5b); however, the hydroxyl bands are evident unless the film is heated to 100°C (Figure 2.5c). Additionally, when the film is heated rapidly to 75°C , the broad absorbance disappears before the loss of the sharp band (not shown). A small band at

3639 cm^{-1} is restored upon cooling (Figure 2.5d) and exposure to ambient air for 30 minutes results in the partial restoration of the broad hydroxyl absorbance (Figure 2.5e). Continued exposure to ambient air did not cause any additional increase in the intensity of this band. Again, the low temperature required for removal of the hydroxyl absorption bands indicates that water, not hydroxyl ligands are the primary source of the bands.

We tentatively ascribe the non-H-bonded hydroxyl absorbance to water coordinated to Zr centers. We attribute H-bonded hydroxyl absorbances to sorbed water. During slow heating an equilibrium is maintained between the two types of water. Rapid heating results indicate that non-H-bonded water is more difficult to remove, perhaps due to a combination of steric hindrance and coordination with Zr. It also may be energetically more stable since the sharp absorbance band returns first upon cooling. Partial restoration of the broad absorbance upon exposure to ambient air is further evidence that this band is due to sorbed water.

Water may be present due to condensation reactions occurring during spin casting or due to trapping of water present in precursor solutions. Water is probably also present due to exposure to ambient moisture during spincasting and drying. Zirconium can accommodate a larger coordination sphere than titanium. As a consequence, hydration of zirconium may occur leading to films with a higher water content than the titanium films. Factors such as porosity may also contribute to the extent of water sorption in the films.

Backbone. The low frequency region of the Ti00 and Ti24 spectra (Figures 2.4a and 2.4b, respectively) contains a broad absorbance between 980 and 530 cm^{-1} that is commonly attributed to an envelope of phonon bands in the titanium oxide network [50]. Similar features have been reported by Doeuff *et al.* [22] in the spectra of titanium acetate

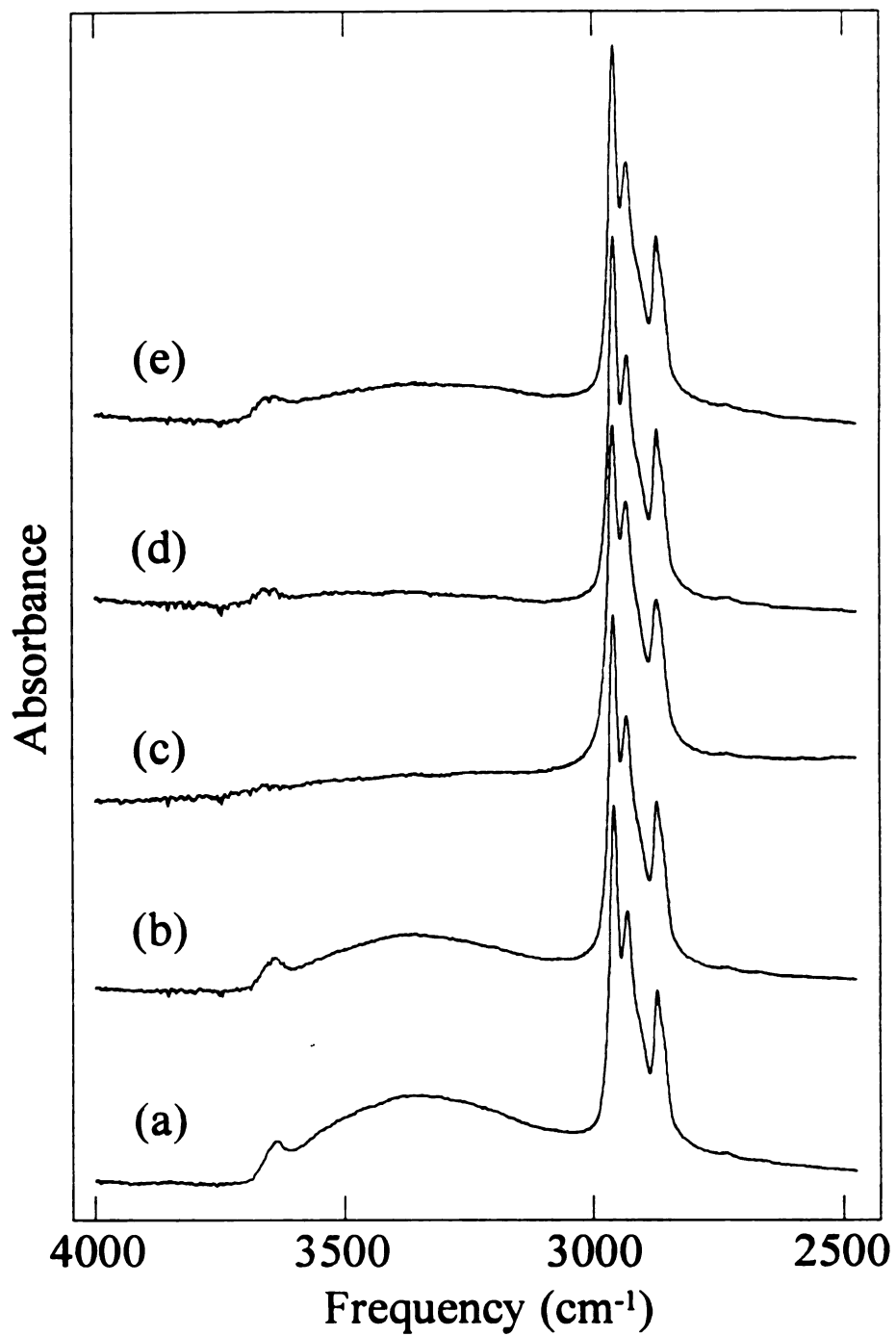


Figure 2.5 FTIR spectra of hydroxyl region: *in situ* heating of ZrO₂ film (a) before heating; (b) heated to 50°C; (c) heated to 100°C; (d) cooled to room temperature in dry nitrogen; (e) exposed to ambient air for 30 minutes.

gels and were also present in our solution spectra (Figure 2.2d). Though the shape of this broad absorbance is essentially unchanged with increased precursor solution age, its relative intensity is decreased with respect to carboxylate absorbances. The low frequency region of the FTIR spectra of the zirconium films (Figure 2.4c) show two major bands at 654 and 462 cm^{-1} which we attribute to backbone $\nu(\text{Zr-O})$. These bands are similar to those in the solution spectra after the addition of water (Figure 2.3d). Atik and Aegerter [23] ascribed bands at 666 and 363 cm^{-1} to Zr-O-Zr stretches and Sanchez and In [55] attributed a broad band between 600 and 300 cm^{-1} to these vibrations in a zirconium oxide based network.

XPS Characterization of Valerate Films. The XPS metal core peak binding energies measured for titanium ($\text{Ti } 2p_{3/2} = 458.7 \text{ eV}$) and zirconium ($\text{Zr } 3d_{5/2} = 182.3 \text{ eV}$) are independent of solution aging and typical of values measured for tetravalent forms of the elements [56]. The XPS C 1s spectra measured for the films consist of peaks at 284.6 eV (reference peak) and 288.5 eV due to alkyl and carboxylate carbon, respectively. No features due to alkoxide carbon ($\sim 286 \text{ eV}$) are observed in the spectra which is consistent with the FTIR analysis of the films. The XPS O 1s spectra measured for the films consist of peaks at 530.1 eV and 531.8 eV that are attributed to backbone and ligand (carboxylate, hydroxyl, or water) oxygen, respectively. Figure 2.6 shows the XPS O 1s spectra of Ti00, Ti24, and Zr00 films. The relative intensity of the ligand oxygen peak increases with respect to that of the backbone oxygen peak with titanium solution aging. For the zirconium films, the relative intensities of the backbone and ligand oxygen peaks are independent of the age of solution used to cast the film.

Atomic ratios derived from XPS intensity ratios are presented in Table 2.1. When combined with interpretation based upon the FTIR analysis of the films, these values provide a quantitative assessment of the chemical species present in the films. FTIR analysis indicates that the films consist primarily of a metal oxygen network with valerate ligands coordinated to metal centers. Water is also present in the films. The concentration of valerate ligands is indicated by carboxyl carbon/metal atomic ratios determined by the XPS analysis. Since each carboxylate carbon is associated with two ligand oxygens, a film containing only carboxylate ligands is expected to have a ligand oxygen/carboxyl carbon ratio close to two. Thus, ligand oxygen/carboxylate carbon values greater than two indicate the presence of water or hydroxyl groups in the films.

It is important to note that if water is present in valeric acid when it is mixed with the alkoxide, levels of carboxylation are lower. This is in agreement with the results of Doeuff *et al.* [27] who found that adding titanium alkoxide to a mixture of water and acetic acid led to the formation of a gel with a low level of carboxylation. In order to achieve the level of carboxylation indicated by our results, the use of dry reactants is imperative.

Titanium Films. The concentration of valerate ligands in the films [57] increases from the Ti00 film (1.16 ± 0.10) to the Ti24 film (1.42 ± 0.05) indicating that these ligands add to titanium during solution aging. Accompanying the increase in valerate ligand content is a corresponding decrease in the backbone oxygen concentration with solution aging. Backbone oxygen to titanium atomic ratios decrease from 1.40 ± 0.01 for Ti00 films to 1.12 ± 0.03 for Ti24 films. The change in the relative concentrations of

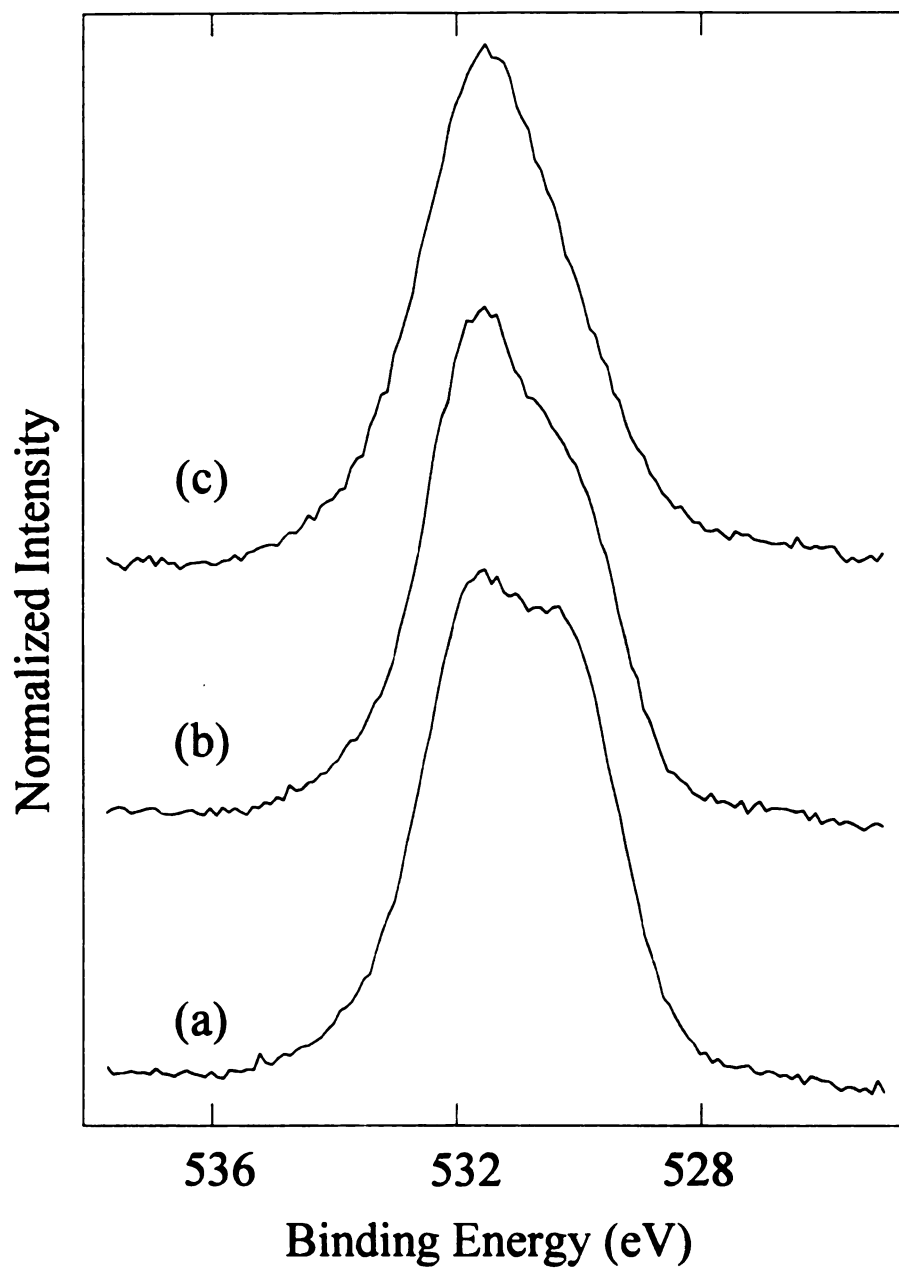


Figure 2.6 Oxygen 1s photoelectron spectra measured for (a) Ti00, (b) Ti24, and (c) Zr00 films.

Table 2.1 Atomic Ratios of Carbon and Oxygen Species Calculated from XPS Intensity Ratios.

<u>Film</u>	Atomic Ratios*			
	<u>Backbone Oxygen</u> Metal	<u>Carboxyl Carbon</u> Metal	<u>Ligand Oxygen</u> Metal	<u>Ligand Oxygen</u> Carboxyl Carbon
Ti00	1.4	1.2	2.2	1.9
Ti24	1.1	1.4	2.6	1.8
Zr00	1.0	1.8	2.5	2.1
Zr24	1.0	1.9	2.5	2.0

* Relative standard deviations for atomic ratios are $\leq \pm 10\%$.

these two species is also apparent by comparing the FTIR spectra of the Ti00 and Ti24 films (Figure 2.4).

These changes can be understood based upon solution compositions. Recall that the FTIR spectra of freshly prepared titanium solutions contain absorbances due to alkoxide ligands. This indicates that hydrolysis and condensation reactions have not gone to completion in these solutions. We believe that the removal of the solvent that occurs during spincoating and drying facilitates completion of these processes and the formation of backbone oxygen linkages. Because valerates are strong ligands, their presence limits the extent of condensation. In contrast, alkoxide groups are absent in the aged film solutions. Film solutions contain a large excess of valeric acid and during solution aging, valerate ligands may displace remaining alkoxide and/or hydroxyl ligands. The extent of carboxylation is increased while the extent of condensation has been accordingly decreased.

A slow rate of carboxylation for titanium valerate alkoxide complexes is consistent with their slow rate of hydrolysis since both are nucleophilic substitution reactions. Though isopropoxide ligands form good leaving groups, their bulkiness may hinder the approach of nucleophiles to titanium. In addition, solution studies indicated that a second valerate ligand was not readily added to titanium since it required the breaking of relatively stable dimeric units. Bridging alkoxide ligands were preferentially hydrolyzed and subsequent condensation reactions lead to completely new oligomeric structures. These species may be more easily carboxylated than the titanium valerate alkoxide dimers.

The ligand oxygen/carboxyl carbon ratio for titanium films is slightly less than two indicating that little water is present in these films. Sorbed water evident in the FTIR spectra is pumped away in the vacuum required for XPS analysis. *In situ* FTIR heating experiments indicated that water is not strongly bound to the titanium films.

Zirconium Films. The compositions of zirconium films prepared from fresh and day old solutions are nearly identical. This is consistent with FTIR results which indicate that aging has little effect on the structure of the films. The number of valerate ligands per zirconium is the same within experimental error in zirconium films prepared from fresh (1.80 ± 0.12) and aged (1.90 ± 0.15) solutions and all zirconium films have a backbone oxygen/metal atomic ratio of approximately one.

The ligand oxygen/carboxyl carbon ratio for zirconium films is slightly greater than that for titanium films. However, its value also indicates that little water is present in these films. Again, sorbed water observed with FTIR is removed by the vacuum prior to XPS analysis. A small amount may remain in the zirconium films. This is consistent with the higher concentration of water in the zirconium films as indicated by the FTIR analysis and the higher temperature required for its removal. The presence of a small concentration of hydroxyl ligands can not be ruled out.

Additional Comments. It should be noted that film compositions calculated using XPS intensity ratios have the appropriate number of ligands per metal center. Titanium and zirconium have +4 oxidation states, backbone oxygen has a -2 oxidation state, and a carboxylate group can be assigned a charge of -1. Using this accounting system, the anion charge calculated for the Ti00 film (1.4 backbone oxygens and 1.2 carboxylate species per

metal center) is -4.0. Similar calculations for the Ti24, Zr00, and Zr24 films lead to charges of -3.7, -3.9, and -3.9, respectively. Within experimental error, these results indicate the formation of neutral molecules and further demonstrate the use of XPS to determine film composition.

The levels of carboxylation determined for the films are consistent with that observed in the solution studies. According to the solution studies, between 1 and 1.5 valerate ligands displace alkoxide ligands on $\text{Ti}(\text{OPr}^i)_4$. The Ti00 and Ti24 films contain 1.2 and 1.4 valerate ligands per metal center. $\text{Zr}(\text{OPr}^n)_4$ were shown to react readily with just under two valeric acid molecules which is the level of carboxylation measured in the zirconium films.

2.5 References

- 1 . Ulrich, D.R. *J. Non-Cryst. Solids* **1988**, *100*, 174.
- 2 . *Better Ceramics Through Chemistry V*, Hampden-Smith, M.J.; Klemperer, W.G.; Brinker, C.J.; Eds.; Mater. Res. Soc. Symp. Proc. 271: Pittsburgh, PA, 1992.
- 3 . *Ultrastructure Processing of Advanced Ceramics*, Mackenzie, J.D.; Ulrich, D.R., Eds.; North Holland: New York, 1988.
- 4 . *Sol-Gel Technology for Thin Films, Fibers, Preforms, Electronics, and Specialty Shapes*, Klein, L.C., Ed.; Noyes Publications: Park Ridge, New Jersey, 1988.
- 5 . Brinker, C.J.; Scherrer, G. *Sol-Gel Science, the Physics and Chemistry of Sol-Gel Processing*, Academic Press: San Diego, 1990.
- 6 . Scriven, L.E. in *Better Ceramics Through Chemistry III*, Brinker, C.J.; Clark, D.E.; Ulrich, D.R., Eds., Mat. Res. Soc., Pittsburgh, PA, 1988, 717.
- 7 . Brinker, C.J.; Hurd, A.J.; Schunk, P.R.; Frye, G.C.; Ashley, C.S. *J. Non-Cryst. Solids* **1992**, *147&148*, 424.
- 8 . Hench, L.L.; West, J.K. *Chem. Rev.* **1990**, *90*, 33.
- 9 . Schaeffer, D.W. *Science* **1989**, *243*, 1023.
- 10 . Klemperer, W.G.; Ramamurthi, S.D. in *Better Ceramics Through Chemistry III*; Brinker, C.J.; Clark, D.E.; Ulrich, D.R.; Eds.; Materials Research Society, Pittsburgh, 1988, 1.
- 11 . Klemperer, W.G.; Mainz, V.V.; Millar, D.M. in *Better Ceramics Through Chemistry II*; Brinker, C.J.; Clark, D.E.; Ulrich, D.R.; Eds.; Materials Research Society, Pittsburgh, 1986, 3.
- 12 . Klemperer, W.G.; Mainz, V.V.; Millar, D.M, *ibid.*, 15.
- 13 . Bradley, D.C., Mehrotra, R.C.; Gaur, D.P. *Metal Alkoxides*; Academic Press: London, 1978.
- 14 . Mehrotra, R.C. *J. Non-Cryst. Solids* **1988**, *100*, 1.
- 15 . Livage, J.; Henry, M.; Sanchez, C. *Prog. Solid St. Chem.* **1988**, *18*, 259.
- 16 . Hubert-Pfalzgraf, L.G. *New J. Chem.* **1987**, *11*, 663.

- 17 . Mehrotra, R.C.; Gaur, D.P.; Bohra, R. *Metal β -diketonates and Allied Derivatives*, Academic Press, London, 1978.
- 18 . Mehrotra, R.C.; Bohra, R. *Metal Carboxylates*, Academic Press, London, 1983.
- 19 . Sanchez, C.; Livage, J.; Henry, M.; Babonneau, F. *J. Non-Cryst. Solids* **1988**, *100*, 65.
- 20 . Debsikar, J.C. *J. Non-Cryst. Solids* **1986**, *87*, 343.
- 21 . Doeuff, S.; Henry, M.; Sanchez, C.; Livage, J. *J. Non-Cryst. Solids*. **1987**, *89*, 84.
- 22 . Doeuff, S.; Henry, M.; Sanchez, C.; Livage, J. *J. Non-Cryst. Solids* **1987**, *89*, 206.
- 23 . Atik, M.; Aegerter, M.A. *J. Non-Cryst. Solids*. **1992**, *147&148*, 813.
- 24 . Chaumont, D.; Craievich, A.; Zarzycki *J. Non-Cryst. Solids* **1992**, *147&148*, 127.
- 25 . Yoldas, B.E. *J. Mater. Sci.* **1986**, *21*, 1080.
- 26 . Leautic, A.; Riman, R.E. *J. Non-Cryst. Solids*. **1991**, *135*, 259.
- 27 . Assink, R.A.; Schwartz, R.W. *Chem. Mater.* **1993**, *5*, 511.
- 28 . Laaziz, I.; Larbot, A.; Julbe, A.; Guizard, C.; Cot, L. *J. Solid St. Chem.* **1992**, *98*, 393.
- 29 . Doeuff, S.; Henry, M.; Sanchez, C. *Mat. Res. Bull.* **1990**, *25*, 1519.
- 30 . Sanchez, C.; Babonneau, F.; Doeuff, S.; Leautic, A. *Ultrastructure Processing of Advanced Ceramics*, Mackenzie, J.D.; Ulrich, D.R., Eds.; North Holland: New York, 1988; 77.
- 31 . Larbot, A.; Alary, J.A.; Guizard, C.; Cot, L.; Gillot *J. Non-Cryst. Solids* **1988**, *104*, 161.
- 32 . Gagliardi, C.D.; Berglund, K.A. in *Processing Science of Advanced Ceramics*, Aksay, I.A.; McVay, G.L.; Ulrich, D.R., Eds.; Mater. Res. Soc. Proc. 155: Pittsburgh, PA, 1986; 127.

- 33 . Gagliardi, C.D.; Dunuwila, D.; Berglund, K.A. in *Better Ceramics Through Chemistry IV*, Zelinsky, B.J.J.; Brinker, C.J.; Clark, D.E.; Ulrich, D.R., Eds.; Mater. Res. Soc. Proc. 180: Pittsburgh, PA, 1990; 801.
- 34 . Sanchez, C.; Livage, J. *New J. Chem.* **1990**, *14*, 513.
- 35 . Schroeder, H. in *Physics of Thin Films*, Hass, G., Ed., Vol. 5, Academic Press, New York, 1969, 87.
- 36 . Doeuff, S.; Dromzee, Y.; Taulelle, J.; Sanchez, C. *Inorg. Chem.* **1989**, *28*, 4439.
- 37 . Deacon, G.B.; Phillips, R.J. *Coord. Chem. Rev.* **1980**, *33*, 227.
- 38 . Grigor'ev, A.I. *Russ. J. Inorg. Chem.* **1963**, *8(4)*, 409.
- 39 . Wagner, C.D.; Davis, L.E.; Zeller, M.V.; Taylor, J.A.; Gale, L.H. *Surf. Interface Anal.* **1981**, *3*, 211.
- 40 . Software provided by Dr. Andrew Proctor, University of Pittsburgh, Pittsburgh, PA.
- 41 . Colthup, N.B.; Daly, L.H.; Wiberley, S.E. *Introduction to Infrared and Raman Spectroscopy*, 3rd Ed. Academic Press: San Diego, 1990.
- 42 . Silverstein, R.M.; Bassler, C.G.; Morrill, T.C. *Spectrometric Identification of Organic Compounds*, 3rd Ed. John Wiley & Sons, Inc.: New York, 1974.
- 43 . Barraclough, C.G.; Bradley, D.C.; Lewis, J.; Thomas, I.M. *J. Chem. Soc.* **1961**, 2601.
- 44 . Zeitler, V.A.; Brown, C.A. *J. Phys. Chem.* **1957**, *61*, 1174.
- 45 . Babonneau, F.; Doeuff, S.; Leautic, A.; Sanchez, C.; Cartier, C.; Verdaguer, M. *Inorg. Chem.* **1988**, *27*, 3166.
- 46 . Bradley, D.C.; Carter, D.G. *Can. J. Chem.* **1961**, *39*, 1434.
- 47 . Livage, J.; Sanchez, C. *J. Non-Cryst. Solids* **1992**, *145*, 11.
- 48 . Spinner, E. *J. Chem. Soc.* **1964**, 4217.

49. Sanchez, C.; Toledano, P.; Ribot, F. in *Better Ceramics Through Chemistry IV*, Zelinsky, B.J.J.; Brinker, C.J.; Clark, D.E.; Ulrich, D.R., Eds.; Mater. Res. Soc. Proc. 180: Pittsburgh, PA, 1990; 47.
50. McDevitt, N.T.; Baun, W.L. *Spectrochimica Acta* **1964**, *20*, 799.
51. Greenwood, N.N.; Earnshaw, A. *Chemistry of the Elements*; Pergamon Press: New York, 1984.
52. Morrison, R.T.; Boyd, R.N. *Organic Chemistry*, 3rd Ed; Allyn and Bacon, Inc.: Boston, 1974.
53. In all film spectra, the $\nu_s(\text{COO})$ band is as broad as the $\nu_m(\text{COO})$ band, however, only one well-resolved maximum is observed. All $\Delta\nu$ values are reported with respect to this maximum which is on the high energy side of the peak. Therefore, separations of the outer peaks may actually be greater than the values reported.
54. Paul, R.C.; Baidya, O.B.; Kumar, R.C.; Kapoor, R. *Aust. J. Chem.* **1976**, *29*, 1605.
55. Sanchez, C.; In, M. *J. Non-Cryst. Solids* **1992**, *147&148*, 1.
56. *Handbook of X-ray Photoelectron Spectroscopy*; Wagner, C.D.; Riggs, W.M.; Davis, L.E.; Moulder, J.F.; Muilenburg, G.E., Eds.; Perkin Elmer, 1979.
57. In this discussion, values are reported to two decimal places and the standard deviation of the values measured for three different films is given to indicate the actual precision of the measurements.

Chapter 3

Synthesis and Characterization of Tin Valerate and Tin Oxide Thin Films

3.1 Abstract

Tin valerate films have been prepared by spincoating solutions produced from the hydrolysis of tin(II) methoxide or tin(IV) isopropoxide in alcohol and valeric acid. Tin oxide films were made from tin valerate films using two methods: calcination at 400°C in air and by room temperature hydrogen peroxide treatment. All tin valerate and tin oxide films are transparent and exhibit uniform adhesion to quartz substrates. FTIR and XPS analyses indicate that the structure and composition of valerate films prepared from either alkoxide are similar despite differences in precursor oxidation state and concentrations of acid and alcohol used for the syntheses. Tin valerate films are comprised of an oxygen-tin polymer backbone coordinated with valerate ligands. Both monodentate and bidentate carboxylates are present, the former apparently stabilized by hydrogen bonding with sorbed water. Quantitative XPS analysis indicates that valerate/tin and hydroxyl/tin ratios are 0.26 and 0.55, respectively. This level of film carboxylation is consistent with the extent of carboxylate formation in tin(IV) isopropoxide/valeric acid solutions. Hydrogen peroxide treatment of tin valerate films removes organic ligands and increases the level of backbone oxygen. Hydrogen peroxide treatment or calcination results in the formation of amorphous tin (IV) oxide films.

3.2 Introduction

Tin oxide is a commonly used material in conductimetric sensor [1] and heterogeneous catalyst applications [2]. Properties such as transparency and semiconductivity also make tin oxide a fundamental component of solar cells [3], transparent electrodes [4], thin film resistors [5], and far IR detectors [6]. Thin films of tin oxide are conventionally prepared by reactive sputtering [7], spray pyrolysis [8], or CVD [9]. While these methods produce high quality oxide films, they do have limitations that can be addressed by the development of sol-gel techniques. First, sol-gel derived materials can be prepared with high surface areas and controlled porosity, properties which are important in catalyst and sensor applications [10,11]. Second, electronic and optical properties can be tailored by mixing tin oxide with other metal oxides or by doping with noble metals. Sol-gel synthesis of these materials would be advantageous since molecularly mixed oxides can be produced from metal alkoxide precursors [12].

Sol-gel synthesis of materials from silicon and transition metal alkoxides has been extensively investigated [10,13]. Under the proper conditions, addition of water to alkoxides causes hydrolysis and condensation reactions. Transition metal alkoxides are highly reactive and tend to form oxyhydroxide precipitates when exposed to moisture. Limiting alkoxide reactivity inhibits precipitate formation and allows the preparation of polymeric gels and thin films [13]. Control is achieved through complexation of the metal alkoxides with strong ligands such as carboxylates and β -diketonates. Valeric acid (pentanoic acid) modified transition metal alkoxides produce especially stable, uniform,

and transparent films which exhibit good adhesion to glass and quartz substrates [14, 15]. Previously we have shown that titanium and zirconium valerate films are comprised of a metal-oxygen network coordinated with valerate ligands [15].

Despite the importance of tin oxide thin films in a number of technologies, the study of tin alkoxide sol-gel routes to these materials has been relatively limited [16, 17]. Like transition metal alkoxides, tin alkoxides are known to react rapidly with water [16]. It is reasonable to suppose that methods demonstrated to produce high quality films from transition metal alkoxides could be successfully applied to the synthesis of films from tin alkoxides. In this work uniform, transparent tin valerate films have been prepared from tin(IV) isopropoxide ($\text{Sn}(\text{OPr}^i)_4$) or tin(II) methoxide ($\text{Sn}(\text{OMe})_2$) and valeric acid using methods found to produce high quality films from titanium and zirconium alkoxides [14, 15]. Two different methods: room temperature hydrogen peroxide treatment and calcination in air at 400°C were used to produce oxide films from tin valerate films.

All films in this study were characterized using a combination of bulk and surface spectroscopies in a manner similar to that used to study titanium and zirconium valerate films [15]. Structural information was obtained by Fourier transform infrared spectroscopy (FTIR). X-ray photoelectron spectroscopy (XPS) was used to provide information about the chemical species present in film surfaces and their relative concentrations. The oxidation state of tin in the films was examined using valence band XPS.

3.3 Experimental

Materials. Tin(II) methoxide (Johnson Matthey) and tin(IV) isopropoxide 10% w/v in isopropanol (Chemat Technologies), absolute methanol (Photrex reagent, J.T. Baker), hydrogen peroxide, 30% (Baker analyzed reagent, J.T. Baker), and valeric acid (99+%, Aldrich Chemical Company) were used without further purification. Distilled, deionized water was used for all syntheses. Tin(IV) oxide (99.995+%, Aldrich Chemical Company) was pressed into pellets and calcined in dry air (80 cm³/min, medical grade, AGA Gas Co.) at 425°C for 4 h before XPS analysis.

Film Preparation. The methods used to synthesize films were based on techniques developed for the preparation of transition metal carboxylate thin films [14]. Modifications were necessary to obtain clear, particle free solutions and transparent, uniform films using the tin alkoxide precursors. Molar ratios of 15 methanol : 9 valeric acid : 1.5 water : 1 metal alkoxide were used to prepare films from Sn(OMe)₂. Films synthesized from Sn(OPrⁱ)₄ were prepared using mixtures of 40 isopropanol : 20 valeric acid : 1.5 water : 1 metal alkoxide. Reactions were carried out at room temperature in capped vials. Sn(OMe)₂ was dispersed in methanol using sonication. Valeric acid was added to the alkoxide-alcohol mixtures followed by water. A vortex mixer was used to vigorously stir solutions following the addition of each reactant.

Addition of valeric acid to Sn(OMe)₂-methanol suspensions caused brief but vigorous foaming and produced a faintly yellow, opalescent, particle free solution. No further changes were observed upon addition of water to these mixtures. No reaction was visually apparent when mixing Sn(OPrⁱ)₄ and isopropanol with valeric acid; however,

addition of water resulted in the formation of a white precipitate which dissolved immediately upon mixing. Though initially these solutions had an opalescent appearance (perhaps due to unreacted water dispersed in the solutions), within five minutes the solutions were transparent and colorless.

Freshly prepared solutions were dispersed on the desired substrate (quartz or KBr crystal) and spun for five minutes. All films prepared in this study were transparent, colorless, and exhibited complete and uniform adhesion to quartz substrates. Films were air-dried overnight and stored in a desiccator. Films studied without further treatment are referred to as tin valerate films (SnV). Calcined films (SnC) were prepared by heating SnV films in a tube furnace in dry air (80 cm³/min, medical grade, AGA Gas Co.) at 400°C for 4 h. Peroxide treated films (SnP) were obtained by immersing SnV films coated on quartz or Si crystals in a 30% hydrogen peroxide solution for 4h followed by drying at 110°C in air for 30 min. The FTIR spectrum of Si crystals was found to be unchanged by hydrogen peroxide treatment.

To clarify the analysis of the hydrogen peroxide treated films, tin valerate gels and peroxide treated gels were prepared. Tin valerate gels were synthesized from a 1:1:1.5 mixture of Sn(OPrⁱ)₄ (as received in isopropanol), valeric acid, and water. Gels were allowed to dry at room temperature and were spread on KBr crystals for analysis. Peroxide treated gels were obtained using the same procedures described for the preparation of SnP films.

Fourier Transform Infrared Spectroscopy (FTIR). FTIR spectra were obtained using a Mattson Instruments Galaxy 3020 Fourier transform infrared

spectrometer. Data acquisition and processing were performed using an Enhanced First software package. The mid-IR region ($4000\text{--}400\text{ cm}^{-1}$) was examined with a resolution of 2 cm^{-1} . Spectral features were the same for films cast on both KBr and Si. For titration experiments, solutions were prepared in capped vials and stirred with a vortex mixer. FTIR spectra of all liquids were obtained from samples prepared by placing a drop between KBr windows. *In situ* heating experiments were performed under nitrogen purge (99.95%, AGA Gas Co.) using a stainless-steel sample holder equipped with cartridge heaters (Omega). The temperature was fixed using an Omega CN 1200 controller.

X-ray Photoelectron Spectroscopy (XPS). Films cast on quartz slides were analyzed with a VG Microtech spectrometer using a Clam2 hemispherical analyzer. All XPS spectra were collected using a Mg anode (1253.6 eV) operated at a power of 300 W (15 kV and 20 mA emission current) with an analyzer pass energy of 50 eV . Four regions were scanned for each film: C $1s$, O $1s$, Sn $3d$, and the valence band. Binding energies were referenced to adventitious carbon (C $1s = 284.6\text{ eV}$) and were measured with a precision of $\pm 0.1\text{ eV}$. Quantitative XPS calculations were performed using sensitivity factors determined by the analysis of titanium valerate films [15] and tin(IV) oxide. XPS peaks were fitted with 20% Lorentzian-Gaussian mix Voigt functions using a non-linear least squares curve fitting program [18]. This program was also used to remove X-ray satellites from valence band spectra. It must be noted that the use of XPS to evaluate film composition assumes that the films are homogeneous.

X-ray Diffraction (XRD). XRD diffraction patterns of tin oxide films on quartz slides were obtained with a Rigaku XRD diffractometer employing Cu $K\alpha$ radiation ($\lambda =$

1.541838 Å). The X-ray was operated at 45 kV and 100 mA. Diffraction patterns were collected with a scan rate of 0.20 degree (2θ)/min and DD and DS slit widths of 1° .

3.4 Results and Discussion

Solution Chemistry. We have previously reported an FTIR investigation of solution chemistry leading to the production of titanium and zirconium valerate polymers [15]. In addition to examining ligand formation and hydrolysis reactions, we found that FTIR analysis of solutions containing different valeric acid : metal alkoxide ratios provided an estimate of the extent of carboxylation of the metal valerate polymers. A similar study of tin film solutions is presented here.

FTIR spectra of solutions that contain varying concentrations of $\text{Sn}(\text{OPr}^i)_4$, valeric acid, and water are shown in Figure 3.1. For valeric acid (Figure 3.1a), the strong absorbance at 1711 cm^{-1} is attributed to a dimeric asymmetric carbonyl stretch [19,20]. $\text{Sn}(\text{OPr}^i)_4$ is dissolved in a large excess of isopropanol ($\sim 1:40$) and, for this reason, its FTIR spectrum (Figure 3.1b) largely resembles that of the alcohol solvent. Valerate ligands formed when valeric acid and $\text{Sn}(\text{OPr}^i)_4$ are mixed (Figures 3.1c - 3.1e) have asymmetric carboxyl stretch ($\nu_{\text{as}}(\text{COO})$) vibrations which occur between about 1700 and 1500 cm^{-1} . Corresponding symmetric stretch ($\nu_{\text{s}}(\text{COO})$) bands (1500 to 1250 cm^{-1}) are not shown because they are obscured by strong isopropanol absorbances [21]. Carboxylate coordination mode can be inferred from the frequency of the $\nu_{\text{as}}(\text{COO})$ absorbance band. Grigor'ev reported that the $\nu_{\text{as}}(\text{COO})$ frequency decreased with decreasing OCO bond angle [22]. Since bond angle tends to decrease with coordination mode as follows: monodentate > bidentate bridging > bidentate chelating, $\nu_{\text{as}}(\text{COO})$ bands

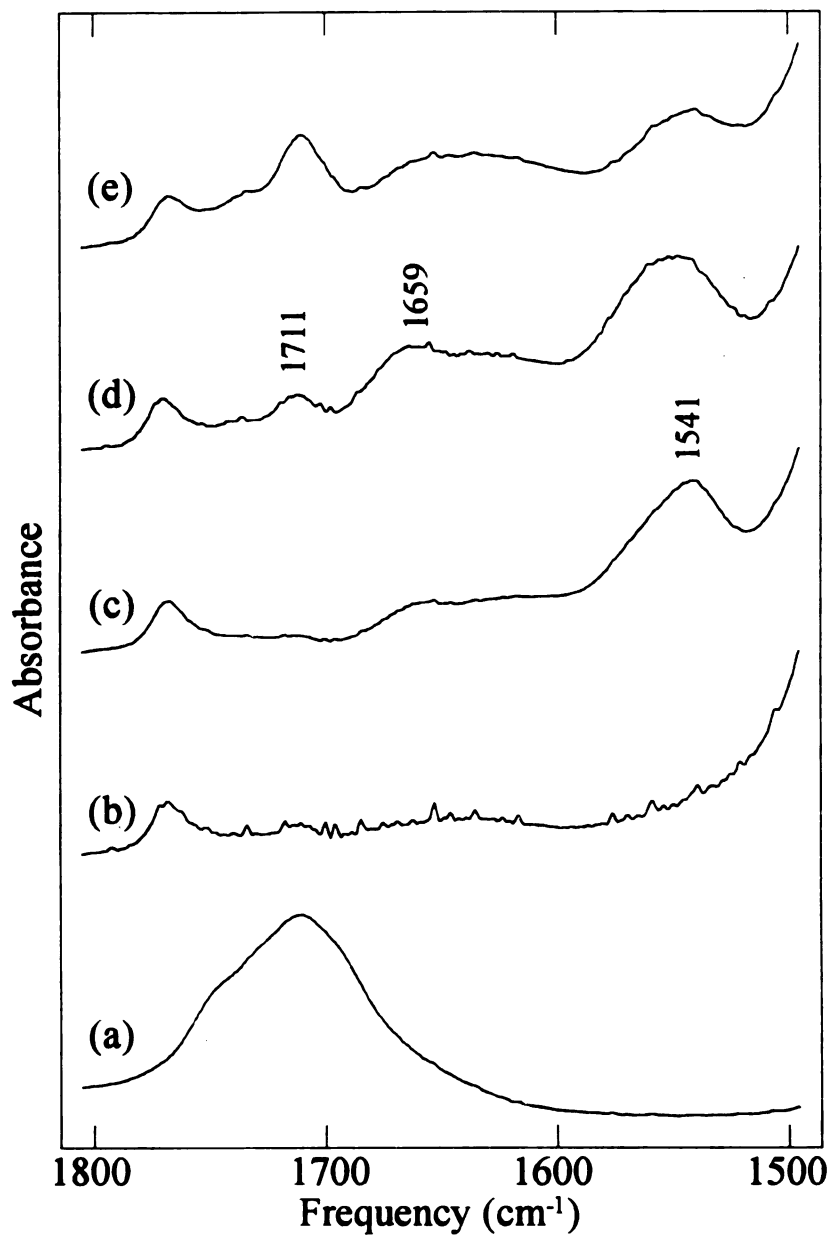


Figure 3.1 FTIR spectra of (a) valeric acid and (b) $\text{Sn}(\text{OPr}^i)_4$ in isopropanol and spectra of solutions containing different concentrations of valeric acid and water. $\text{Sn}(\text{OPr}^i)_4$: valeric acid : water ratios are: (c) 1 : 0.5 : 0, (d) 1 : 1 : 0, and (e) 1 : 1 : 2. Spectra are normalized to the isopropanol band 1769 cm^{-1} .

of consider

presence of

band is 156

In t

ratio (Figur

unreacted

bidentate v

and 1600 c

FTIR spect

3 1d) conta

cm⁻¹) valen

Apparently

Additionall

doubling th

concentrati

increased

accommoda

isopropanol

metal cente

Sn(OPrⁱ)₄

each dimer

of considerably higher frequency than observed for the ionic form of the ligand suggest the presence of monodentate ligands. For sodium valerate, the frequency of the $\nu_{\text{as}}(\text{COO})$ band is 1562 cm^{-1} [15].

In the spectrum of a solution prepared with a 0.5 valeric acid : $\text{Sn}(\text{OPr}^i)_4$ mole ratio (Figure 3.1c), the absence of a band at 1711 cm^{-1} indicates that there is little unreacted valeric acid in the solution. The absorbance at 1541 cm^{-1} suggests that bidentate valerate ligands have been formed. The broad, low intensity band between 1700 and 1600 cm^{-1} may be due to a small concentration of monodentate valerate ligands. The FTIR spectrum observed for an equimolar mixture of $\text{Sn}(\text{OPr}^i)_4$ and valeric acid (Figure 3.1d) contains bands characteristic of both bidentate (1541 cm^{-1}) and monodentate (1659 cm^{-1}) valerate ligands as well as a small band due to unreacted valeric acid (1711 cm^{-1}). Apparently less than one valerate ligand per tin atom can be formed in this solution. Additionally, a comparison of valerate band intensities in Figures 3.1c and 1d shows that doubling the initial valeric acid concentration has little effect on the bidentate ligand concentration; however, the concentration of monodentate ligands has been slightly increased. This suggests that there is a limit to the number of bidentate ligands that can be accommodated by the metal centers. Hampden-Smith *et al.* [23] reported that in isopropanol, $\text{Sn}(\text{OPr}^i)_4$ is present as solvated dimers of the form $[\text{Sn}(\text{OPr}^i)_4(\text{HOPr}^i)]_2$ with metal centers bridged by two isopropoxide ligands. Considering the dimeric nature of $\text{Sn}(\text{OPr}^i)_4$, our results suggest that one bidentate valerate ligand readily coordinates with each dimer. Since both tin atoms are expected to be equivalent, we believe that the

biden

ligand

Sn(O

Sn(O

hydro

was a

with

sugge

maxim

This

ligand

soluti

by a

isopr

valer

conce

from

is sho

in fil

from

unlike

bidentate valerate ligand may bridge the two metal centers. Further addition of valerate ligands favors monodentate coordination.

Figure 3.1e shows the FTIR spectrum obtained for an equimolar mixture of $\text{Sn}(\text{OPr}^i)_4$ and valeric acid after addition of sufficient water to completely hydrolyze $\text{Sn}(\text{OPr}^i)_4$. The increase in relative intensity of the band at 1711 cm^{-1} indicates that water hydrolyzes some of the valerate ligands. Hydrolysis of a fraction of the valerate ligands was also observed in similarly prepared titanium and zirconium solutions [15]. Reaction with water leads to a lowering of the intensity of the bidentate $\nu_{\text{as}}(\text{COO})$ band. This suggests that bidentate valerate ligands are preferentially hydrolyzed. In addition, the maximum intensity of the monodentate $\nu_{\text{as}}(\text{COO})$ band has shifted to a lower frequency. This may indicate that water is H-bonded to the dangling oxygen of monodentate valerate ligands [21] (*vide infra*). Addition of water to the 0.5 valeric acid : $\text{Sn}(\text{OPr}^i)_4$ mole ratio solution also results in the hydrolysis of valerate ligands (spectrum not shown) as indicated by a small band at 1711 cm^{-1} . The intensities of the $\nu_{\text{as}}(\text{COO})$ bands relative to isopropanol absorbances are the same as seen in Figure 3.1e. Apparently less than 0.5 valerate ligands remain bound to tin after the addition of water. This suggests that the concentration of valerate ligands in the films will be less than 0.5 per tin atom.

Structure of Tin Valerate Films. The FTIR spectra of tin valerate films prepared from $\text{Sn}(\text{OMe})_2$ or $\text{Sn}(\text{OPr}^i)_4$ are essentially identical. A representative SnV film spectrum is shown in Figure 3.2a. The relative intensities of some of the absorbance bands can vary in films prepared at different times (*vide infra*). Since the FTIR spectra of films made from a methoxide in methanol and an isopropoxide in isopropanol are identical, it is unlikely that alkoxides, esters or alcohols are more than trace components of the films.

Absorbance

Figure

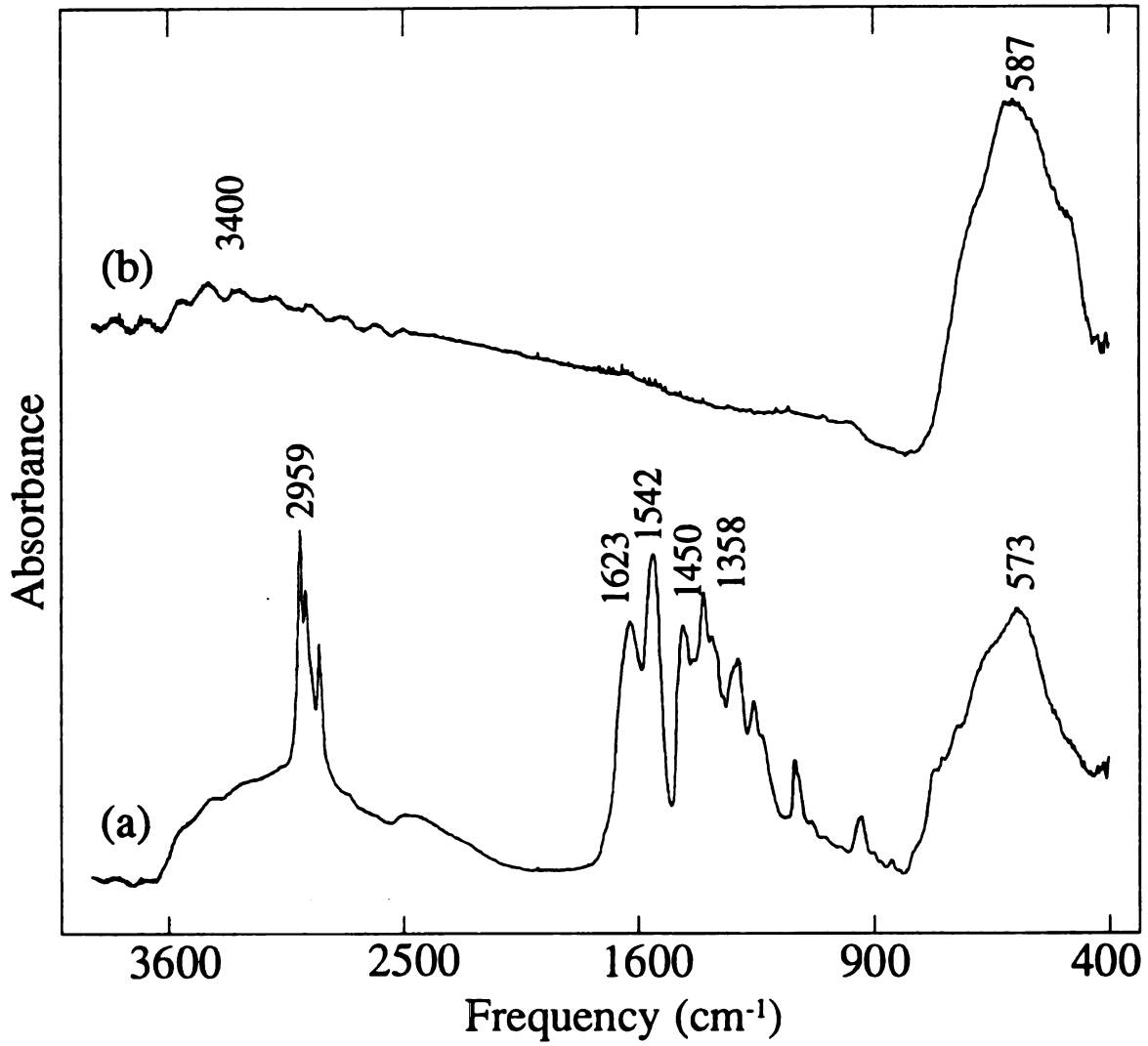


Figure 3.2 FTIR spectra of (a) SnV and (b) SnC films.

Indeed, there are no absorbances in any film spectrum that can be attributed to the presence of these species. All bands in the SnV spectrum can be attributed to vibrational modes of either valerate ligands, sorbed water and/or hydroxyl ligands, or tin-oxygen bonds.

Valerate Ligands. As in titanium and zirconium valerate film spectra [15], three bands at 2959, 2933, and 2873 cm^{-1} are present in the SnV spectrum which are similar in frequency, shape, and relative intensity to the C-H stretching absorbances observed for valeric acid. Alkyl group vibrations at 1109 and 752 cm^{-1} are also present in all valerate film spectra and in the valeric acid spectrum. The absence of the characteristic valeric acid absorbance at 1711 cm^{-1} indicates that these bands are due to valerate ligands in the films, not to valeric acid. Additionally, bands which can be attributed to coordinated valerate ligands can be readily identified in SnV film spectra. Bands at 1623 and 1542 cm^{-1} are due to $\nu_{\text{as}}(\text{COO})$ vibrations and those at 1450 and 1358 cm^{-1} to $\nu_{\text{s}}(\text{COO})$ vibrations of the valerate ligands [21, 24]. The frequencies of the asymmetric stretch vibrations are very similar to those observed for these polymers in solution (Figure 3.1e).

The coordination mode of carboxylate ligands to a metal center is commonly inferred by comparing the difference between the asymmetric and symmetric COO stretch vibrations ($\Delta\nu$) with that of the ionic form of the ligand [21,24]. A separation greater than that in the spectrum of the ionic species indicates monodentate ligands, whereas smaller separations are indicative of bidentate coordination [24]. The value of $\Delta\nu$ for sodium valerate is 142 cm^{-1} [15]. The bands at 1623 cm^{-1} and 1358 cm^{-1} are proposed to be a pair of asymmetric and symmetric COO stretches, as are those at 1542 cm^{-1} and 1450 cm^{-1} .

The sep

inner pe

these ar

carboxy

modes

Alcock

includin

1575, 1

approac

1635, 1

groups.

stretchi

(Figure

absorba

disting

[19].

the spe

species

them f

The separation of the outermost peaks is 265 cm^{-1} indicating monodentate ligands. The inner peaks are 92 cm^{-1} apart, a separation characteristic of bidentate ligands. Whether these are bridging or chelating bidentate ligands cannot be determined from $\Delta\nu$.

The presence of both monodentate and bidentate carboxylate ligands in tin carboxylate compounds is not unusual. Garner *et al.* [25] reported both coordination modes present in $\text{Sn}(\text{O}_2\text{CEt})_4$ with absorbances at 1690, 1565, 1445, and 1301 cm^{-1} . Alcock *et al.* [26] studied the structure and infrared spectra of metal carboxylates including two tin compounds: $\text{Sn}(\text{O}_2\text{CMe})_4$ which has COO stretching vibrations at 1635, 1575, 1513, and 1400 cm^{-1} and is bidentate chelating with one asymmetric ligand approaching a monodentate structure, and $(\text{Me}_4\text{N})\text{Sn}(\text{O}_2\text{CMe})_5$ with absorption bands at 1635, 1570, 1430, and 1365 cm^{-1} due to two bidentate and three monodentate acetate groups.

Sorbed Water and/or Hydroxyl Ligands. A broad absorbance due to O-H stretching vibrations is observed near 3000 cm^{-1} in the spectra of all tin valerate films (Figure 3.2a). Since there is little, if any, valeric acid or alcohol present in these films, this absorbance is attributed to hydroxyl ligands and/or sorbed water. In general, water can be distinguished from hydroxyl ligands by the $\delta(\text{H-O-H})$ band at approximately 1620 cm^{-1} [19]. Unfortunately, strong absorbances due to valerate ligands dominate this region of the spectrum making it impossible to use this feature to differentiate between the two species in these films.

Water and hydroxyl ligands can be distinguished by the energy required to remove them from the film [15]. Most sorbed water will be removed by heating at 100°C ,

wherea

a tin va

and the

relative

$v_{\text{max}}(\text{COO})$

band as

film is h

the film

carboxy

minutes

substan

H-bond

band i

destabi

oxygen

monod

water

feature

simulta

carbox

whereas, hydroxyl ligands will not. Figure 3.3 shows the changes in the FTIR spectrum of a tin valerate film heated from 25°C (Figure 3.3a) to 100°C (Figure 3.3d) in dry nitrogen and then cooled to room temperature (Figures 3.3e and 3.3f). Heating decreases the relative intensities of both the broad hydroxyl absorbance centered at 3000 cm^{-1} and the $\nu_{\text{as}}(\text{COO})$ band at 1623 cm^{-1} . An absorbance between 1400 and 1300 cm^{-1} (the $\nu_{\text{s}}(\text{COO})$ band associated with the $\nu_{\text{as}}(\text{COO})$ band at 1623 cm^{-1}) also decreases in intensity as the film is heated. These absorption bands are largely removed by heating at 100°C. Cooling the film to room temperature in dry nitrogen results in a small increase in the hydroxyl and carboxylate features (Figure 3.3e). Subsequent exposure of the film to ambient air for 15 minutes restores these bands (Figure 3.3f).

The hydroxyl absorbance band can be largely attributed to sorbed water since it is substantially decreased by heating the films to 100°C. Its frequency is typical of strongly H-bonded O-H groups [20]. The simultaneous decrease in hydroxyl band and $\nu_{\text{as}}(\text{COO})$ band intensities suggests that the monodentate form of the carboxylate ligand is destabilized by the removal of water. Sorbed water may be H-bonded to the dangling oxygen of the monodentate carboxylic acid. As water is removed from the film, the monodentate form is destabilized and a bidentate coordination is assumed. (Although water has a vibrational mode at about 1620 cm^{-1} and part of the loss of the carboxylate feature at 1623 cm^{-1} may be due to loss of water, this would not account for the simultaneous loss of the band between 1400 and 1300 cm^{-1} . Complete removal of carboxylate groups could also account for these spectral changes. This is unlikely,

Absorbance

Figure

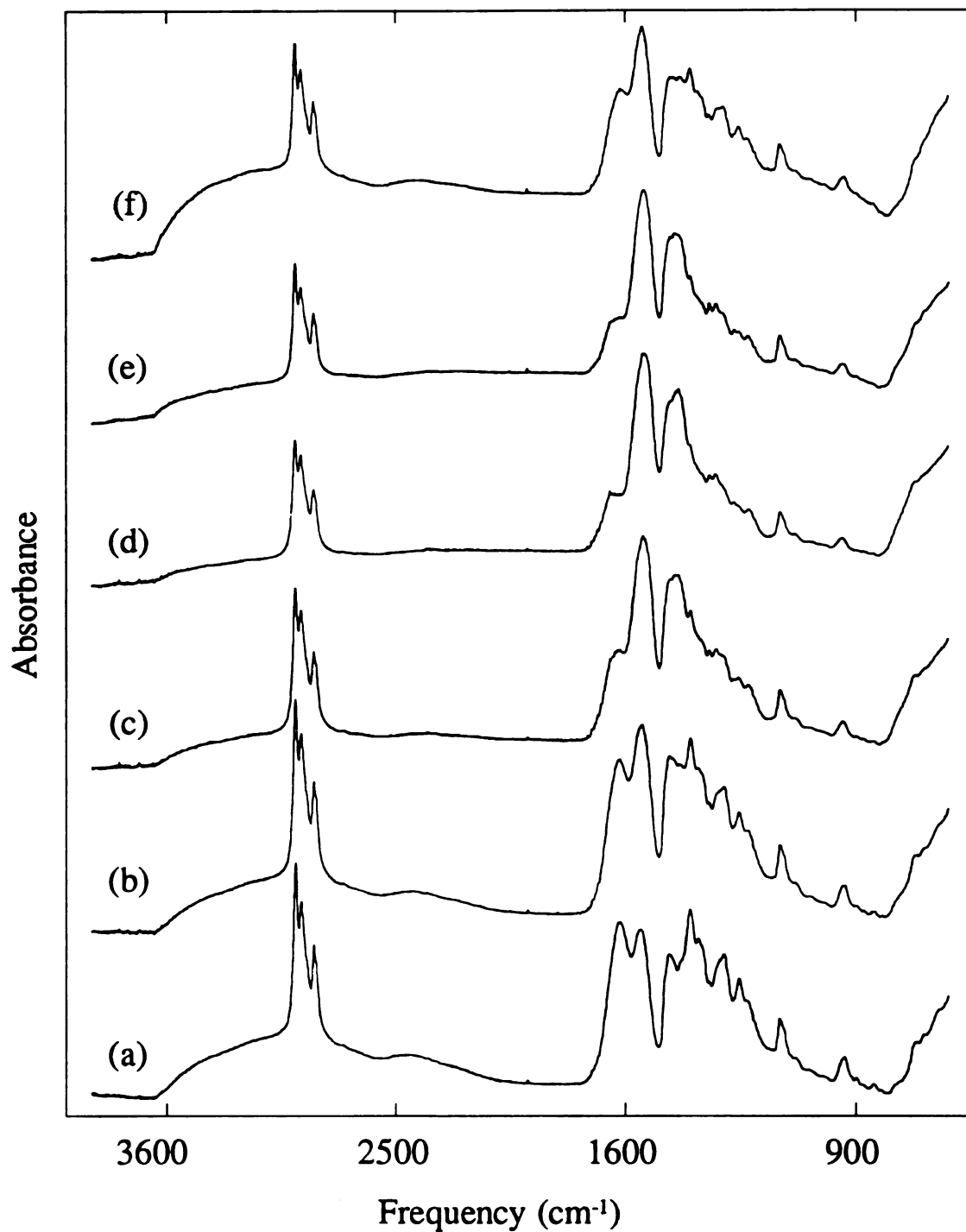


Figure 3.3 FTIR spectra of sequential treatments of an SnV film: (a) initial spectrum collected at 25°C; heated in nitrogen to: (b) 50°C, (c) 75°C, and (d) 100°C; (e) cooled to 25°C in nitrogen, and (f) exposed to ambient air at 25°C.

howev

expos

observ

prepar

relativ

results

functi

the tim

3.2a).

Orel e

v(Sn-

simila

low e

of vib

as we

consi

modif

coord

simila

however, since monodentate carboxylate features are restored after the heated film is exposed to ambient air.)

Variation in the relative intensity of the carboxylate stretching frequencies was observed for films prepared at different times. The SnV film shown in Figure 3.3a was prepared under higher humidity conditions than the one shown in Figure 3.2a and it has a relatively higher monodentate carboxylate concentration. This is consistent with the results of the thermal study. The concentration of water in these films may, in part, be a function of ambient conditions when the solution is prepared and the film is cast.

Metal-Oxygen Bonds. The low energy region of the FTIR spectrum observed for the tin valerate film shows a broad absorbance band between 800 and 400 cm^{-1} (Figure 3.2a). A broad band in this frequency range was also reported for tin gels prepared by Orel *et al.* [27] and by Giuntini *et al.* [28]. Orel *et al.* [27] ascribed bands 551 cm^{-1} to $\nu(\text{Sn-O})$ modes and those at 667 cm^{-1} to $\nu(\text{Sn-O-Sn})$ vibrations. Giuntini *et al.* [28] made similar assignments to bands at 540 cm^{-1} and 680 cm^{-1} , respectively. The maximum of the low energy absorbance band in the SnV spectrum occurs at 573 cm^{-1} . The broad envelope of vibrational bands includes Sn-O vibrations associated with hydroxyl and valerate ligands as well as Sn-O-Sn vibrations associated with a metal oxygen backbone.

In summary, the structure of the SnV films as determined by FTIR analyses is consistent with that expected from the hydrolysis and condensation of valeric acid modified tin alkoxides. SnV films are comprised of a metal - oxygen backbone coordinated with both monodentate and bidentate valerate ligands. This structure is similar to that of titanium and zirconium valerate films [15], however, no evidence of

monodentate valerate ligands was found in the titanium or zirconium films. Sorbed water is present in the SnV films and some tin centers may be coordinated with hydroxyl ligands.

XPS Analysis. XPS was primarily used to identify and quantitate the species in the surface of the films. In the C 1s spectra of SnV films, peaks observed at 284.6 eV (reference peak) and 288.5 eV are attributed to alkyl/adventitious carbon and carboxyl carbon (valerate group), respectively. Oxygen in films can be categorized into two types: backbone oxygen (530.6 eV) and ligand oxygen (531.9 eV) [15]. FTIR analysis of SnV films suggests that ligand oxygen in these films includes both valerate and hydroxyl oxygen. Since XPS measurements were carried out under UHV conditions, most sorbed water was removed from the films prior to the analysis and, as a consequence, does not contribute significantly to the O 1s spectra. The XPS Sn 3d_{5/2} binding energy measured for these films (486.7 eV) is 0.3 - 0.4 eV higher than typically reported for tin oxide materials [29]. The separation of 43.9 eV between the backbone oxygen 1s and Sn 3d_{5/2} peaks is characteristic of tin oxides [30].

Table 3.1 shows concentrations of valerate ligands, hydroxyl ligands, and backbone oxygen relative to the tin concentration in the SnV films as calculated from XPS intensity ratios. The valerate concentration was determined directly from the carboxyl C 1s / Sn 3d_{5/2} intensity ratio. The difference between the total ligand oxygen and valerate oxygen (two per valerate group) established the concentration of hydroxyl ligands in the films. As with the FTIR analysis, XPS analysis of SnV films made from either alkoxide precursor gave identical results, within experimental error.

The level of carboxylation in the SnV films (0.26 valerate ligand per tin) is quite low compared to values reported for titanium (1.2) and zirconium (1.8) valerate films

Table

Film
SnV
SnP
SnC

*Rela
10%,

Table 3.1 **Composition of Films: Ratios^a of Ligands and Backbone Oxygen to Tin and Estimated Average Tin Oxidation State as Determined by Quantitative XPS Analysis**

Film	<u>Valerate</u> Sn	<u>Hydroxyl</u> Sn	<u>Backbone O</u> Sn	Tin Oxidation State
SnV	0.26	0.55	1.6	4.0
SnP	-	0.52	1.8	4.1
SnC	-	0.33	1.85	4.0

^a Relative standard deviations for valerate, hydroxyl, and backbone oxygen ratios are $\leq \pm 10\%$, $\leq \pm 10\%$, and $\leq \pm 5\%$, respectively.

[15]. Ho

value exp

concentr

reaction

with car

the alc

$\text{Sn}(\text{OM}$

concer

acid is

films

each

neutr

calcu

in thi

ident

tin is

prec

obse

redu

oxid

oxid

[15]. However, the relative extent of carboxylation of SnV films is consistent with the value expected from the FTIR study of the valeric acid-Sn(OPrⁱ)₄ solutions. Low valerate concentrations in tin valerate films may be related to high levels of alcohol in tin alkoxide reaction mixtures. It is well-known that the maximum replacement of alkoxide ligands with carboxylates can only be achieved if alcohol is removed during synthesis [21]. While the alcohol concentration of the Sn(OPrⁱ)₄ solutions is nearly three times that of the Sn(OMe)₂ solutions, in both Sn(OMe)₂ and Sn(OPrⁱ)₄ precursor solutions, the initial concentration of alcohol is approximately twice that of valeric acid. In contrast, valeric acid is the major component of zirconium and titanium film solutions [15].

Quantitative XPS results can also be used to infer the oxidation state of metals in films [15, 31]. Assuming a charge of -1 for carboxylate and hydroxyl ligands and -2 for each backbone oxygen, a net negative charge in each film can be determined. Electrical neutrality requires that metal atoms have a charge equal and opposite to this. These calculations indicate that tin has an average oxidation state of approximately +4 in all films in this study (Table 3.1). As stated previously, SnV films made from either precursor are identical according to FTIR and XPS analyses. This suggests that the oxidation state of tin is the same in all valerate films even though the oxidation states are different in the precursor alkoxides. Oxidation of Sn(OMe)₂ is consistent with the vigorous bubbling observed when it is mixed with valeric acid: protons oxidize Sn²⁺ to Sn⁴⁺ and are in turn reduced to form hydrogen gas. It is also known that most Sn²⁺ solutions are readily oxidized to Sn⁴⁺ and must be protected from exposure to air [32]. Therefore, a tin oxidation state of +4 in a film derived from Sn(OMe)₂ is not surprising.

to use

basis

oxidat

The lo

2p - d

Sn 5s

the ox

used

Sn^{4+} i

band

films.

oxyge

oxide

minu

with

easily

leads

state

photo

This

featur

Since Sn^{2+} and Sn^{4+} oxides have similar XPS Sn $3d_{5/2}$ binding energies, it is difficult to use Sn core level binding energies to confirm the oxidation state of tin calculated on the basis of ligand and metal charge balancing. It has been established, however, that the oxidation state can be determined from the valence band spectra of tin oxides [30, 33-35]. The lowest binding energy feature in the valence band spectrum of SnO_2 is a prominent O $2p$ - derived peak with a binding energy of approximately 5 eV. In SnO , there is a strong Sn $5s$ - derived feature at about 2 eV. Valence band spectra have been used to determine the oxidation state of tin in different forms of tin oxide. For example, Themlin *et al.* [34] used the areas of these two features to determine the relative concentrations of Sn^{2+} and Sn^{4+} in single crystal and polycrystalline tin oxides. Sanjinés *et al.* [35] used the valence band spectrum to determine the oxidation state of tin in amorphous sputter deposited films.

While SnV films contain organic ligands, they are primarily comprised of metal oxygen polymers with limited valerate ligand coordination. They are, therefore, largely tin oxide - like materials. The valence band spectrum of a SnV film collected in the first 15 minutes of X-ray exposure time (Figure 3.4a) is similar to that of SnO_2 . This is consistent with our charge balance calculation (Table 3.1). We have found that the SnV films are easily photoreduced during XPS analysis. Extended exposure of SnV films to X-rays leads to the formation of a peak indicative of Sn^{2+} (2 eV) and a decrease in the oxidation state calculated from core level intensities. An extreme example of the effects of X-ray photoreduction on the valence band spectrum of an SnV film is shown in Figure 3.4b. This valence band spectrum was collected after 12 hours of X-ray exposure and contains features similar to those reported for Sn^{2+} oxides [30,34]. The calculated oxidation state

Intensity

Figure

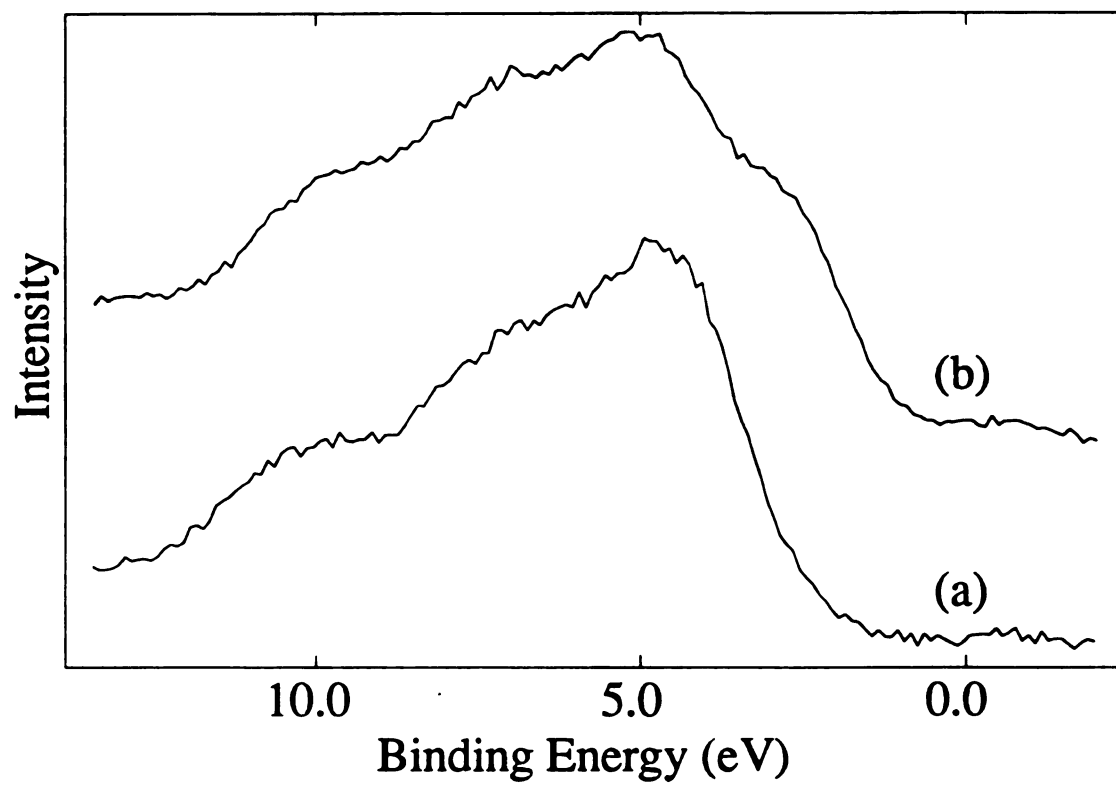


Figure 3.4 Valence band photoelectron spectra of SnV film (a) initially and (b) after 12h of X-ray exposure.

of tin

analys

film st

spectr

3400

1620

ligand

spectr

and 4

occu

band

Char

grou

cryst

FTIR

cons

to a

of v

the

of tin in this photoreduced film is approximately +2.8. For this reason, all core band XPS analyses of SnV films were conducted within the first 5 minutes of X-ray exposure.

Structure of Tin Oxide Films. Calcined Tin Films. XRD analysis of the SnC film showed no peaks other than a broad feature due to the quartz substrate. The FTIR spectrum of the SnC film is shown in Figure 3.2b. A broad O-H stretch absorbance near 3400 cm^{-1} is typical of hydroxyl ligands and/or sorbed water in tin oxide [36]. The band at 1620 cm^{-1} , characteristic of sorbed water, is relatively small indicating that hydroxyl ligands predominate. No bands characteristic of organic groups are observed in the SnC spectrum. The spectrum of a calcined tin film shows a strong, broad band between 800 and 400 cm^{-1} due to $\nu(\text{Sn-O-Sn})$ and $\nu(\text{Sn-O})$ vibrations. The maximum absorbance occurs at 587 cm^{-1} , a slightly higher frequency than seen for the SnV films.

Giuntini *et al.* [28] noted an increase in the relative intensity of the $\nu(\text{Sn-O-Sn})$ band at 680 cm^{-1} compared to the $\nu(\text{Sn-O})$ band at 540 cm^{-1} upon heating gels to 350°C . Changes were attributed to the formation of O-Sn-O bridges from structural hydroxyl groups. Orel *et al.* [27] noted similar changes for their gels and correlated it with crystallization. We believe that the similarity of the low frequency bands observed in the FTIR spectra of SnC and SnV films suggests that the SnC films are amorphous. This is consistent with XRD results obtained for the calcined films.

The XPS C 1s spectrum obtained for SnC films contains peaks that can be ascribed to adventitious carbon (284.6 eV) and carbonate species (288.8 eV). These features are of very low intensity compared to the carbon peaks observed in the SnV films. Based on the trace levels of carbonate species detected in SnC films ($<0.04/\text{Sn}$), SnC 1s oxygen

peaks

The b

decre

calcin

to ad

the X

its va

SnO₂

the l

of th

cast

per

tre

Co

spe

Th

the

in

bo

th

tr

a

peaks are ascribed to backbone oxygen (530.3 eV) and hydroxyl groups (531.9 eV) only. The binding energy of the Sn $3d_{5/2}$ peak is 486.4 eV, typical of tin oxides [29]. The decrease in hydroxyl concentration and increase in backbone oxygen observed following calcination (Table 3.1) suggests that removal of the carboxylate and hydroxyl ligands leads to additional metal - oxygen backbone formation. Charge balance calculations based upon the XPS results leads to a +4 oxidation state for tin in SnC films. This is consistent with its valence band spectrum (Figure 3.5b) which is very similar to that of polycrystalline SnO₂ (Figure 3.5a).

Hydrogen Peroxide Treated Films. The effect of hydrogen peroxide treatment on the FTIR spectrum observed for a tin valerate film is shown in Figure 3.6. The spectrum of the untreated SnV film on Si (Figure 3.6a) is similar to the spectrum obtained for a film cast on KBr (Figure 3.2a). Figure 3.6b is the spectrum of the same film after hydrogen peroxide treatment (SnP), and Figure 3.6c shows the spectrum of a hydrogen peroxide treated, uncoated Si crystal. The spectra are normalized to the Si band at 1108 cm⁻¹. Comparison of the valerate ligand absorbance bands in the treated and untreated film spectra shows that hydrogen peroxide treatment removes most of the valerate ligands. The hydroxyl absorbance intensity in the SnP and SnV film spectra are similar, however, the maximum intensity is shifted to higher frequency in the SnP film spectrum. Recall that in the SnV films, the lower frequency hydroxyl absorbances were attributed to water H-bonded to monodentate valerate ligands. The frequency shift is therefore consistent with the removal of the valerate ligands. C-H stretch bands at about 2900 cm⁻¹ may be due to traces of a hydrocarbon residue remaining after removal of valerate ligands. An absorbance band centered at 1620 cm⁻¹ in the SnP spectrum can be largely attributed to

Intensity

Figur

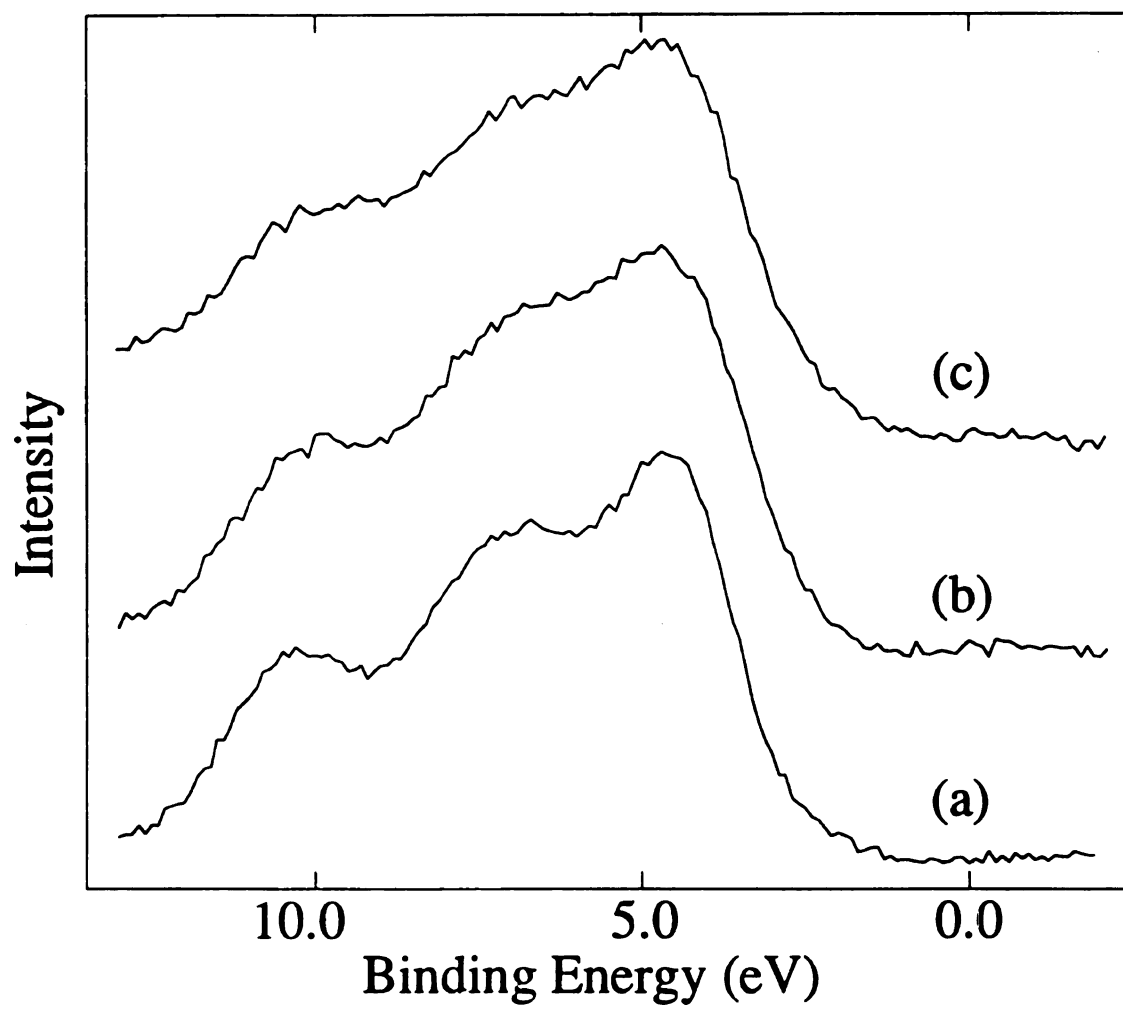


Figure 3.5 Valence band photoelectron spectra of (a) tin(IV) oxide, (b) SnC film, and (c) SnP film.

Absorbance

Figure

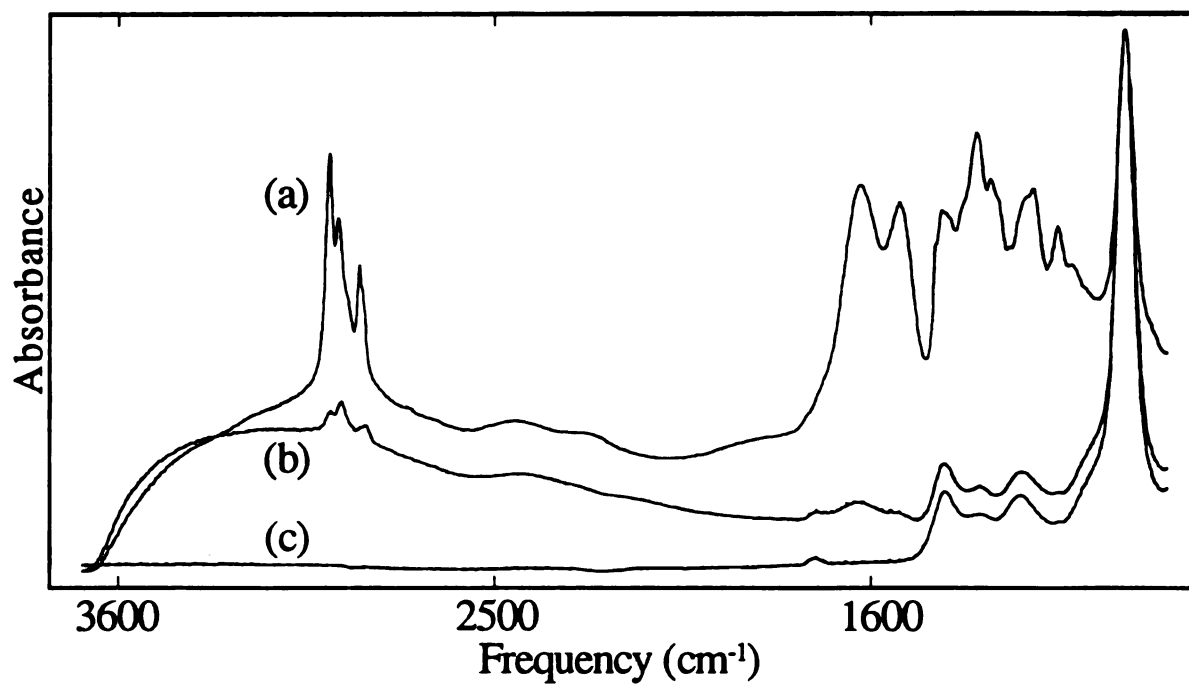


Figure 3.6 FTIR spectra of SnV film on Si crystal (a) before and (b) after hydrogen peroxide treatment (SnP), and (c) the uncoated Si crystal.

sorbed w

attributab

T

vibration

absorba

gels wa

SnV fi

hydrog

the ch

hydro

perox

Hydr

400

uncl

Sn

spe

eV

att

de

all

eV

co

sorbed water. As noted for the SnC film, XRD analysis of the SnP film showed no peaks attributable to the film.

The effect of hydrogen peroxide treatment on the low frequency tin-oxygen vibrations cannot be determined using films coated on Si crystals because Si has strong absorbances below 1250 cm^{-1} . For this reason hydrogen peroxide treatment of tin valerate gels was also studied. The tin valerate gel spectrum (Figure 3.7a) is similar to that of the SnV film with an additional, strong contribution from sorbed valeric acid. The effects of hydrogen peroxide treatment on the hydroxyl and valerate absorbance bands are similar to the changes induced in the SnV film: most valerate groups are removed and the maximum hydroxyl absorbance is shifted to higher frequency (Figure 3.7b). The spectrum of the peroxide treated gel also contains an absorbance at 1620 cm^{-1} due in part to sorbed water. Hydrogen peroxide treatment has little effect on the strong absorbance between 800 and 400 cm^{-1} , suggesting that the structure of the tin oxide polymer network is largely unchanged by carboxylate removal.

XPS binding energies of backbone O 1s (530.7 eV), ligand O 1s (531.9 eV), and Sn $3d_{5/2}$ (486.7 eV) peaks have the same values as measured for SnV films. The C 1s spectrum of an SnP film contains three peaks with binding energies of 284.6 eV , 286.4 eV , and 288.7 eV . Since FTIR analysis detects only traces of residual carbon species, we attribute the SnP carbon to a residue of hydrogen peroxide reaction products which have deposited on the film surface. The lowest binding energy peak is due to a combination of alkyl and adventitious carbon. Carbon 1s peaks with binding energies of 288.7 and 286.4 eV are typical of carbon-oxygen moieties with a variety of carbon to oxygen ratios. The combined concentration of these species is about 0.2 per tin atom in the surface of the

Absorbance

Figure

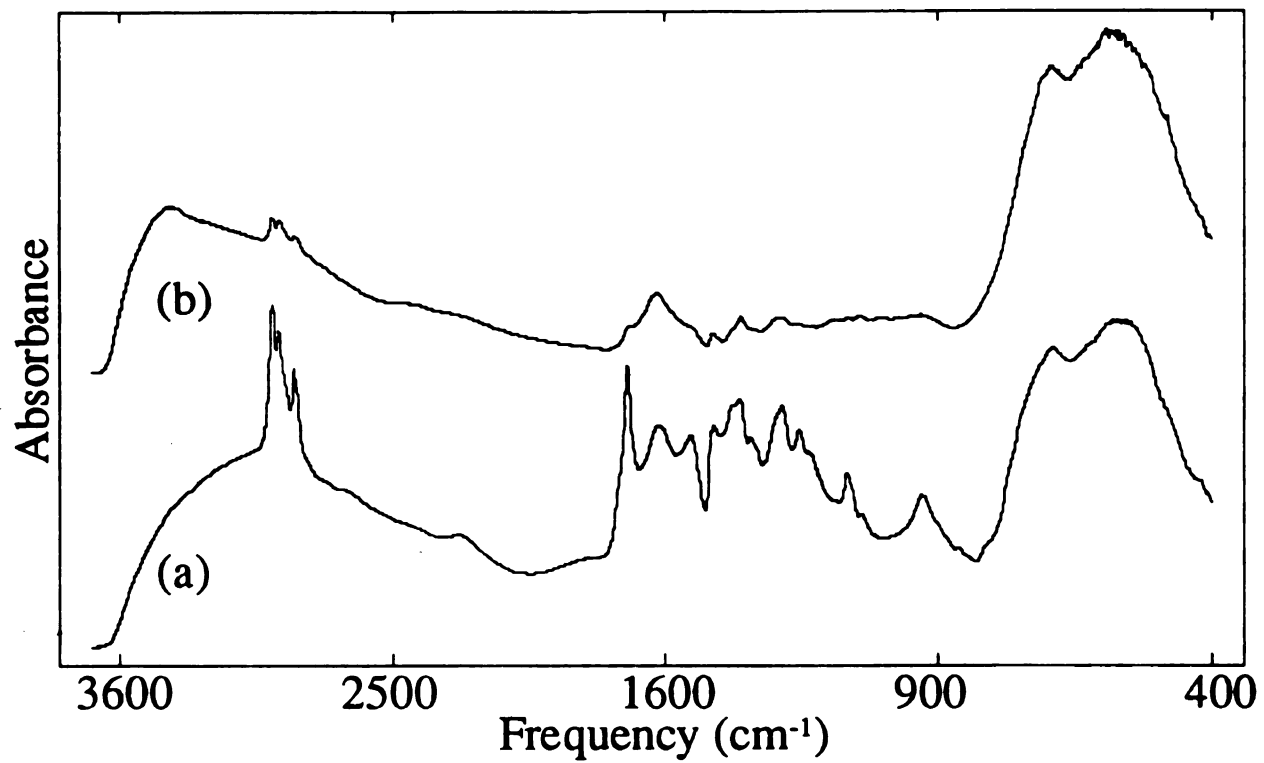


Figure 3.7 FTIR spectra of tin valerate gel (a) before and (b) after hydrogen peroxide treatment.

films. For

each cart

determin

associate

it results

expected

the vacu

that no

establis

metal c

carboxy

increas

valence

to the

respec

consis

films a

X-ray

to be s

films. For our calculations, it was assumed that there was one oxygen associated with each carbon of these binding energies. The hydroxyl concentration (Table 3.1) was then determined from the intensity of the ligand oxygen peak after subtraction of oxygen associated with surface carbon contamination. While this assumption is only approximate, it results in a reasonable value for the hydroxyl concentration. Again, sorbed water is not expected to make a significant contribution to O 1s spectra since it is largely removed by the vacuum system of the XPS instrument prior to analysis. We should also emphasize that no Si (quartz substrate) was detected in the XPS analysis of SnP films. This further establishes the belief that hydrogen peroxide treatment does not significantly damage the metal oxide polymer structure. However, as noted for SnC films, removal of the carboxylate ligands increases the backbone oxygen content (Table 3.1), presumably by increasing the extent of polymer crosslinking.

Our analyses have suggested that SnP films are tin oxide - like materials. The valence band spectrum of an SnP film (Figure 3.6c) is similar in shape and binding energy to the valence band spectra of polycrystalline SnO₂ and SnC films (Figures 3.6a and 3.6b, respectively). This indicates that tin is in a +4 oxidation state in SnP films. This is consistent with the quantitative XPS charge balance (Table 3.1). Like SnV films, SnP films are subject to X-ray photoreduction and thus analyses were performed using minimal X-ray exposure times. Calcined tin oxide films and polycrystalline SnO₂ were not found to be susceptible to photoreduction under our analysis conditions.

35 Re

1. M
A

2. F
F

3. S
A

4. Y

5.

6.

7.

8.

9.

10.

11.

12.

3.5 References

1. Madou, M.J.; Morrison, S.R. *Chemical Sensing with Solid State Devices*; Academic Press: San Diego, CA, 1989.
2. Fuller, M.J.; Warwick, M.E. *J.Catal.* **1973**, *29*, 441. McAleer, J. *J. Chem. Soc. Faraday Trans. I* **1979**, *75*, 2768. Berry, F.J. *Adv. Catal.* **1981**, *30*, 97.
3. Shewchun, J.; Singh, R.; Green, M.A. *J. Appl. Phys.* **1977**, *48*, 765. Bucher, E. *Appl. Phys.* **1978**, *17*, 1.
4. Peaker, A.R.; Horsley, B. *Rev. Sci. Instrum.* **1971**, *42*, 1825.
5. Cocco, G.; Enzo, S.; Carturan, G.; Giordano Orsis, P.; Scardi, P. *Mater. Chem. Phys.* **1987**, *17*, 541-551.
6. Von Ortenberg, M.; Link, J.; Helbig, R. *J. Opt. Soc. Am.* **1977**, *67*, 968.
7. Kohl, D. *Sens. Actuators* **1989**, *18*, 71. Ippommatsu, M.; Sasaki, H. *J. Electrochem. Soc.* **1989**, *136(7)*, 2123. Capehart, T.W.; Chang, S.C. *J. Vac. Sci. Technol.*, **1981**, *18(2)*, 393.
8. Pink, H.; Treitinger, L. Vite, L. *Japan. J. Appl. Phys.* **1980**, *19(3)*, 513. Tomar, M.S.; Garcia, F.J. *Prog. Cryst. Growth Charact.* **1981**, *4*, 221.
9. Lalauze, R.; Pijolat, C.; Vincent, S.; Bruno, L. *Sens. Actuators* **1992**, *8*, 237. Kim, K.; Finstad, T.G.; Chu, W.K.; Cox, X.B.; Linton, R.W. *Solar Cells* **1985**, *13*, 301.
10. Brinker, C.J.; Scherer, G. *Sol-Gel Science*; Academic Press: San Diego, 1990.
11. Roger, C.; Hampden Smith, M.J.; Brinker, C.J. In *Better Ceramics Through Chemistry V*, Hampden Smith, M.J., Klemperer, W.G., Brinker, C.J., Eds.; Mater. Res. Soc. Symp. Proc. 271; MRS: Pittsburgh, PA, 1992; 51.
12. Yoldas, B.E. *J. Non-Cryst. Solids* **1980**, *38&39*, 81. Thomas, I.M. In *Sol-Gel Technology for Thin Films, Fibers, Preforms, Electronics and Specialty Shapes*, Klein, L.C., Ed.; Noyes Publications: Park Ridge, N.J., 1988; 2. Wark, T.A.; Gulliver, E.A.; Jones, L.C.; Hampden-Smith, M.J.; Rheingold, A.L.; Huffman, J.C. in *Better Ceramics Through Chemistry IV*, Zelinsky, B.J.J.; Brinker, C.J.; Clark, D.E.; Ulrich, D.R., Eds.; Mater. Res. Soc. Proc. 180; Pittsburgh, PA, 1990; 61. Wellbrock, U.; Beier, W.; Frischat, G.H. *J. Non-Cryst. Solids* **1992**, *147&148*, 350.
13. Livage, J.; Henry, M.; Sanchez, C. *Prog. Solid State Chem.* **1989**, *18*, 259.

14.

15.

16.

17.

18.

19.

20.

21.

22.

23.

24.

25.

26.

27.

28.

14. Gagliardi, C.D.; Berglund, K.A. in *Processing Science of Advanced Ceramics*, Aksay, K.A.; McVay, G.L.; Ulrich, D.R., Eds.; Mater. Res.Soc. Proc. 155: Pittsburgh, PA, 1986; 127. Gagliardi, C.D.; Dunuwila, D.; Berglund, K.A. in *Better Ceramics Through Chemistry IV*, Zelinsky, B.J.J.; Brinker, C.J.; Clark, D.E.; Ulrich, D.R., Eds.; Mater. Res. Soc. Proc. 180: Pittsburgh, AA, 1990; 801. Dunawila, D.; Berglund, K.A. *Chem. Mater.* **1994**, 6(9), 1556.
15. Severin, K.G.; Ledford, J.S.; Torgerson, B.A.; Berglund, K.A. *Chem. Mater.* **1994**, 6(7), 890.
16. Hampden-Smith, M.J.; Wark, T.A.; Brinker, C.J. *Coor. Chem. Rev.* **1992**, 112, 81.
17. Takahashi, Y.; Wada, Y. *J. Electrochem. Soc.* **1990**, 137, 267.
18. Software provided by Dr. Andrew Proctor, University of Pittsburgh, Pittsburgh, PA.
19. Colthup, N.B.; Daly, L.H.; Wiberley, S.E. *Introduction to Infrared and Raman Spectroscopy*; 3rd Ed. Academic Press: San Diego, 1990.
20. Silverstein, R.M.; Bassler, C.G.; Morrill, T.C. *Spectrometric Identification of Organic Compounds*; 3rd Ed. John Wiley & Sons, Inc.: New York, 1974.
21. Mehrotra, R.C.; Bohra, R. *Metal Carboxylates*; Academic Press: London, 1983.
22. Grigor'ev, A.I. *Russ. J. Inorg. Chem.* **1963**, 8(4), 409.
23. Hampden-Smith, M.J.; Wark, T.A.; Rheingold, A.; Huffman, J.C. *Can. J. Chem.* **1991**, 69, 121.
24. Deacon, G.B.; Phillips, R.J. *Coord. Chem. Rev.* **1980**, 33, 227-250.
25. Garner, C.D.; Hughes, B.; King, T.J. *J. Chem. Soc., Dalton Trans.* **1975**, 562.
26. Alcock, N.W.; Tracy, V.M.; Waddington, T.C. *J. Chem. Soc., Dalton Trans.* **1976**, 2243.
27. Orel, B.; Lavrencic-Stangar, U.; Crnjak-Orel, Z.; Bukovec, P.; Kosec, M. *J. Non-Cryst. Solids* **1994**, 167, 272.
28. Giuntini, J.C.; Granier, W.; Zanchetta, J.V.; Taha, A. *J. Mater. Sci. Lett.* **1990**, 9, 1383.

29. He
Da

30. La

31. N

32. D

33. S

34. T

35.

36.

29. *Handbook of X-ray Photoelectron Spectroscopy*; Wagner, C.D.; Riggs, W.M.; Davis, L.E.; Moulder, J.F.; Muilenburg, G.E., Eds.; Perkin Elmer, 1979.
30. Lau, C.L.; Wertheim, G.K. *J. Vac. Sci. Technol.* **1978**, *15*(2), 622.
31. Noonan, G.O.; Ledford, J.S. *Chem. Mater.* **1995**, *7*(6), 1117.
32. Donaldson, J.D. *Prog. Inorg. Chem.* **1968**, *8*, 287.
33. Sherwood, P.M.A. *Phys. Rev. B* **1990**, *41*(14), 10 151.
34. Themlin, J.M.; Chtaib, M.; Henrard, L.; Lambin, P.; Darville, J.; Gilles, J.-M. *Phys. Rev. B* **1992**, *46*(4), 2460.
35. Sanjinés, R.; Coluzza, C.; Rosenfeld, F.; Gozzo, F.; Alméras, Ph.; Lévy, F.; Margaritondo, G. *J. Appl. Phys.* **1993**, *73*(8), 3997.
36. Thorton, E.W.; Harrison, P.G. *J.C.S. Faraday I* **1975**, *71*, 461.

4.1

prepare

of 100

solution

calcini

stable

tempe

transf

ultra

films

films

Sn w

surfa

com

at 4

dete

Chapter 4

Synthesis and Characterization of Sol-Gel Derived Titanium-Tin Oxide Films

4.1 Abstract

In this study the homogeneity and properties of titanium-tin oxide thin films prepared using a modified sol-gel technique are examined. Films with Ti:Sn atomic ratios of 100:0, 75:25, 50:50, 25:75, and 0:100 have been formed by spin casting hydrolyzed solutions of tin(IV) and titanium(IV) isopropoxides and valeric acid onto quartz slides and calcining in air at temperatures between 250 and 1000 °C. All films are transparent, stable, and exhibit uniform adhesion to quartz. The effect of composition and calcination temperature has been determined using X-ray photoelectron spectroscopy (XPS), Fourier transform infrared spectroscopy (FTIR), X-ray diffraction (XRD), ellipsometry, and ultraviolet-visible spectroscopy (UV-Vis). Additionally, the homogeneity of the mixed films has been explored with angle resolved XPS (AR-XPS). It was found that “as cast” films prepared by mixing separately hydrolyzed alkoxides have a surface enhancement of Sn which is not present if the alkoxides are hydrolyzed together. Calcination causes Ti to surface segregate and the degree of surface segregation is a function of both film composition and calcination temperature. Mixing suppresses the formation of crystallites at 400 °C and at higher temperatures only mixed TiO₂ and SnO₂ rutile phases are detected. Depending upon the composition, “as cast” films range in thickness from 400 -

300 nm and

250 °C. Re

4.2 Intr

Mi

chemical

titanium c

higher co

[2, 3].

strongly

candida

and im

Madde

was i

applic

TiO₂

2000

Dis

ion

inh

co

de

300 nm and collapse between 50% and 20% upon calcination at temperatures as low as 250 °C. Refractive indices were also found to be related to film composition.

4.2 Introduction

Mixing metal oxides is a promising approach for tailoring the physical and chemical properties of materials for use in a wide range of applications [1]. Tin and titanium oxides have been mixed to produce catalysts with modified reactivity [2] and higher concentrations of strong acid sites than present in either of the single metal oxides [2, 3]. Takahashi and Wada [4] found that the conductivity of TiO₂-SnO₂ films was strongly dependent upon the components of the ambient gas, making them ideal candidates for gas sensing materials. Indeed, gas sensors with enhanced sensitivity [5,6] and improved response times [5, 7] have been produced from mixed TiO₂-SnO₂ materials. Maddelena *et al.*[8] also demonstrated that the electrical conductivity of tin oxide glasses was increased by doping with titanium oxide. In addition to catalytic and sensor applications, the ability to control refractive indices and conductivities may make mixed TiO₂-SnO₂ thin films useful as new transparent coatings.

Classically, mixed metal oxides are prepared by repeated high temperature (1000-2000 °C) heating and grinding of single metal oxides in the desired atomic ratios. Disadvantages of this method include high processing temperatures, contamination from ionic impurities in raw materials, irreproducible stoichiometry, and the production of inhomogeneous materials [1, 9]. Other researchers have prepared TiO₂-SnO₂ powders by coprecipitation of alkoxides [3, 10] or chlorides [2,5] and films using chemical vapor deposition (CVD) [4] and sol-gel [5,8] techniques. Sol-gel synthesis from metal alkoxides

is especially

Multicom

high purit

and it is

homogen

of the so

sensing

sol-gel s

depend

phases

charac

films.

[12,13

experi

depos

on the

as can

theref

metho

produ

is especially advantageous because it avoids the problems inherent in classical methods. Multicomponent oxides can be synthesized at relatively low temperatures, reactants are of high purity, there are no residual impurities introduced from the presence of counterions, and it is a wet chemical method which allows better control over the stoichiometry and homogeneity of the materials produced [1,9, 11]. Additionally, the rheological properties of the sols make them ideal for the production of thin films which are useful for both gas sensing and coatings applications [9]. In the current study we explore the use a modified sol-gel synthesis method to make $\text{TiO}_2\text{-SnO}_2$ thin films from metal alkoxides.

The catalytic, physical, optical, and electronic properties of thin films are strongly dependent, not only upon the particular metal oxide(s) in the films, but also upon the phases present and in the case of crystalline materials, orientation of the crystallites. These characteristics are, in turn, strongly dependent upon the method used to synthesize the films. For instance, TiO_2 films have different characteristics when produced using CVD [12,13], sputter deposition [14,15], sol-gel [16,17], or atomic layer epitaxy [18,19]. Also, experimental conditions such as gas pressure and substrate temperature for sputter deposition [14] and additives used in a sol-gel synthesis [16] can have a strong influence on the phases present, phase transition temperatures, and preferred crystallite orientations, as can impurities or dopants [20] and the type of substrate used [13]. It is important, therefore, to determine the unique characteristics of films produced using a particular method.

In the first part of this paper we evaluate variations of the sol-gel method for producing homogeneously mixed films. We have previously reported the synthesis of

titanium

22]. The

would b

alkoxide

extent c

oligome

Alkoxid

polyme

oligom

favor i

been d

togeth

homo

alkox

are q

the a

prepa

and p

solu

spe

titanium valerate and tin valerate films from $\text{Ti}(\text{OPr}^i)_4$ and $\text{Sn}(\text{OPr}^i)_4$, respectively [21, 22]. The simplest method for preparing mixed metal oxide films from these alkoxides would be to mix them together and then carry out the synthesis as for the individual alkoxides. Factors which may influence the homogeneity of the resultant films are the extent of oligomerization of the alkoxides and their relative hydrolysis rates. Highly oligomeric alkoxides would be expected to produce heterogeneous mixed materials. Alkoxides with different hydrolysis rates have a kinetic incompatibility that favors self-polymerization [23].

The alkoxides chosen for the synthesis: $\text{Ti}(\text{OPr}^i)_4$ and $\text{Sn}(\text{OPr}^i)_4$ have low levels of oligomerization: they are monomeric [24] and dimeric [25], respectively, and this should favor intimate mixing of the two alkoxides before polymerization. Additionally, it has been demonstrated that double metal alkoxides can be formed by refluxing the alkoxides together [26]. This could potentially further enhance the likelihood of producing homogeneously mixed materials. The relative hydrolysis and condensation rates of these alkoxides after complexation with valerate ligands is unknown but if the hydrolysis rates are quite dissimilar, the resultant material would resemble one prepared by polymerizing the alkoxides separately, followed by mixing. In this study, three variations are used to prepare 50:50 mixtures: mixing the alkoxides with and without refluxing before hydrolysis, and polymerizing the alkoxides separately, followed by mixing. Films prepared from these solutions are compared.

The methods used to evaluate these films are Fourier transform infrared spectroscopy (FTIR), X-ray photoelectron spectroscopy (XPS), and angle resolved XPS

(AR-X)

Ti-O-S

provid

or Sn

surfac

the st

(XRD

chara

25:7:

Addi

films

4.3

titan

Che

was

tech

pre

tho

our

(AR-XPS). Identification of a band in the FTIR spectrum which could be attributed to a Ti-O-Sn stretch or a peak in the O 1s XPS spectrum due to oxygen in this moiety would provide direct evidence of mixing. AR-XPS is used to detect a surface enhancement of Ti or Sn. Commonly one component of an inhomogeneous material will segregate at the surface and this could be identified and characterized with AR-XPS.

In the second part of the paper, the effect of calcination (250 °C to 1000 °C) on the structure and properties of TiO₂ and SnO₂ films is examined using X-ray diffraction (XRD), XPS, ultraviolet-visible spectroscopy (UV-Vis), and ellipsometry. The characteristics of these films are compared with that of films prepared with Ti:Sn ratios of 25:75, 50:50, and 75:25 and calcined at temperatures between 400 and 1000 °C. Additionally, AR-XPS is used to characterize surface segregation of oxides in mixed oxide films and XRD to identify crystalline mixed oxide phases.

4.3 Experimental

Materials. Tin(IV) isopropoxide 10% w/v in isopropanol (Chemat Technologies), titanium(IV) isopropoxide (Aldrich Chemical Company), and valeric acid (99+%, Aldrich Chemical Company) were used without further purification. Distilled, deionized water was used for all syntheses.

Film Preparation. The methods used to synthesize films were based on techniques developed previously [21, 22]. Films synthesized from Sn(OPrⁱ)₄ were prepared using mixtures of 40 isopropanol : 9 valeric acid : 1.5 water : 1 Sn(OPrⁱ)₄ and those from Ti(OPrⁱ)₄ from 9 valeric acid : 1.5 water : 1 Ti(OPrⁱ)₄. Reactions were carried out at room temperature in capped vials in a N₂ purged glovebox. Valeric acid was added

to the alk

following

Ti

an equim

was adde

1.5 : 1.

solution

the alk

Method

previo

stirred

1 with

quart

temp

air (

Film

were

all fi

and

Ti 2

to the alkoxide followed by water. A vortex mixer was used to vigorously stir solutions following the addition of each reactant.

Three different methods were used to synthesize 50:50 mixed films. In Method 1, an equimolar mixture of $\text{Sn}(\text{OPr}^i)_4$ and $\text{Ti}(\text{OPr}^i)_4$ was stirred vigorously and valeric acid was added immediately, followed by water. The acid to water to alkoxide ratios were 9 : 1.5 : 1. Isopropanol, from the $\text{Sn}(\text{OPr}^i)_4$ precursor solution, was also present in these solutions in a 20 alcohol : 1 alkoxide ratio. Method 2 is the same as Method 1 except that the alkoxide mixture was refluxed for one hour before the addition of valeric acid. In Method 3 separate solutions were prepared from the two alkoxides as described in the previous paragraph. After standing for three hours, the two solutions were combined and stirred with a vortex mixer. For the calcination study, films were prepared using Method 1 with the appropriate relative molar concentrations of the alkoxides.

Freshly prepared solutions were dispersed on cleaned, acetone rinsed and dried quartz slides, spun for five minutes, and air-dried overnight. Films calcined at temperatures ≤ 600 °C were prepared by heating films in a tube furnace under a flow of dry air ($100 \text{ cm}^3/\text{min}$, medical grade, AGA Gas Co.) at the desired temperature for 24 h. Films calcined at 800 °C or 1000 °C were heated in a muffle furnace for 24 h. All films were stored in a desiccator before analysis or further treatment. Unless otherwise noted, all films prepared in this study were visually transparent, colorless, and exhibited complete and uniform adhesion to quartz substrates.

Samples are designated with the following abbreviations: 100 % Ti film = Ti, 75% Ti 25% Sn = TS, 50% Ti 50% Sn = EM (equimolar), 25% Ti 75% Sn = ST, and 100% Sn

= Sr

and

valen

films

75%

analy

XPS

(15 k

were

refer

of \pm

sensi

fitted

curve

films

in the

0° (d

regio

regio

2p p

= Sn. Films studied without further treatment are referred to as valerate or “as cast” films and designated with “Val” (i.e. 100 % Sn “as cast” film = SnVal or a 75% Ti 25% Sn valerate film = TSVal). Films which were heated in air are referred to as calcined or oxide films and designated with a “C” followed by the calcination temperature (i.e. a 25% Ti 75% Sn film which has been calcined at 400 °C = STC400).

X-ray Photoelectron Spectroscopy (XPS). Films cast on quartz slides were analyzed with a VG Microtech spectrometer using a Clam2 hemispherical analyzer. All XPS spectra were collected using a Mg anode (1253.6 eV) operated at a power of 300 W (15 kV and 20 mA emission current) with an analyzer pass energy of 50 eV. Four regions were scanned for each film: C 1s, O 1s, Sn 3d, and Ti 2p. Binding energies were referenced to adventitious carbon (C 1s = 284.6 eV) and were measured with a precision of ± 0.1 eV. Quantitative XPS calculations were performed using empirically derived sensitivity factors previously determined in this laboratory [21, 22]. XPS peaks were fitted with 20% Lorentzian-Gaussian mix Voigt functions using a non-linear least squares curve fitting program [27]. Unless otherwise noted, composition of mixed metal oxide films are reported as a molar ratio with respect to the total metal concentration (Ti + Sn) in the film. Values reported have a standard deviation of < 10%.

Angle Resolved XPS (AR-XPS). Mixed films were analyzed at angles between 0° (deepest) and 90° (shallowest) with respect to the surface normal at 15° intervals. Two regions were scanned: the C 1s region to provide a binding energy reference and a 100 eV region (binding energy range: 545 eV to 445 eV) which contained the O 1s, Sn 3d, and Ti 2p peaks. Over this narrow range of kinetic energies it is valid to assume that the

photoelect

was deter

3λ. Usin

Å was ca

areas of t

sensitiv

determin

reported

prepare

<5%.

each ot

surface

showed

In ord

sensitiv

slides w

1.5418

collect

was re

Peak w

photoelectrons have similar escape depths. The mean free path (λ) of the photoelectrons was determined from the universal curve [28] and the sampling depth was assumed to be 3λ . Using a monolayer thickness of 3 Å, a maximum sampling depth of approximately 50 Å was calculated. Relative concentrations of Sn and Ti were determined by measuring the areas of the Sn $3d_{5/2}$ peak and the Ti 2p peaks and applying a sensitivity factor. The Ti/Sn sensitivity factor was determined by taking a ratio of the O/Sn and O/Ti sensitivity factors determined by analysis of SnO₂ and TiO₂ polycrystalline powders, respectively. Values reported are normalized by dividing by the relative concentration of Ti and Sn used to prepare the films. While all standard deviations of reported values are <10%, most are <5%.

In our instrument configuration the X-ray source and the analyzer are at 90° from each other. Since X-ray emission is parallel to the sample surface for a 0° analysis angle, a surface sensitivity due to the source is created. In all cases, samples collected at 0° showed a higher concentration of the surface enhanced species than was measured at 15°. In order to avoid confusion due to the convolution of source and analyzer surface sensitivity, data collected with a 0° angle is not reported in this study.

X-ray Diffraction (XRD). XRD diffraction patterns of calcined films on quartz slides were obtained with a Rigaku XRD diffractometer employing Cu K α radiation ($\lambda=1.541838$ Å). The X-ray was operated at 45 kV and 100 mA. Diffraction patterns were collected using DD and DS slit widths of 1°. The background due to the quartz substrate was removed from the patterns by subtracting the XRD pattern of a blank quartz slide. Peak widths and locations were determined using a non-linear least squares curve fitting

pro

us

qu

ra

qu

w

B

0.

A

63

le

sig

wi

th

are

program [27] and assuming Gaussian line shapes. Mean particle sizes were calculated using the Scherrer equation [29] assuming no line broadening due to stress.

Ultraviolet-Visible Spectroscopy (UV-Vis). Absorbance spectra of films cast on quartz slides were collected with a Hitachi U4001 UV-Vis spectrophotometer over a range of 190-750 nm using a scan speed of 300 nm/min and a 2 nm slit width. A blank quartz slide was used in the reference beam.

Absorption coefficient (α) data was fitted to:

$$\alpha hv = A(hv - E_g)^2 \quad 4.1$$

where hv is the photon energy, E_g is the optical band gap energy, and A is a constant [30]. Band gaps were then determined from plots of $(\alpha hv)^{1/2}$ versus hv . Values reported are ± 0.15 eV.

Ellipsometry. Refractive indices and film thicknesses were determined using an Auto EL II (Rudolph Research International, USA) ellipsometer using a He-Ne laser ($\lambda = 632.8$ nm) as the light source. The reported values are the result of measurements of at least three films and four or more measurements were made on each film. There was no significant difference in values measured at different places on a single film, indicating that within experimental error, the films were of uniform thickness and refractive index over the entire surface. Standard deviations for thickness and refractive index measurements are less than 5% and 3%, respectively.

4.4

4.4.1

and

Ident

spect

high

while

poly

spec

film

com

ligar

two

band

due

band

vale

whic

indiv

show

also

4.4 Results and Discussion

4.4.1 Effect of preparation method on film homogeneity.

The FTIR spectra of valerate films made from range of relative concentration of Ti and Sn are shown in Figure 4.1. The mixed films were prepared using Method 1. Identification of bands in tin valerate (Figure 4.1a) and titanium valerate (Figure 4.1e) film spectra have been previously reported [21, 22]. In general, the bands at frequencies higher than 1000 cm^{-1} are due to the presence of the valerate ligands and hydroxyl groups, while those at lower frequencies are primarily due to metal - oxygen stretches, both in the polymer backbone and due to ligand coordination to the metal centers. The mixed film spectra (Figures 4.1b - 4.1d) appear to be largely a combination of the SnVal and TiVal film spectra and indicate that, like the single metal films, the mixed valerate films are comprised of metal - oxygen polymer backbones coordinated with valerate and hydroxyl ligands.

The low frequency region of all spectra shows strong, broad bands. Unless the two metals alternate rigorously in the polymer networks both $\nu(\text{Ti-O-Ti})$ and $\nu(\text{Sn-O-Sn})$ bands will be present in the mixed film spectra, as will bands from metal-oxygen stretches due to ligand coordination. Unfortunately, because of the breadth and intensity of these bands, it is difficult to identify the presence of a $\nu(\text{Ti-O-Sn})$ band in any of the mixed valerate film spectra. Additionally, the FTIR spectra of 50:50 films made from alkoxides which were heated together (Method 2) and the spectra of films made by mixing individually polymerized alkoxides (Method 3) are not significantly different from that shown in Figure 4.1c. FTIR spectra of the three 50:50 mixed films calcined at $250\text{ }^{\circ}\text{C}$ are also indistinguishable from one another (not shown) and again, no bands could be

Normalized Absorbance

Figure

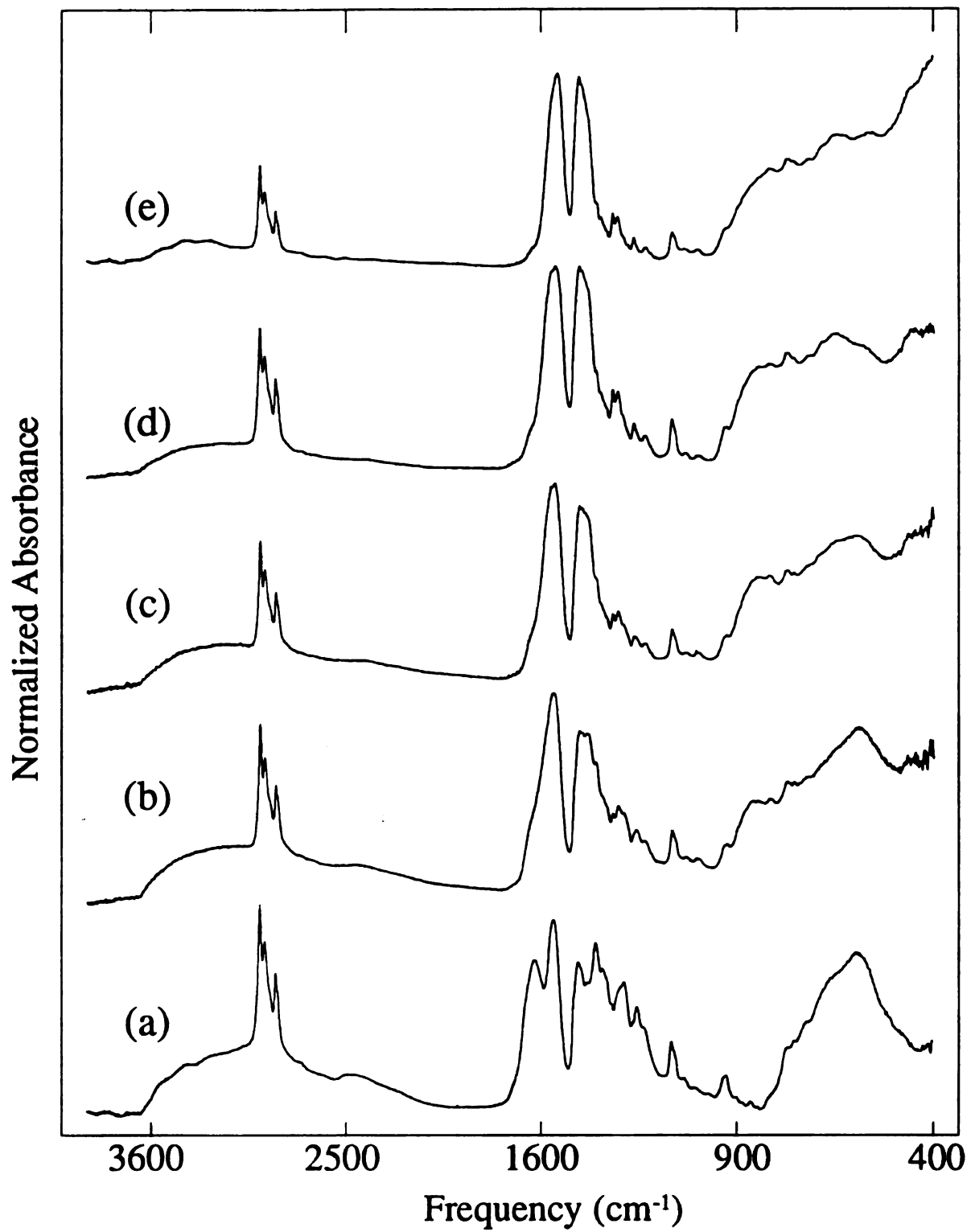


Figure 4.1 FTIR spectra of valerate films: (a) SnVal, (b) STVal, (c) EMVal, (d) TSVaI, and (e) TiVal.

identi

al. [3

synth

stretc

not s

they

resul

the e

O 1s

529.

two

sepa

(this

have

peak

(530

2p_{3/2}

Ti v

occe

inhe

identified that were not present in the TiC250 and SnC250 film spectra. Nakabayashi *et al.* [3] used Raman spectroscopy to study the formation of mixed TiO₂-SnO₂ powders synthesized by coprecipitation of metal alkoxides and reported that bands due to Ti-O-Sn stretches were present between 770 and 430 cm⁻¹. These bands were very broad so it is not surprising that we are unable to isolate these stretches in the FTIR spectra, though they occur in the frequency range we are scanning and should be infrared active. These results are inconclusive and indicate that this is not a promising approach for evaluating the extent of mixing.

XPS analysis was also explored as a method for evaluating film homogeneity. The O 1s binding energies for backbone oxygen in SnVal and TiVal films are 530.6 eV and 529.7 eV, respectively. This separation should be adequate to distinguish between the two peaks, if tin valerate and titanium valerate polymers have polymerized completely separately. Assuming equal intensities and a FWHM of 2 eV for each of the O 1s peaks (this is the FWHM usually measured for single metal films), the combined peak would have a FWHM of 2.25 eV, an increase of >12 %. Curve fitting the backbone oxygen O 1s peak for all 50:50 mixed films shows a reasonable fit with only one backbone O 1s peak (530.2 eV). In the mixed films, ratios of the O 1s FWHM to that of the Sn 3d_{5/2} and Ti 2p_{3/2} peaks are similar (greater than but within 5%) to that measured for the pure Sn and Ti valerate and calcined films.

Several things are apparent from these results. First, some mixing must be occurring because the O 1s peaks are narrower than expected for a completely inhomogeneous mixture. Second, these results are true for 50:50 mixed films prepared

with

polym

our p

film f

The

probl

bindi

cann

the f

Thos

mixt

titan

three

meas

steep

enha

4.2.

samp

with

relat

the

with any of the three methods. This means that even when the alkoxides have been polymerized separately (Method 3) some mixing does occur. This is not surprising since our previous study of titanium valerate films indicated that polymerization occurs during film formation [21]. This technique is not useful for determining the extent of mixing. The peaks are quite featureless and there is no unique curve fitting solution to this problem. There may be a range of bonding environments and therefore a range of O 1s binding energies present in these samples.

Ti-O-Sn moieties are undoubtedly present in these films, but FTIR and XPS cannot be used to determine the extent of mixing. AR-XPS is more indirect and relies on the fact that frequently in heterogeneous mixtures, one component may surface segregate. Those films prepared by Method 3 are expected to produce the most inhomogeneous mixtures and therefore, are the most likely to show a surface enhancement of either tin or titanium. Figure 4.2 shows the result of AR-XPS study of 50:50 films prepared using the three different methods. Films prepared with Method 3 have a Ti/Sn ratio of 0.55 when measured at the surface. This ratio increases to 0.80 as the sampling depth increases. The steep gradient in the measurements suggests that there is a thin surface layer which is enhanced in tin species.

AR-XPS depth profiles of films prepared using Method 1 are also shown in Figure 4.2. First, the Ti/Sn ratio is relatively constant, ranging from 0.85 to 0.90 over the sampling depth, indicating that these films are uniform perpendicular to the film surface with only a slight surface enrichment of Sn. Second, the Ti/Sn ratio is close to 1, the relative concentration of the two alkoxides used to prepare the films. Since the films have the expected bulk composition throughout the near surface region, this is another

Figure 4

indicated

the depth

measured

XPS results

are more

This study

two results

and T.

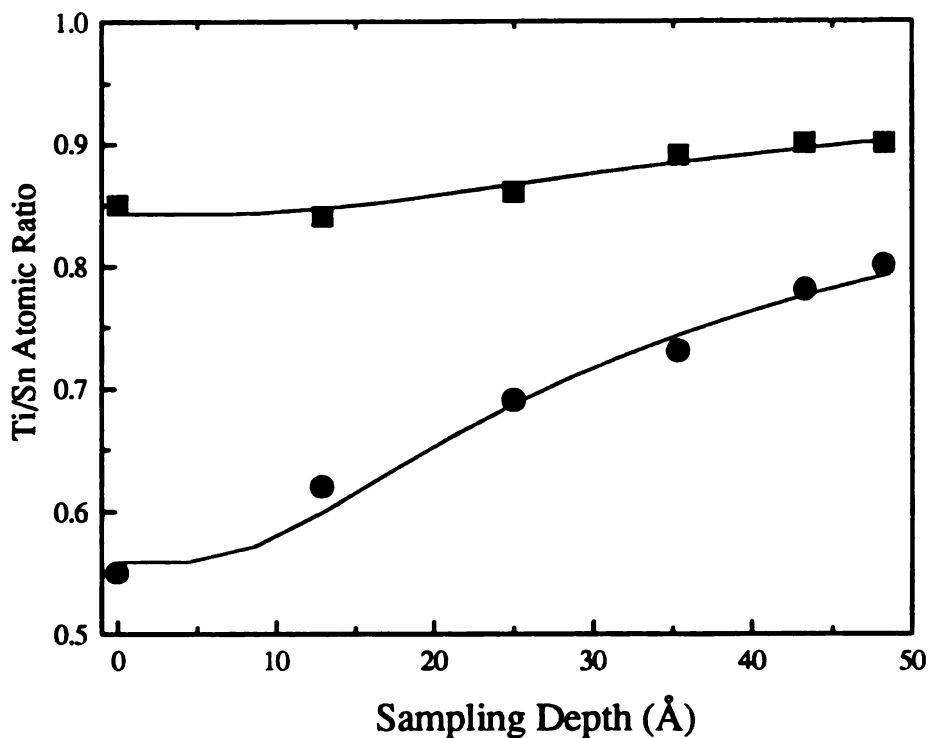


Figure 4.2 AR-XPS analysis of 50%Ti 50% Sn valerate films prepared using Methods 1 and 2 ■ and using Method 3 ●. The curves represent the best fit to the model.

indication that the films are well mixed. In addition, there is no significant difference in the depth profiles of films prepared from Methods 1 and 2. This shows that there is no measurable benefit to refluxing the alkoxides together before hydrolysis. Overall, AR-XPS results indicate that films prepared by mixing the alkoxides together before hydrolysis are more homogeneous than those obtained from a mixture of the hydrolyzed solutions. This suggests that the hydrolysis rates of the two carboxylated alkoxides may be similar.

These films can be modeled most simply by considering that they are comprised of two regions: an enriched surface layer and the bulk. The thickness of the surface layer (d) and Ti/Sn ratio for the surface layer (R_s) can be estimated assuming exponential

attenuation of photoelectrons with depth [31]. The measured ratios (R) are related to the analysis angle (θ) by the following equation:

$$R = R_s(1 - e^{-d/\lambda \cos\theta}) + R_b(e^{-d/\lambda \cos\theta}) \quad 4.2$$

Estimates can be obtained by minimizing the sum of difference between the collected data and values generated using this equation. R_b is the bulk ratio and is assumed to be 1. Results show that the Method 1 films have a 15 Å surface layer with $R_s = 0.85$ (correlation coefficient: 0.97) and the Method 3 films have a 10 Å surface layer $R_s = 0.56$ (correlation coefficient : 0.99).

The reason for the surface enhancement of Sn is not readily evident and the identity of the Sn species at the surface is not clear, though the Sn $3d_{5/2}$ binding energy (486.8 eV) is the same as that in the bulk and consistent with a Sn^{4+} oxide. As determined with AR-XPS, levels of hydroxyl groups and carboxylate groups are lower when measured at film surfaces than when a deeper cross-section of the film is analyzed. Backbone oxygen (oxide) concentrations do not change with analysis depth. This means that the surface is reduced but this may only reflect the sensitivity of the surface to x-ray induced photoreduction [22] and not the true nature of the surface species. Possibly the segregation is related to the relative concentration of uncondensed species in the film solutions. These species may rise and condense at the surface during the spin casting process. In solutions prepared using Method 1, the alkoxides are intimately mixed and hydrolyzed together so the relative concentration of uncondensed Sn and Ti species may be similar. In the separately hydrolyzed solutions (Method 3) the concentrations may be dissimilar, ultimately resulting in films with an enhanced surface concentration of Sn.

Based upon these results, for the remainder of this study mixed oxide films are prepared using Method 1. Before examining the mixed $\text{TiO}_2\text{-SnO}_2$ films, the characteristics of the single metal oxide films will be established.

4.4.2 Effect of Calcination Temperature on Titanium Valerate Films.

Calcined titanium valerate films contain approximately 1.85 backbone oxygen and 0.30 hydroxyl groups per Ti, as determined with XPS. Binding energies are 458.5 eV, 529.7 eV, and 531.6 eV for Ti $2p_{3/2}$, oxide O 1s, and hydroxyl O 1s peaks, respectively. Film composition and binding energies do not change significantly with calcination temperature and are the same as measured for polycrystalline TiO_2 . Though films are visually uniform, traces of Si from the quartz substrate are evident in the XPS spectra of films calcined at ≥ 600 °C. This indicates that the films are cracked. The extent of cracking, as reflected by the relative Si concentration, increases with calcination temperature. Cracks may develop due to a difference in the expansion coefficients of the substrate and the film or due to the formation of crystallites within the film.

XRD analysis indicates that TiVal films are amorphous and that crystallization occurs as a result of calcination at temperatures ≥ 400 °C. Figure 4.3 shows the XRD patterns collected between 25° and 29° (2θ) for films calcined between 250 °C and 1000 °C. Films calcined at 250 °C show no evidence of crystallinity. Those calcined at 400 °C contain anatase crystallites with an average particle size of 10 nm. Anatase crystallites are larger (average: 25 nm) after calcination at 600 °C and a weak rutile $\langle 110 \rangle$ peak indicates that there are traces of rutile crystallites in this film (average size: 8 nm). These peak locations correspond to lattice constants “a” of 3.78 Å (anatase) and 4.59 Å (rutile).

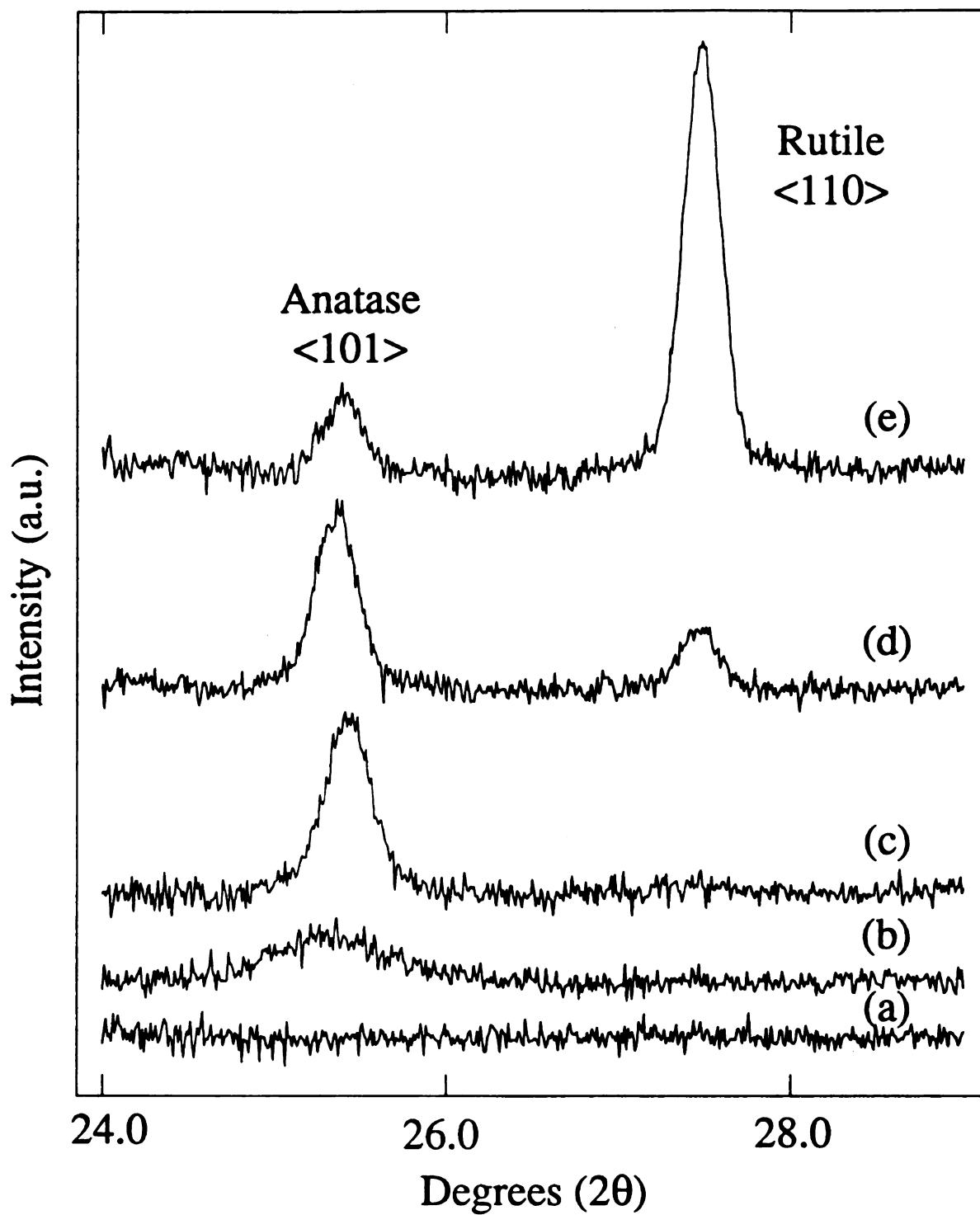


Figure 4.3 XRD patterns of calcined TiVal films: (a) TiC250, (b) TiC400, (c) TiC600, (d) TiC800, and (e) TiC1000.

These values are consistent with literature values [32]. Calcination at 800 °C results in a film which contains both anatase and rutile crystallites with average particle sizes of 25 nm and 30 nm. Calcination at 1000 °C dramatically increases the intensity of the rutile <110> peak by ~ 7 times and decreases that of the anatase <101> peak by one half, but particle sizes are approximately the same as in the TiC800 film.

Figure 4.4e shows a wider range of the XRD pattern for the TiC1000 film. The relative intensity of the <101>/<110> in polycrystalline rutile is 0.50 [33], however, in these films the ratio is 0.04. Additionally, there are no other peaks discernible in the film XRD pattern collected between 20° and 80° (2 θ). This indicates that there is a strong preferential orientation of the rutile crystallites with the <110> planes parallel to the film surface. In films calcined at lower temperatures, the <110> rutile peak and the <101> anatase peaks are the only ones present in the XRD patterns indicating strong preferential orientation for crystallites in these films as well.

Overall, the XRD results indicate anatase crystallites, largely orientated in the <101> direction, are formed when films are calcined at ≥ 400 °C. Rutile forms at temperatures ≥ 600 °C with a preferential <110> orientation and it is the predominant phase after calcination at 1000 °C. In films calcined at 1000 °C, the number of rutile crystallites dramatically increases but crystallite growth is not enhanced.

Film thicknesses and refractive indices are reported in Table 4.1. TiVal films are 386 nm thick with a refractive index of 1.66. This is similar to the refractive index of films spin cast from acidic ethanol solutions of titanium ethoxide (1.61) reported by Exarhos and Hess [17]. Titanium valerate films collapse upon calcination, however they are not completely collapsed unless calcined at ≥ 400 °C. TiC250 films are 239 nm thick with a

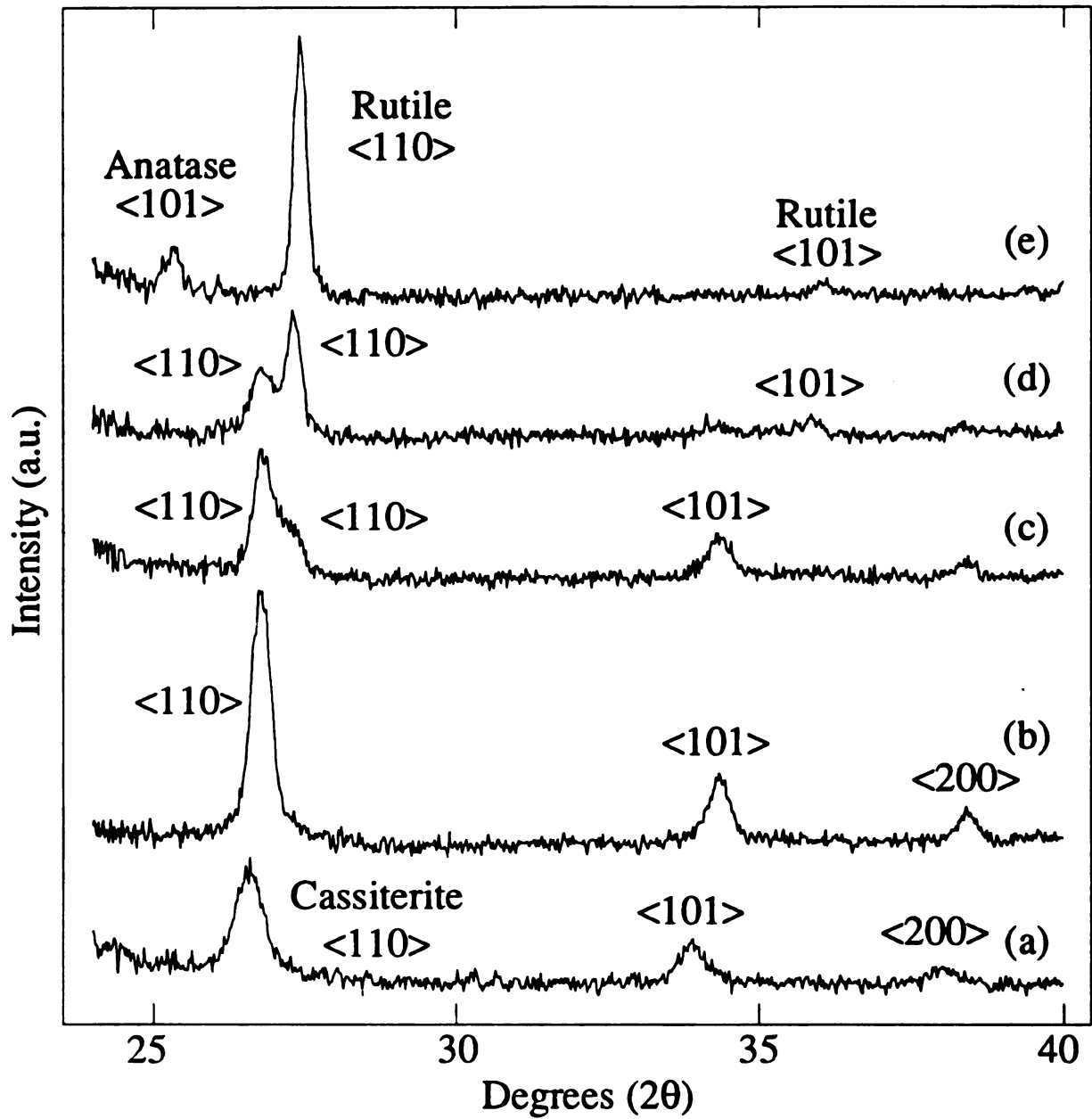


Figure 4.4 XRD patterns of films calcined at 1000 °C: (a) SnC1000, (b) STC1000, (c) EMC1000, (d) TSC1000, and (e) TiC1000.

Table 4.1 Thickness "d" (nm) and *refractive index* "n" of films as a function of composition and calcination temperature. Standard deviations are < 5% for thicknesses and < 3% for refractive indices.

Film	Ti		TS		EM		ST		Sn	
	d	n	d	n	d	n	d	n	d	n
Valerate	386	1.66	354	1.65	346	1.60	335	1.63	303	1.57
250 °C	239	2.04							237	1.75
400 °C	209	2.17	232	1.96	251	1.85	278	1.72	247	1.72
600 °C	205	2.20	231	1.95	253	1.81	252	1.80	234	1.78
800 °C	205	2.19	229	1.97	244	1.78	261	1.73	244	1.72
1000 °C	--	--	230	2.00	253	1.80	216	2.00	242	1.71

refractive index of 2.00 whereas those calcined at temperatures between 400 °C and 800 °C are ~205 nm thick with refractive indices of approximately 2.2. Accurate measurements of the thickness and refractive indices of films calcined at 1000 °C could not be obtained using ellipsometry, probably because the films were extensively fractured.

These results show that calcination at 400 °C leads to a collapse in the films of almost 50%. Dramatic collapse in sol-gel materials at such low temperatures is not uncommon, especially after such a extensive calcination time (24 h) [34]. Generally, gels collapse after the organic portions of the material have been burned away and through *in situ* FTIR studies, we found that calcination at 250 °C is adequate to do this [35]. In addition, increasing the calcination temperature above 400 °C does not cause additional collapse or change the refractive index. Brinker and Harrington [36] found that the refractive index of mixed 90% TiO₂ - 10% SiO₂ films reached the maximum value of 2.1 when calcined at 400 °C and interpreted this as indication that the films are fully densified at this temperature. This reasoning suggests that TiVal films calcined at ≥400 °C are also fully densified. This is an advantage for coating materials but a disadvantage for sensor and catalysis applications where high surface area is desired.

The refractive indices for these films are less than that reported for pure polycrystalline anatase or rutile (2.57 and 2.95, respectively [37]). This is commonly the case for sol-gel thin films [16] and may be due to the fact that these films are comprised of a mixture of crystalline and amorphous phases [17]. These films collapse upon calcination at much lower temperatures than needed to induce crystallization. Ritala *et al.* [19] proposed that crystallization may be retarded in a dense material and this may account for

the limited extent of crystallization in these films. Highly crystalline materials are not obtained unless the films are calcined at 1000 °C.

TiVal films have a band gap of 3.5 eV and calcination narrows the gap. The band gap steadily decreases with calcination temperature from 3.4 eV for films calcined at 250 °C to 3.1 eV for films calcined at 800 °C. The band gap of the TiC1000 film is 2.8 eV (assuming film thickness of 200 nm). The trend is consistent with the formation of crystallites. Band gaps are reported to be 3.2 eV and 3.0 eV for anatase and rutile, respectively [38]. Values of 3.3-3.4 are commonly reported for TiO₂ thin films containing crystallites of either anatase, rutile, or a combination of both [14, 15].

In the films calcined at temperatures between 400 and 800 °C there is a maximum in the absorption curve at 4.85 eV (Figure 4.6e). We speculate that this is due to the presence of anatase in these films because this peak is present only in those films which are known to contain a predominant anatase phase; however, we have found no literature precedent for this. The transmittance of the films in the visible region is nearly 100% for the TiVal films and decreases from approximately 91% to 83% for films calcined at temperatures between 250 °C to 1000 °C, respectively.

4.4.3 Effect of Calcination Temperature on Tin Valerate Films.

The XPS results indicate that all calcined films have compositions and binding energies similar to that of polycrystalline SnO₂. The oxide and hydroxyl concentrations are 1.85 and 0.30 per Sn and binding energies are 486.7 eV, 530.6 eV, and 532.0 eV for Sn 3d_{5/2}, oxide O 1s, and hydroxyl O 1s peaks, respectively. Traces of Si from the quartz substrate due to film cracking are evident in films calcined at 600 °C and higher. Si 2p

peaks are more intense in the spectra of films calcined at higher temperatures, indicating that the extent of cracking increases with calcination temperature. Films calcined between 250 °C and 600 °C are conductive [35] which indicates that though SnC600 films contain cracks, cracking is not extensive enough to render them completely discontinuous.

As determined with XRD, SnVal films are amorphous. Crystallites are evident in XRD patterns of films calcined at temperatures ≥ 400 °C (Figure 4.5). Peaks are most intense in the pattern of the film calcined at 1000 °C (Figure 4.4a) and are characteristic of cassiterite, a rutile form of tin oxide. Only lines due to the $\langle 110 \rangle$, $\langle 101 \rangle$, and $\langle 200 \rangle$ planes are present in the XRD patterns between 20° and 40° (2θ). Calculation of the lattice constants results in values of 4.74 Å and 3.19 Å for “a” and “c”, respectively, which is consistent with values reported in the literature for polycrystalline cassiterite [39]. Relative intensities are different, however, and $\langle 101 \rangle / \langle 110 \rangle$ and $\langle 200 \rangle / \langle 110 \rangle$ values are 0.35 and 0.15 for the films instead of 0.80 and 0.25, respectively, reported for the powders [39]. This indicates that there is a preferred orientation for the $\langle 110 \rangle$ planes parallel to the surface of the films, though it is not as pronounced as in the calcined titanium films. The intensity of the $\langle 110 \rangle$ line increases and narrows with calcination temperature (Figure 4.5). Average particle size increases from 4 nm in films calcined at 400 °C up to 13 nm in films calcined at 1000 °C.

As reported in Table 4.1, SnVal films are 303 nm thick and have a refractive index of 1.57. Calcination at 250 °C leads to a collapse of films to ~240 nm and an increase in the refractive index to 1.74. Additional calcination at up to 1000 °C does not lead to a significant change in film thickness or refractive index. This indicates that SnVal films are densified at a very low temperature. Other researchers have reported refractive indices

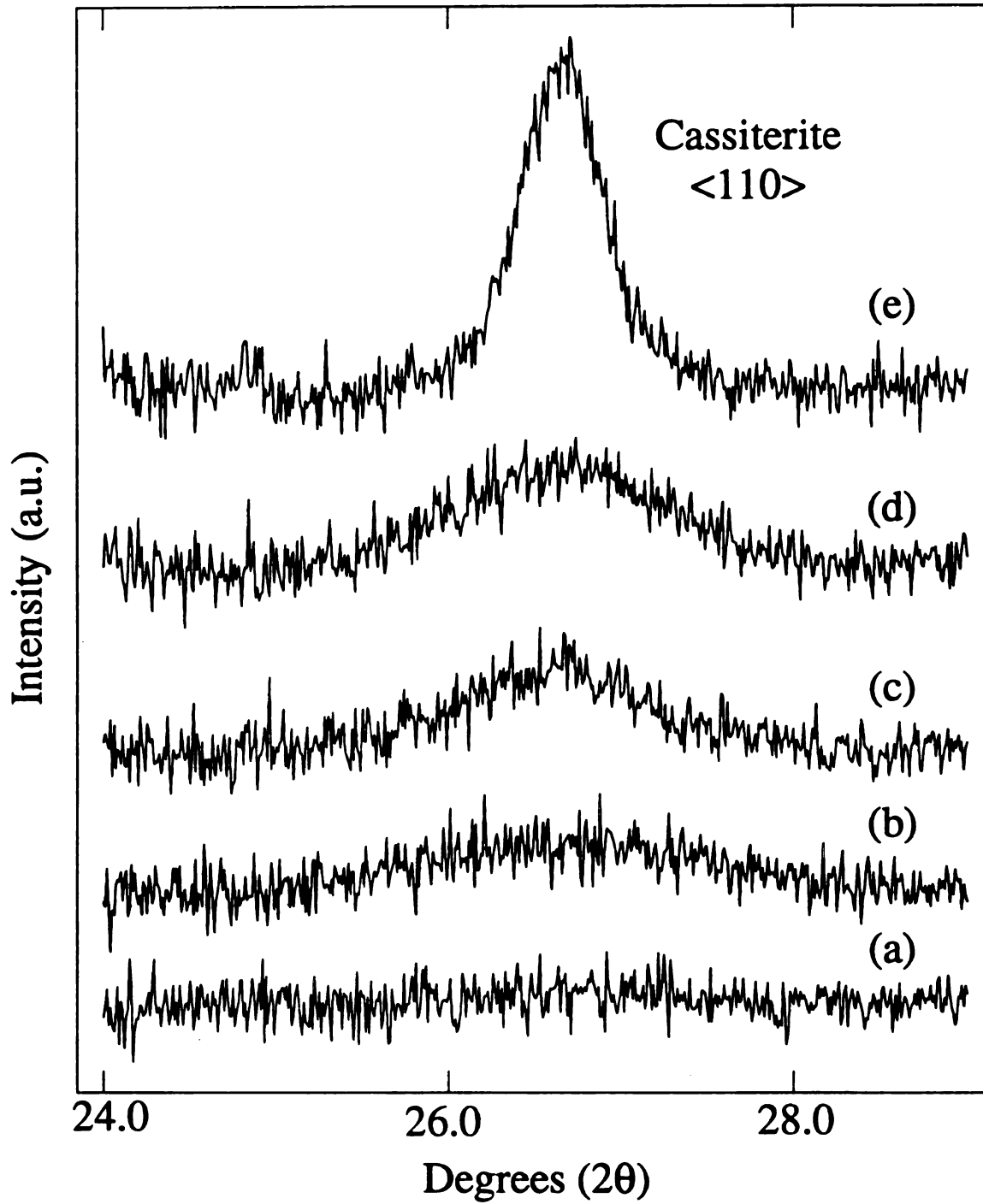


Figure 4.5 XRD patterns of calcined SnVal films: (a) SnC250, (b) SnC400, (c) SnC600, (d) SnC800, and (e) SnC1000.

between 1.8 and 2.2 for polycrystalline SnO₂ films [40, 41]. The low value measured for films in this study may reflect their largely amorphous nature. As indicated in the discussion of the calcined titanium films, densification of films at temperatures below the crystallization temperature may inhibit the formation of crystallites.

SnVal films may be thinner than TiVal films because the solutions used to prepare the SnVal films have nearly a factor of 10 higher alcohol concentration than the TiVal solutions. It is well-known that the thickness of dipcoated sol-gel films can be controlled by the addition of a solvent [34] and it may also be true for spin-coated films. TiVal films collapse almost 50% when calcined at 400 °C compared with a 20% for SnVal films. TiVal films are more highly carboxylated (1.2 valerate/Ti [21]) than SnVal films (0.26 valerate/Sn [22]) and therefore it is not surprising that the loss of the organic components of the film which occurs upon calcination would have a more dramatic effect on the TiVal film.

Preliminary results indicate that both the thickness and extent of carboxylation can be controlled by dilution with isopropanol. A TiVal film prepared from a solution with an isopropanol concentration equal to that of a SnVal solution has approximately the same valerate concentration and thickness as a SnVal film. Unlike the SnVal films, however, the extent of collapse of the TiVal film is much greater, about 35%. This suggests that while the extent of compaction is a function of the carboxylate concentration, it is also a function of the metal in the film.

Analysis of the UV-Vis spectra of these films shows that the optical band gap of the valerate film is 3.8 eV while all calcined films have a band gap of approximately 2.8

eV. The band gap for cassiterite is reported to be 3.6 eV [42]. Other researchers [43, 44] have found that amorphous tin oxide films have smaller band gap energies than crystalline films and thus our low value (2.8 eV) may be another indication of the largely amorphous nature of these films. Melsheimer and Ziegler [44] also reported band gap energies of ~2.8 eV for their amorphous tin dioxide thin films. The transmittance of the SnVal films and all of the calcined Sn films is >97% in the visible range.

In summary, calcination of tin valerate films leads to film collapse, but other than an increase in the extent of crystallization and the size of the crystallites, there is little change in film characteristics with calcination temperature.

4.4.4 Effect of Mixing and Calcination at 400 °C on Film Properties.

All mixed valerate films are amorphous and have flat AR-XPS depth profiles with normalized Ti/Sn ratios of approximately 0.9. XPS binding energies for Sn 3d_{5/2} and Ti 2p_{3/2} peaks are 486.8 eV and 458.5 eV, respectively. These values are similar to those measured for the single metal films and consistent with +4 oxidation states. In the mixed valerate films, binding energies for ligand (hydroxyl and carboxylate) O 1s (531.8 eV) and carboxylate C 1s (288.7 eV) do not change with composition and again are similar to those measured for the single metal films. The oxide O 1s binding energies are 529.7 eV and 530.6 eV for TiVal and SnVal films, respectively, and intermediate values are measured for the mixed films (TSVal: 530.1 eV, EMVal: 530.2 eV, and STVal: 530.3 eV). The O 1s peaks were fitted assuming only one type of backbone oxygen.

The composition of the valerate films is shown in Table 4.2. It can be seen that the valerate concentrations increase and hydroxyl concentrations decrease from SnVal to

Table 4.2 Composition of Valerate Films: Ratios of Ligands and Backbone Oxygen to Metal and Estimated Average Metal Oxidation State as Determined by Quantitative XPS Analysis

Ti:Sn	<u>Valerate</u> Metal	<u>Hydroxyl</u> Metal	<u>Backbone O</u> Metal	Metal Oxidation State
100:0	1.2	--	1.4	4.0
75:25	0.65	0.36	1.6	4.2
50:50	0.56	0.41	1.5	4.0
25:75	0.36	0.65	1.5	4.0
0:100	0.26	0.55	1.6	4.0

TiVal films. Note that these trends are consistent with the increase in isopropanol concentrations in the film solutions. Backbone oxygen concentrations are approximately the same in all films.

In calcined mixed films, the average oxide/metal and hydroxyl/metal ratios are 1.85 and 0.29, respectively, the same as in the calcined single metal films. O 1s and Ti 2p_{3/2} binding energies are unchanged by calcination. The Sn 3d_{5/2} binding energy is slightly lower in calcined films (486.6 eV), but still consistent with a +4 oxidation state. Though both SnC400 and TiC400 films contain crystallites, there is no evidence of crystallization in any of the mixed films after calcination at 400 °C. This may be an indication that the metals are well-mixed in these films or it may be that they mutually inhibit crystallization. It is not uncommon for additives to change, either inhibit or enhance, the crystallization behavior of oxides [20].

As with the single metal films, all mixed films collapse with calcination at 400 °C and increasing the calcination temperature up to 800 °C does not cause significant

additional compaction (Table 4.1). The extent of collapse does seem to be roughly correlated with the Ti (and valerate, see Table 4.2) concentration the films. TSVaI films collapse 35%, EMVaI films 28%, and STVaI films 21%.

The refractive indices of the mixed films are intermediate between those of the single metal films (Table 4.1). As with film thickness, the refractive indices of the films change dramatically upon calcination at 400 °C but there is no significant additional change with calcination up to 800 °C. Refractive indices of the mixed valerate films are all close to 1.60. Values for calcined films are 2.17, 1.96, 1.85, 1.72, and 1.72 for TiC400 TSC400, EMC400, STC400, and SnC400 films, respectively. Results show that films with refractive indices between approximately 1.7 and 2.2 can be prepared by controlling the relative Ti/Sn concentration.

The band gaps of the mixed valerate films are between those of the single metal films (3.5 - 3.8 eV) and the transmittance of all valerate films is >97% in the visible region of the spectrum. Like the Ti films, the band gaps of the mixed films tend to decrease with calcination temperature (Table 4.3). Changes in the band gap are probably related to phase changes and changes in crystallite concentration (*vide infra*).

Absorption coefficients are higher for titanium films than for tin films and mixed films have intermediate values. This can be seen in the UV-Vis spectra of the films calcined at 400 °C presented in Figure 4.6. Calcination does not change absorption coefficients in the UV region significantly, but the transmittance of the mixed films at visible wavelength tends to decrease as films are calcined at higher temperatures. In general, the transmittance decreases from approximately 95% to 85% as films are calcined

Table 4.3 Band Gap Energies for Films as a Function of Calcination Temperature and Composition.

Film	Ti	TS	EM	ST	Sn
Valerate	3.5	3.5	3.6	3.8	3.8
250 °C	3.4				2.8
400 °C	3.3	3.3	3.3	3.4	2.8
600 °C	3.3	3.2	3.1	3.5	2.9
800 °C	3.1	3.0	2.7	3.0	2.8
1000 °C	2.8	3.0	3.0	2.5	3.0

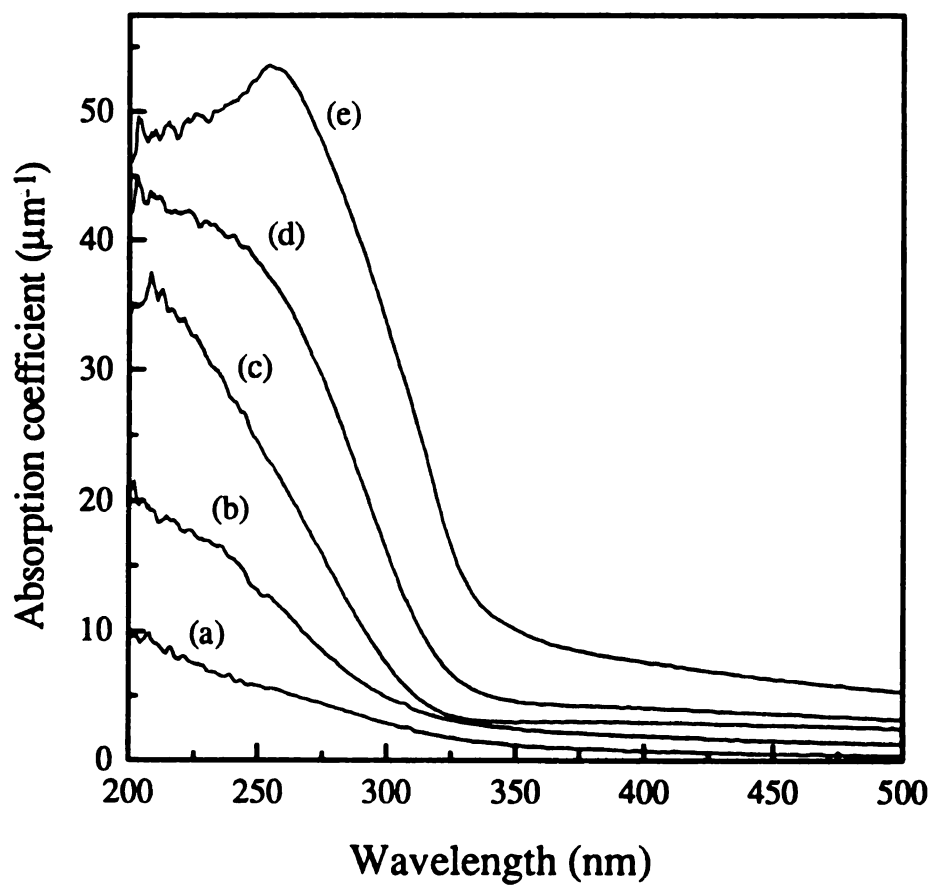


Figure 4.6 UV-Vis spectra of films calcined at 400 °C: (a) SnC400, (b) STC400, (c) EMC400, (d) TSC400, and (e) TiC400.

from 400 °C to 1000 °C. Reflections at phase interfaces, due to partial crystallization, may be responsible for decreases in measured transmittance with increased calcination temperature.

4.4.5 Effect of Mixing and Calcination at 600 °C to 1000 °C.

As with the single metal films, all mixed films calcined at ≥ 600 °C contain cracks. Si 2p peak intensity, as determined with XPS, is very low in the C600 films and increases with calcination temperature.

XRD patterns of mixed metal oxide films which have been calcined at 600 °C have broad, low intensity peaks due to small crystallites (Figures 4.7b, 4.9b, and 4.11b). Average particle sizes are less than 11 nm in all mixtures. These lines become more intense and narrower as the calcination temperature increases, but line positions do not change appreciably. This indicates that though crystallite size increases with calcination temperature and perhaps the number of crystallites also increases, no new crystalline phases develop. In all films there is no evidence of pure tin oxide (cassiterite) or titanium oxide (anatase and rutile) phases seen in the single metal oxide films.

Crystalline Mixed Oxide Phases. There are two distinct phases present in the mixed oxide films. These can be seen most clearly in the XRD patterns of films calcined at 1000 °C (Figure 4.4). The first is a Sn-rich rutile phase, similar in nature to cassiterite. The same lines are present in the STC1000 film pattern (Figure 4.4b) as in that of the SnC1000 film (Figure 4.4a) but the lines are shifted to slightly larger angles (2θ). The lattice constants "a" and "c" are 4.70 Å and 3.13 Å, respectively for the mixed phase, which are slightly smaller than those measured for the cassiterite crystallites ($a = 4.74$ Å

and $c = 3.19 \text{ \AA}$). This contraction of the unit cell is consistent with the substitution of Ti for Sn in the cassiterite lattice. Considering that lattice constants for the TiO_2 rutile phase are 4.59 \AA and 2.96 \AA , the approximate relative concentration of Ti in the lattice can be estimated assuming a linear relationship between the composition and the lattice constants. Results indicate a 25% Ti - 75% Sn mixture in these crystallites, the same relative concentration used to prepare the films.

The relative intensities of the lines indicate that the Sn-rich rutile phase has an even stronger $\langle 110 \rangle$ preferential orientation than the cassiterite crystallites in pure tin oxide films. Also crystallites are larger in the STC1000 film (20 nm) than in the SnC1000 film (13 nm) and the $\langle 110 \rangle$ peak is more than twice as intense. This suggests that the Sn-rich rutile phase is very stable.

The second phase seen in the mixed oxide films is a Ti-rich phase similar to rutile and is most apparent in the XRD pattern of the TSC1000 film (Figure 4.4d). There are only two lines present due to this phase, an intense $\langle 110 \rangle$ line and a very low intensity $\langle 101 \rangle$ line, at slightly smaller angles than seen in the TiC1000 film pattern (Figure 4.4e). Like the rutile crystallites in the titanium oxide films, the Ti-rich rutile phase has a very strong preferential orientation in the $\langle 110 \rangle$ direction. Calculated lattice constants for this phase are $a = 4.61 \text{ \AA}$ and $c = 2.98 \text{ \AA}$, slightly larger than that for rutile TiO_2 . This is consistent with the incorporation of Sn in the lattice and this phase is estimated to have a composition which is approximately 90% Ti and 10% Sn.

Sn-rich rutile crystallites develop upon calcination of ST, EM, and TS mixed oxide films and the lattice constants are the same in all films. The Ti-rich rutile phase is present

in TS and EM mixtures but is not evident in the ST films, even after calcination at 1000 °C. The lattice constant “a” for this phase is the same in TS and EM films. The intensity of the <101> line (if present) is too low to be measured in the latter films, so lattice constant “c” in these films cannot be calculated.

Our results do not suggest the formation of a continuous series of crystalline solid solutions with compositions related to the Ti/Sn ratio used to prepare the films. We see instead, the presence of two distinct phases which have the same composition in all of the mixed films. This result is different than that of other researchers who have prepared TiO₂-SnO₂ mixtures. Nakabashi *et al.*[3] studied TiO₂-SnO₂ powders produced by coprecipitation of alkoxides and found that solid solutions with variable composition were formed. As evidence of this, they show a nearly linear decrease in the rutile lattice constant “c” with increasing TiO₂ concentration. Values drop from 3.19 for the pure SnO₂ powder down to 3.05 for powders which contain only 25% SnO₂.

Takahashi and Wada [4] prepared films with CVD and also showed that the lattice constants for rutile TiO₂ and SnO₂ crystallites are a function of composition, but they found that lattice constants for each phase reached limiting values as the concentration of each oxide decreased. For the TiO₂ phase, lattice constant “a” ranged between 4.61 Å and 4.62 Å for films with TiO₂ molar percents between 75% and 25%, respectively, and “c” was ~2.98 Å in this concentration range. These values are the same as those of our Ti-rich phase (4.61 Å and 2.98 Å) as calculated from the TS films. Lattice constants for Takahashi and Wada’s SnO₂ phase range from 4.73 Å to 4.72 Å for “a” in films prepared with 75% to 25% SnO₂ and have a constant “c” of 3.17 Å. These values are larger than

those calculated for our Sn-rich rutile phase ($a = 4.70 \text{ \AA}$ and $c = 3.13 \text{ \AA}$) over this concentration range. Takahashi and Wada's films do not attain the high level of Ti incorporation in the SnO_2 phase that is present in our films.

Finally, Yoshimura *et al.* [5] studied XRD patterns of 70% TiO_2 -30% SnO_2 films calcined up to 600 °C. They found that SnO_2 was not a solid solution in TiO_2 . These films were prepared from alkoxides using sol-gel techniques; however, $\text{Ti}(\text{OPr}^i)_4$ was hydrolyzed before the addition of the tin alkoxide. This procedure may lead to a more heterogeneous mixture than the methods of other researchers.

There is no evidence of an anatase phase in any of the mixed films, though it was the predominant phase in the TiVal films calcined between 400 and 800 °C. Suwa [10] found that anatase formation was suppressed when the SnO_2 concentration was $\geq 20\%$. Other researchers have also noted that incorporation of SnO_2 suppressed the formation of anatase [2, 4]. Yoshimura *et al.* [5] reported the presence of anatase in their mixed oxide films. This may be further evidence of the heterogeneous nature of their materials.

Now that the identity of the phases in the mixed films has been established, the evolution of the films with increasing calcination temperature can be examined. Calcination of mixtures often results in surface segregation of one component. Surface segregation would have an impact on catalysis and gas sensing applications since surface reactions are fundamental to their functioning. In this final part of this paper, phase changes are correlated with film properties and with surface composition as determined with AR-XPS.

Surface Segregation and Crystallization. In the simplest scenarios, there are two ways in which the surface may become enriched in one of the metals. A surface enhancement may be seen if crystals form with a different Ti/Sn ratio than in the starting amorphous phase. This is expected to lead to flat depth profiles, elevated in either Sn or Ti, if the crystals are either larger than 50 Å and form at the surface, or if they are not within the sampling depth. Alternatively, if one of the metals migrates to the surface forming a surface layer, measured ratios would change with sampling depth, provided that the surface layer is much less than 50 Å. Estimates of layer thickness and composition are made using equation 4.2 as previously described. All fits reported have correlation coefficients of ≥ 0.97 .

As indicated previously, mixed valerate films and films calcined at 400 °C are amorphous. In all three mixtures, valerate films have a normalized Ti/Sn atomic ratio of ~0.9 and 400 °C calcination moves this ratio close to 1. Ratio changes with sampling depth (Figures 4.8, 4.10 and 4.12) may indicate that the 400 °C calcined films have a slight surface segregation of Ti but overall these films and the valerate films appear to be quite homogeneously mixed. All mixed films develop crystallites when calcined at ≥ 600 °C. The crystallinity and surface composition of these films depends upon the initial Ti/Sn ratio and the calcination temperature.

25% Ti 75% Sn (ST) Films. The Sn-rich rutile phase is the only crystalline phase evident in the ST films (Figure 4.7). Average particle sizes increase with calcination temperature with values of 7 nm, 9 nm, and 20 nm for films calcined at 600 °C, 800 °C, and 1000 °C, respectively. Peak intensities double from 600 °C to 800 °C and more than

triple from 800 °C to 1000 °C. The dramatic changes in the crystallinity of the films between 800 °C and 1000 °C may be responsible for the drop in the band gap from 3.0 to 2.5 eV (Table 4.3) and the increase in the refractive index from 1.72 to 2.00 (Table 4.1). The films also collapse about 40% more when calcined at 1000 °C than at lower temperatures (Table 4.1).

Figure 4.8 shows the results of the AR-XPS analysis of the ST films. Calcination at 600 °C leads to an surface enhancement of Ti which is 1.7 times the film ratio. The value steadily decreases almost 20% over the range of sampling depths. This decrease and the low level of crystallization in these films suggests that Ti has migrated to the surface forming a Ti rich surface layer. The thickness of the surface layer is 11 Å as calculated using Equation 4.2. The normalized Ti/Sn ratio is 1.65 for this layer which corresponds to an actual Ti/Sn ratio of 0.55. The model fits this data quite well which suggests that there is not a depletion region below the surface layer. Ti mobility and calcination time may be adequate to eliminate any depletion which may have been created by the surface segregation.

Depth profiles for the STC800 films are flatter, with average normalized Ti/Sn ratios of about 1.3. The drop in Ti concentration at the surface and the flat profile suggests that there is no Ti-rich surface layer on the STC800 films. The elevated Ti level is consistent with a depletion of Sn in the amorphous phase due to crystallization, assuming that the crystals are not forming at the surface. This also suggests that crystallites actually have a Sn concentration >75%, the concentration estimated from the lattice constants.

Calcination at 1000 °C leads to a jump in the surface Ti concentration up to over two times the expected ratio but also to ratios which drop 25% as the sampling depth is

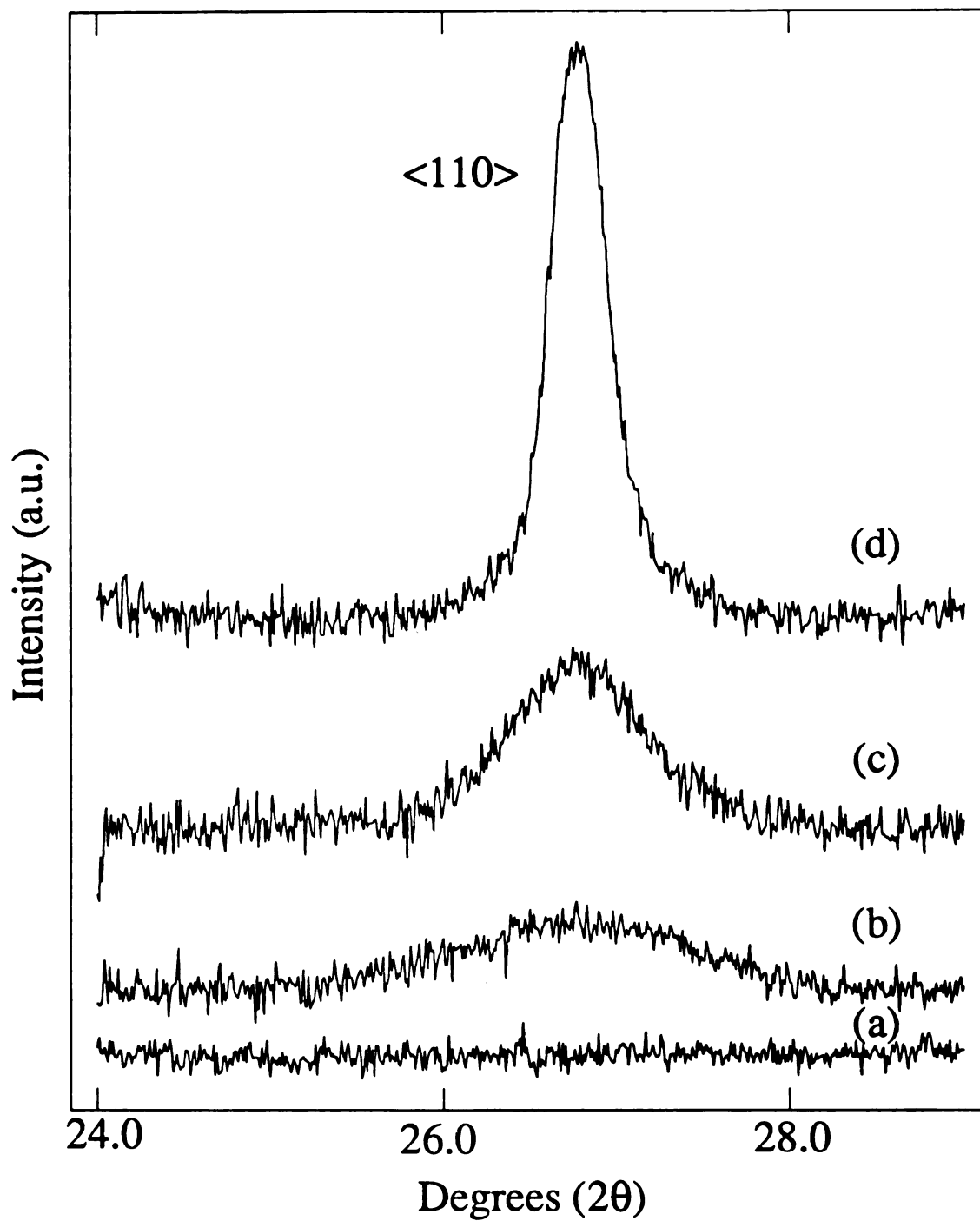


Figure 4.7 XRD patterns of calcined STVal films: (a) STC400, (b) STC600, (c) STC800, and (d) STC1000.

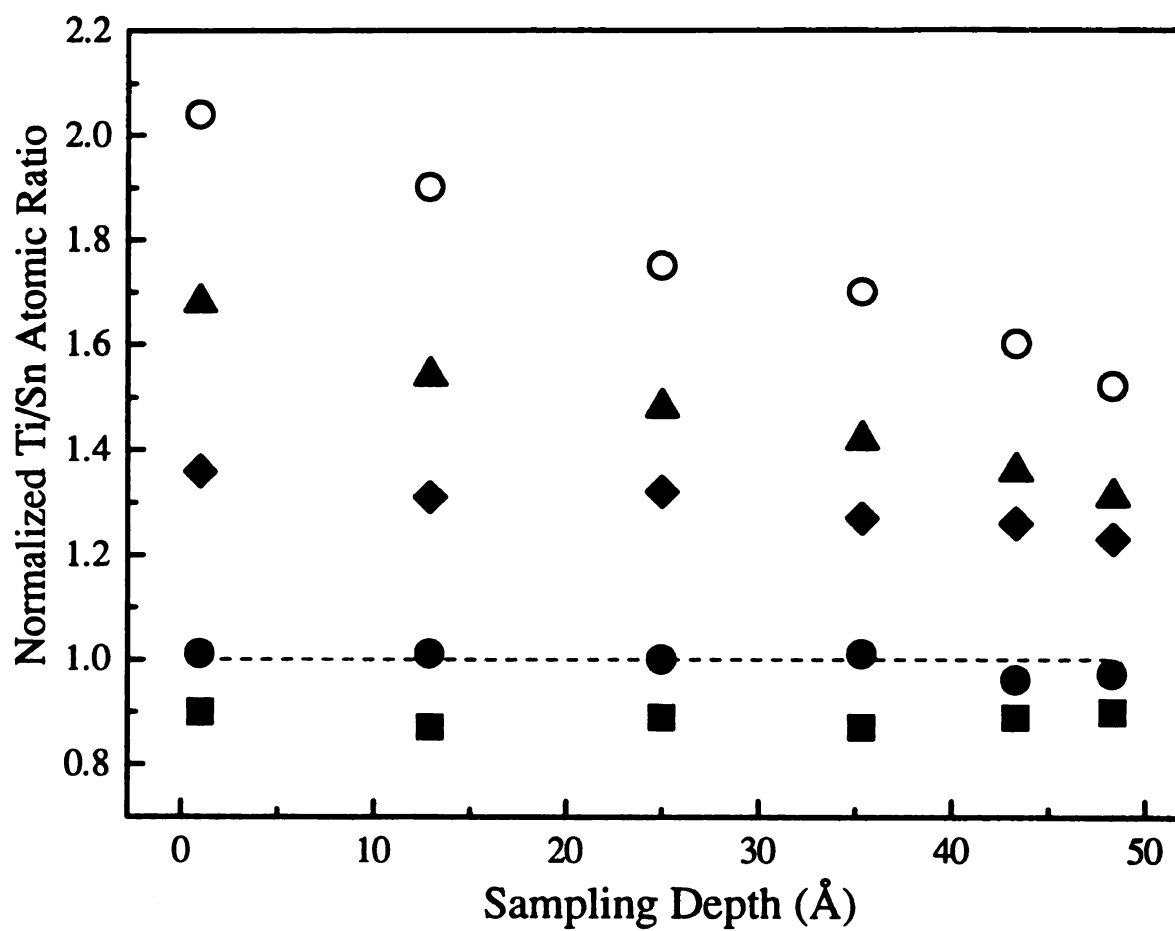


Figure 4.8 AR-XPS analysis of ■STVal, ●STC400, ▲STC600, ◆STC800, and ○STC1000 films.

increased. These elevated and rapidly decreasing levels imply not only a Ti rich surface layer, as in the STC600 films, but perhaps also an amorphous phase rich in Ti as in the STC800 films. Applying the single layer model and allowing the bulk concentration to vary indicates that the normalized surface and bulk Ti/Sn ratios are 2.0 (actual Ti/Sn: 0.67) and 1.2 (actual Ti/Sn: 0.40), respectively. The surface layer thickness is estimated to be 9 Å.

50%Ti 50% Sn (EM) Films. Only one low intensity peak is present in the XRD patterns of the EMC600 films (Figure 4.9). Whether this is a merging of the <110> peaks of the two mixed rutile phases or a single broad peak with an intermediate position ($a = 4.65$ Å) cannot be determined because the peak intensity is too low. Films calcined at 800 °C and 1000 °C contain both mixed phases. The average particles sizes are ~10 nm in the EMC800 films and 18 nm and 24 nm for the Sn-rich and Ti-rich rutile crystallites, respectively, in the EMC1000 films. As with the ST films, the intensity of the <110> peak of the Sn-rich rutile phase more than triples with the increase in calcination temperature from 800 °C to 1000 °C. Despite the difference in crystallinity, the band gap energy, film thickness (250 nm), and refractive index (1.8) are not significantly different between the EMC800 and EMC1000 films (Table 4.1).

As with the ST films, all calcined EM films have a surface enhancement of Ti and like the STC600 film, the EMC600 film may have a Ti-rich surface layer. This can be seen in Figure 4.10 where the Ti/Sn ratio is 1.5 times greater than the expected ratio and it drops about 20% over the range of sampling depths. Calculations show that this could be the result of a 6 Å surface layer with a Ti/Sn ratio of 1.5.

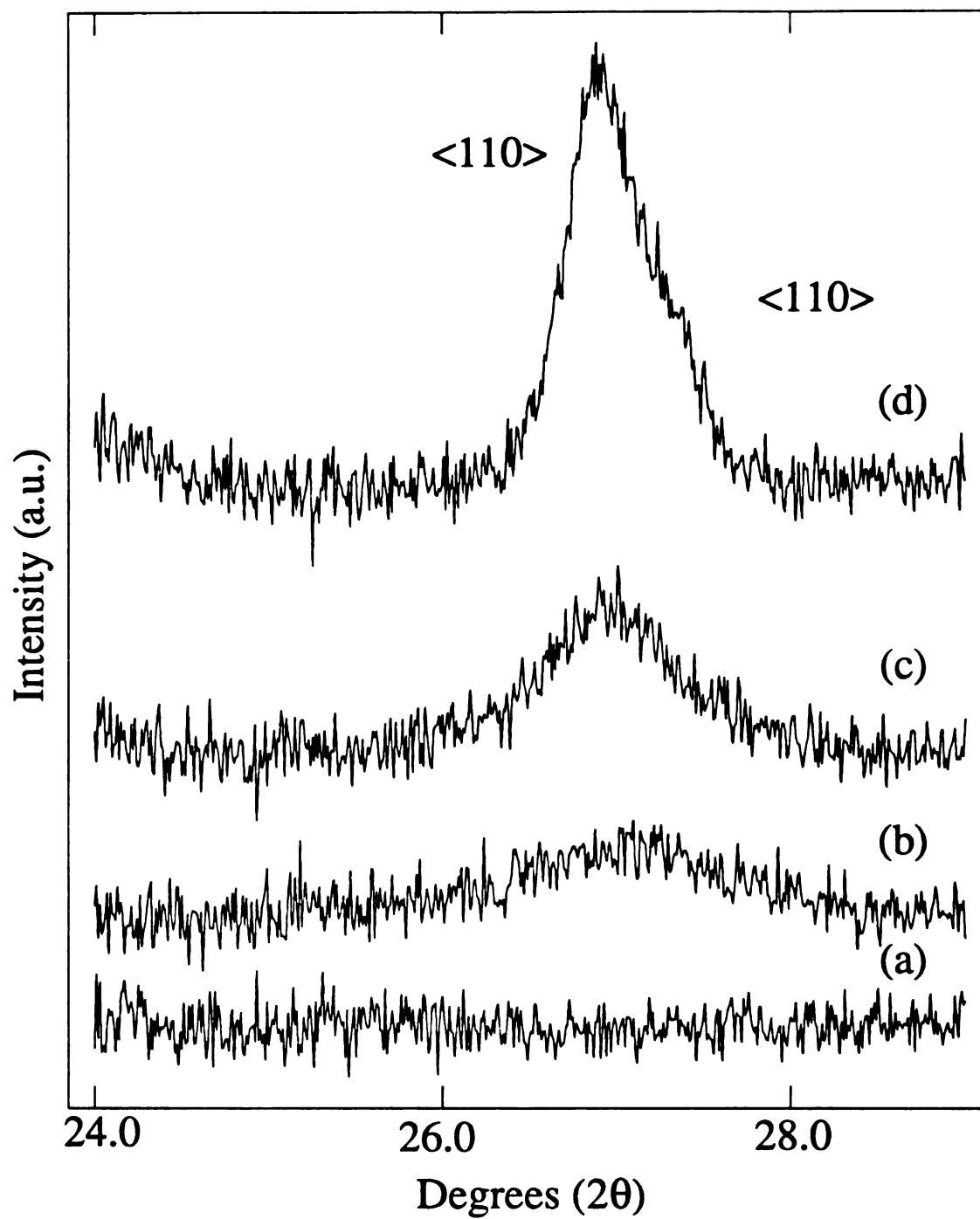


Figure 4.9 XRD patterns of calcined EMVal films: (a) EMC400, (b) EMC600, (c) EMC800, and (d) EMC1000.

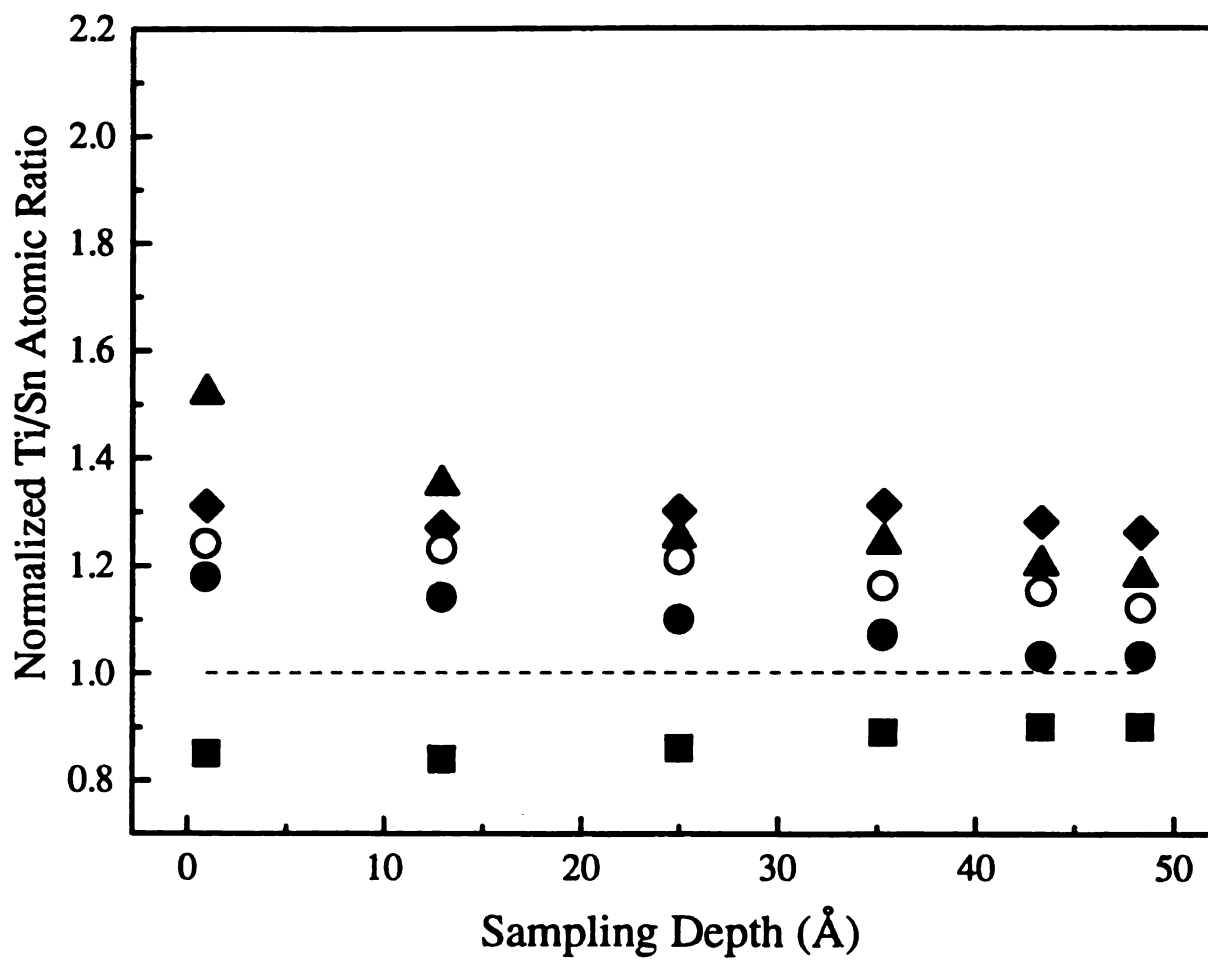


Figure 4.10 AR-XPS analysis of ■EMVal, ●EMC400, ▲EMC600, ◆EMC800, and ○EMC1000 films.

Films calcined at 800 °C and 1000 °C have similar concentration profiles. Both are flat with a relative Ti/Sn concentration of ~1.3 throughout the surface region. The enhancement of Ti is not as great in these films as in the ST films, probably because both phases are crystallizing, leading to less of a Sn depletion in the amorphous phase. Ti is enhanced because the predominant crystalline phase is the Sn-rich one. As with the ST films, this implies that crystallites are not forming at the film surface.

75% Ti 25% Sn (TS) Films. XRD patterns for the TS films are shown in Figure 4.11. Only the Ti-rich rutile phase is evident in the films calcined at 600 °C and 800 °C. Average particle sizes increase from 11 nm up to 14 nm with a tripling of the <110> peak intensity over this temperature range. Films calcined at 1000 °C contain both mixed rutile phases. Both particle size and intensity of the <110> peak of the Ti-rich rutile phase double upon increasing the calcination temperature from 800 °C to 1000 °C. Sn-rich rutile crystallites average about 21 nm. Like the EM films, the band gap energy, film thickness (230 nm), and refractive index (2.0) are not significantly different between the TSC800 and TSC1000 films, despite the difference in crystallinity.

None of the films calcined at ≥ 600 °C show any evidence of a Ti rich surface layer (Figure 4.12). The depth profiles are flat and the relative concentration of Ti/Sn is the same as it is in the uncalcined films. There may not be a strong driving force for Ti to form a surface layer, since it is the majority component of the films.

Crystallization depletes the amorphous phase of the predominant component of the crystallites. In the case of the TSC600 and TSC800 films, Ti should be depleted in the amorphous phase and this may be reflected in the Ti/Sn ratios. Apparently the crystallites

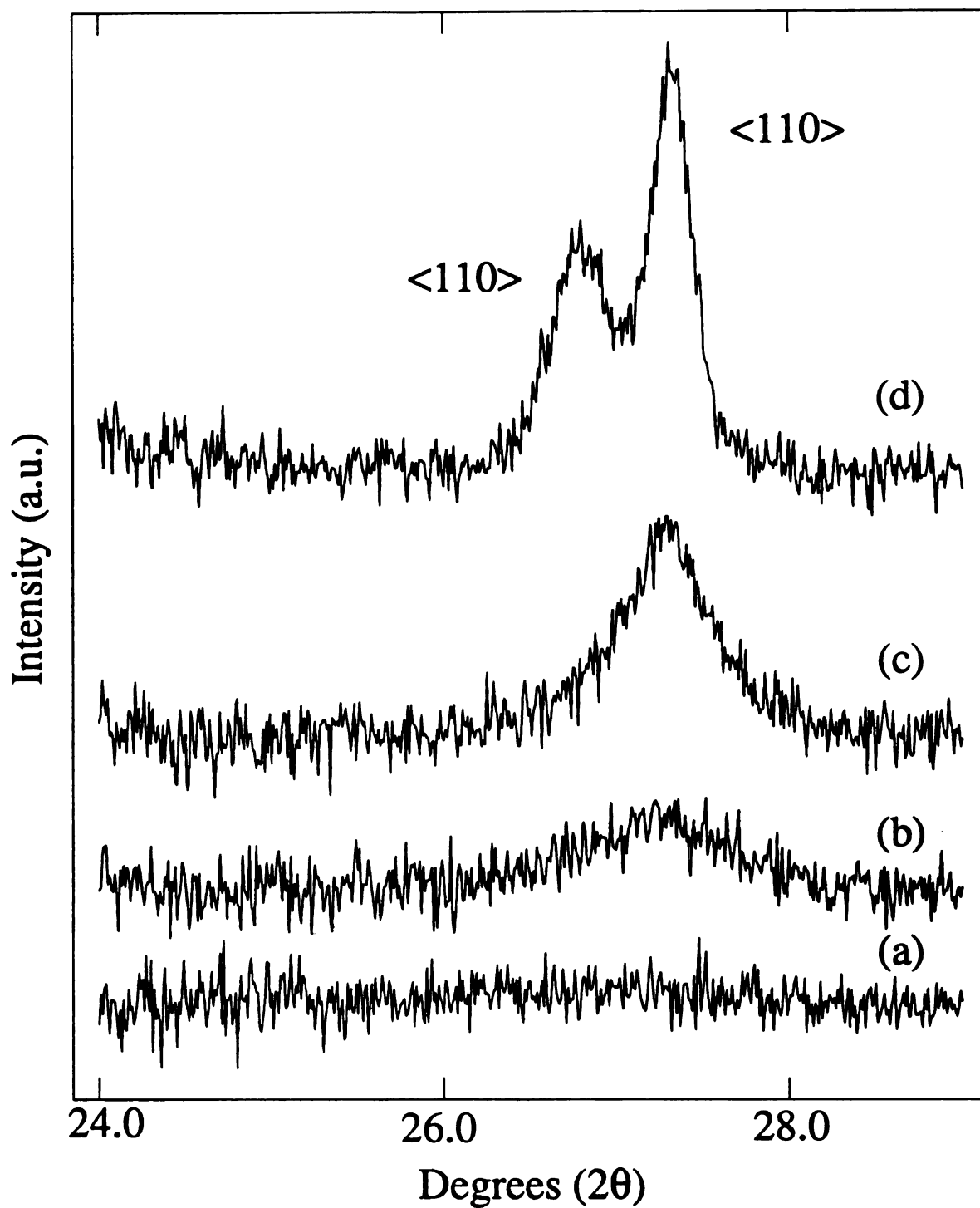


Figure 4.11 XRD patterns of calcined TSVal films: (a) TSC400, (b) TSC600, (c) TSC800, and (d) TSC1000.

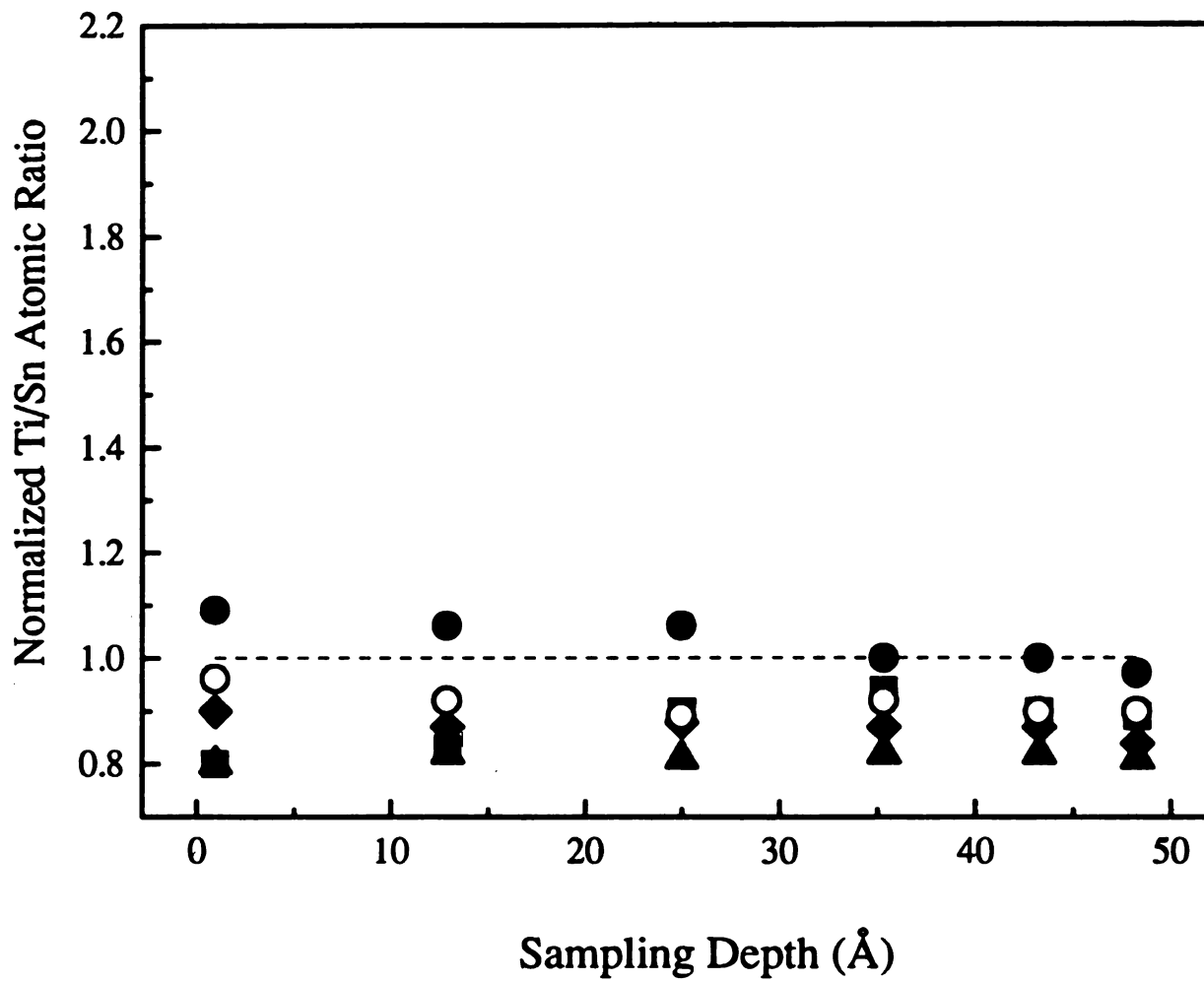


Figure 4.12 AR-XPS analysis of ■TSVa1, ●TSC400, ▲TSC600, ◆TSC800, and ○TSC1000 films.

are fairly homogeneously distributed in the films since there is no significant shift in the vertical distribution of Sn and Ti in the near surface region of the films upon crystallization. Both phases are present in the TSC1000 films and these samples also show little surface enrichment.

4.5 Concluding Remarks

In all calcined films, if a surface layer is formed, it is always enriched in titanium oxide. Our results show that titanium is mobile in films even at 400 °C and tends to surface segregate when films are calcined. According to Seah [45], surface segregation of a component in a mixture is the rule rather than the exception. Lowering the surface free energy is the driving force for the segregation and mobility generally increases with temperature. In relation to this and as a final comment on the study of methods presented at the beginning of this paper, EM films prepared using either Method 1 or Method 3 are indistinguishable with our analysis techniques when they are calcined at temperatures \geq 600 °C. This indicates that at these temperatures, Ti is mobile enough for the films to reach the same (apparently) thermodynamically stable configuration, despite the initial surface enhancement of Sn present in films prepared with Method 3.

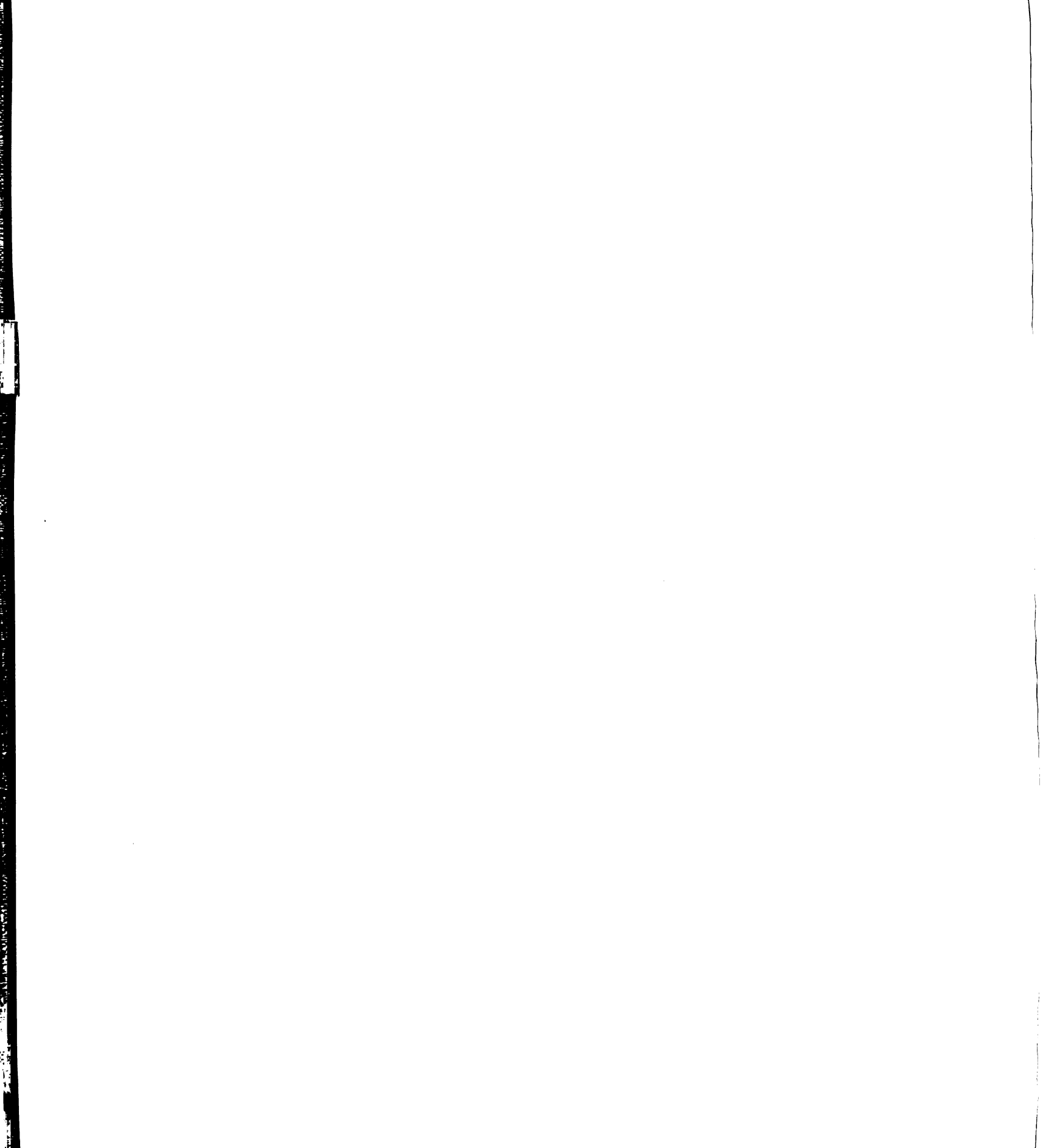
We have shown through this study that homogeneously mixed metal oxide films can be prepared using our modified sol-gel approach. These materials can be calcined at temperatures up to 400 °C without significant crystallization, cracking or surface segregation occurring. The films are highly transparent to visible light, are completely densified, and can be prepared with a range of refractive indices.

Other researchers have found that Sn-Ti oxide materials have interesting catalytic and gas sensing properties [2-8]. Unfortunately for semiconductor gas sensing applications, preliminary results indicate that while tin oxide films calcined between 250 °C and 600 °C are conductive, titanium oxide and mixed oxide films are not. This is surprising since other researchers have shown that TiO_2 and mixed $\text{TiO}_2\text{-SnO}_2$ materials can be conductive [4, 5]. It is known that conductivity in wide band gap semiconductors is due to the presence of defects within the gap and preliminary results show that H_2 reduced TiO_2 films are conductive. Further research is needed to determine if the mixed $\text{TiO}_2\text{-SnO}_2$ films can also be made conductive through a reductive treatment.

4.6 References

1. Hubert-Pfalzgraf, L.G. *New J. Chem.* **1987**, *11*, 663.
2. Itoh, M.; Hattori, H.; Tanabe, K. *J. Catal.* **1976**, *43*, 192.
3. Nakabayashi, H.; Nishiwaki, K.; Kakuta, N.; Ueno, A. *Nippon Kagaku Kaishi* **1991**, *1*, 13.
4. Takahashi, Y.; Wada, Y. *Yogyo-Kyokai-Shi* **1987**, *95(9)*, 864.
5. Yoshimura, N.; Sato, S.; Itoi, M.; Taguchi, H. *Sozai Busseigaku Zasshi* **1990**, *3*, 47.
6. Chung, W.-Y.; Lee, D.-D.; Sohn, B.-K. *Thin Solid Films* **1992**, *221*, 304. Chung, W.-Y.; Lee, D.-D.; Choi, D.-H. *Sens. Actuators B* **1993**, *13-14*, 517.
7. Nakajima, A. *J. Mater. Sci. Lett.* **1993**, *12*, 1778.
8. Maddalena, A.; Dal Maschio, R.; Dire, S.; Raccanelli, A. *J. Non-Cryst. Solids* **1990**, *121*, 365.
9. Hubert-Pfalzgraf, L. G. *New J. Chem.* **1987**, *11(10)*, 663.
10. Suwa, Y.; Kato, Y.; Hirano, S.; Naka, S. **1982**, *31*, 955.
11. Mackenzie, J.D. in *Ultrastructure Processing of Glasses, Ceramics, and Composites*, Hench, L.L.; Ulrich, D.R., Eds.; John Wiley & Sons: New York, 1984, p. 15.
12. Lee, W. G.; Woo, S.I.; Kim, J. C.; Choi, S.H.; Oh, K. H. *Thin Solid Films* **1994**, *237*, 105.
13. Battiston, G. A.; Gerbasi, R.; Porchia, M.; Marigo, A. *Thin Solid Films* **1994**, *239*, 186.
14. Meng, L.; Andritschky, M.; dos Santos, M. P. *Thin Solid Films* **1993**, *223*, 242.
15. Radecka, M.; Zakrzewska, K.; Czernastek, H.; Stapinski, T. *Appl. Surf. Sci.* **1993**, *65/66*, 227.
16. Langlet, M.; Walz, D.; Marage, P.; Joubert, J. C. *Thin Solid Films* **1992**, *221*, 44.
17. Exarhos, G.J.; Hess, N. J. *Thin Solid Films* **1992**, *220*, 254.

18. Ritala, M.; Leskelä, M.; Nykänen, E.; Soininen, P.; Niinistö *Thin Solid Films* **1993**, *225*, 288.
19. Ritala, M.; Leskelä, M.; Niinistö, L.; Haussalo, P. *Chem. Mater.* **1993**, *5*, 1174.
20. Eskelinen, P. *J. Solid State Chem.* **1993**, *106*, 213.
21. Severin, K. G.; Ledford, J. S.; Torgerson, B. A.; Berglund, K. A. *Chem. Mater.* **1994**, *6*, 890.
22. Severin, K.G.; Ledford, J. S. *Langmuir* **1995**, *11*, 2156.
23. Re, N. *J. Non-Cryst. Solids* **1992**, *142*, 1.
24. Babonneau, F.; Doeuff, S.; Leautic, A.; Sanchez, C.; Cartier, C.; Verdaguer, M. *Inorg. Chem.* **1988**, *27*, 3166.
25. Hampden-Smith, M.J.; Wark, T.A.; Rheingold, A.; Huffman, J. C. *Can. J. Chem.* **1991**, *69*, 121.
26. Mehrotra, R.C.; Mehrotra, A. *Inorg. Chim. Acta Rev.* **1971**, *5*, 127.
27. Software provided by Dr. Andrew Proctor, University of Pittsburgh, Pittsburgh, PA.
28. Seah, M. P.; Dench, W.A. *Surf. Interface Anal.* **1979**, *1*, 2.
29. Scherrer, P. *Gött. Nachr.* **1918**, *2*, 98.
30. Mott, N. F.; Davis, E. A. *Electronic Processes in Non-Crystalline Materials*; Clarendon Press: Oxford, 1971.
31. *Practical Surface Analysis, Vol. 1*, Briggs, D.; Seah, M.P., Eds.; John Wiley & Sons, Inc.: New York, 1990.
32. Tang, H.; Levy, F.; Berger, H.; Schmid, P.E. *Phys. Rev. B* **1995**, *52(11)*, 7771.
33. National Bureau of Standards, Mono. 25, Sec. 7, **1969**, 83.
34. Brinker, C.J.; Scherrer, G. *Sol-Gel Science, the Physics and Chemistry of Sol-Gel Processing*; Academic Press: San Diego, 1990.
35. Severin, K.G.; Ledford, J.S. unpublished results



36. Brinker, C.J.; Harrington, M.S. *Solar Energy Materials* **1981**, *5*, 159.
37. Samsonov, G. V. *The Oxide Handbook*; IFI-Plenum: New York, 1982.
38. Kruczynski, L.; Gesser, H. D.; Turner, C. W.; Speers, E. A. *Nature* **1981**, *291*, 399.
39. Swanson; Tatge NBS Circular 539(1), **1953**, 54.
40. Lousa, A.; Gimeno, S.; Marti, J. *Vacuum* **1994**, *45(10/11)*, 1143. Virola, H.; Niinistö, L. *Thin Solid Films* **1994**, *249*, 144. Melsheimer, J.; Ziegler, D. *Thin Solid Films* **1983**, *109*, 71.
41. Meng, L.; dos Santos, M. P. *Thin Solid Films* **1994**, *237*, 112.
42. Agekyan, V.T. *Phys. Status Solidi(a)* **1975**, *43*, 11.
43. Park, S.-S.; Mackenzie, J.D. *Thin Solid Films* **1995**, *258*, 268.
44. Melsheimer, J.; Ziegler, D. *Thin Solid Films* **1985**, *129*, 35.
45. Seah, M. P. in *Practical Surface Analysis, Vol. 1*, Briggs, D.; Seah, M.P., Eds.; John Wiley & Sons, Inc.: New York, 1990, p.311.

Chapter 5

Effect of Preparation Temperature on Tin Oxide Film Reactivity

5.1 Abstract

Tin oxide films are prepared by oxidizing sol-gel derived tin valerate films at room temperature, 200 °C, 400 °C, and 600 °C. Their structures, as determined with X-ray diffraction and X-ray photoelectron spectroscopy (XPS), range from completely amorphous (films oxidized by a room temperature hydrogen peroxide treatment (SnP)) to partially crystalline (films oxidized by calcination in air at 600 °C (SnC600)). The reactivities of these films and a polycrystalline tin oxide powder are evaluated using XPS analyses before and after *in situ* H₂ reduction. Lattice oxygen (oxide) and hydroxyl groups are removed from these materials when they are heated under a flow of H₂. At temperatures ≤ 300 °C, no metal is formed and the oxide/tin ratio decreases with increasing reduction temperature. Reduction at temperatures >300 °C results in the formation of tin metal (β-tin). The degree to which films are reduced by a 300 °C reductive treatment is dependent upon the film structure. SnP films are highly reactive and are reduced to largely Sn²⁺ oxide materials by a 300 °C H₂ treatment, as indicated by surface stoichiometry and XPS valence band spectra. SnC600 films, at the other extreme, are less reactive than the polycrystalline tin oxide powder. SnC200 and SnC400 films have intermediate structures and reactivities. Reoxidation at 200 °C for 1 h. restores the

original composition and reactivity of all except the SnP films, provided the films have not been reduced to metal. Once metallic tin is formed, the films are irreversibly modified.

5.2 Introduction

Many semiconductor gas sensors respond to changes in conductivity that result from reactions occurring at the surface of a metal oxide semiconductor. Tin oxide is commonly used for the detection of reducing gases such as H₂, CO, ethanol, and hydrocarbons. One of the problems with these sensors is that reactions on tin oxide surfaces are not particularly selective. Potentially useful strategies for improving sensor selectivity can be found by analogy to selective oxidation catalysis. Like semiconductor gas sensors, catalyst performance depends upon the selectivity of reactions occurring on metal oxide surfaces [1]. It is known that lattice oxygen reactivity is one of the most important factors in the selectivity of catalysts [2- 4]. It may therefore play an important role in the selectivity of semiconductor gas sensors. In order to test this hypothesis, materials with a wide range of lattice oxygen reactivities are needed. The synthesis, characterization, and reduction properties of these materials is the focus of this study.

The approach used in this study to tailor lattice oxygen reactivity is suggested by the work of Yamazoe *et al.* [5]. They found that when the temperature was adequate for a metal oxide surface to catalytically oxidize a particular gas, it exhibited a maximum in its sensitivity for that gas. Since a different temperature is required to oxidize different gases, this results in a selectivity which is a function of the operating temperature. In our study, instead of increasing the operating temperature to increase the reactivity of the metal oxide, the reactivity of oxide materials is modified by changing their structure. A range of

structures can be obtained through oxidation of amorphous films at different temperatures. The findings of Yamazoe *et al.* [5] suggest that these materials may be sensitive to different gases.

In this study we have chosen to modify the reactivity of tin oxide since it is the semiconductor most commonly used for the detection of reducing gases. Both compressed polycrystalline tin oxide powder and film substrates are used commercially [1]. Use of thin films is advantageous since they are inexpensive to manufacture and compatible with the fabrication of microsensors. Thin films of tin oxide are conventionally prepared by reactive sputtering [6], evaporation [7], spray pyrolysis [8], or chemical vapor deposition [9]. Tin oxide films can also be prepared from tin alkoxides using sol-gel techniques [10]. Previously we have shown that this method can be used to make amorphous tin oxide films which are uniform, transparent, and stable [11]. Sol-gel synthesis is particularly advantageous because it can be used to produce materials with high surface areas and controlled porosity [12, 13], properties which are important for sensor applications. In this study, tin valerate films are synthesized using sol-gel techniques and are then oxidized at temperatures between room temperature and 600 °C to produce tin oxide films with a range of structures.

A method is needed to evaluate the lattice oxygen reactivity of the materials. Typically, temperature programmed reduction (TPR) is used to characterize the reactivity of catalysts. The information obtained using TPR is primarily of a kinetic nature, though some information can be determined about the chemical nature and environment of species in the solid, the number of species present, as well as the relative concentrations of these

species [14]. These are inferred from changes in the uptake of H_2 or in the production of H_2O as the temperature is increased.

For evaluation of oxide reactivity in this study, we have also chosen to reduce our materials at elevated temperatures under a flow of H_2 , but the reactivity is evaluated using X-ray photoelectron spectroscopy (XPS). Materials are reduced at a constant temperature between 200 °C and 400 °C in a reactor attached to the surface science instrument. XPS analysis is used to determine stoichiometry and oxidation state of tin before and after H_2 reduction. In this way changes in concentration and oxidation state of surface species can be measured directly. These surface changes may be different than those that occur in the bulk. This is important because it is surface reactions which are responsible for sensor response.

The presence of tin metal in a sample is easily identified using XPS. The binding energy of Sn $3d_{5/2}$ peak of tin metal (484.6 eV) is significantly lower than that of tin oxide (486.6 eV). Whether there is a chemical shift between the Sn 3d peaks of Sn^{4+} and Sn^{2+} oxides is a matter of active debate. Researchers have proposed that there is either no chemical shift [15,16] or a shift of 0.2 eV [17, 18] or a shift of 0.7 eV [19]. This ambiguity makes it impossible to determine the relative concentrations of Sn^{2+} and Sn^{4+} oxides in a sample from the Sn 3d peak. It has been established, however, that the oxidation state of tin can be determined from the valence band spectra of tin oxides, provided no metallic tin is present in the sample [15, 19-22]. The lowest binding energy feature in the valence band spectrum of a Sn^{4+} oxide is a non-bonding O 2p derived band at approximately 5 eV. In the spectrum of a Sn^{2+} oxide the lowest binding energy feature is at 2 eV and due to photoelectrons from antibonding Sn 5s - O 2p orbitals [19]. An

increase in the relative intensity of the peak at 2 eV is an indication of the formation of a Sn²⁺ oxide material.

In the first part of this study, the reduction properties of polycrystalline tin oxide powder are established. Then, the effect of calcination temperature on the structure and reactivity of tin oxide films is evaluated and film reactivities are compared to that of the powder. There are two important issues. First, do films prepared at different temperatures have significantly different oxide reactivities? If not, this is not a promising approach to making selective sensor materials. Second, do films undergo irreversible restructuring upon reduction? Materials which are suitable for sensors must be able to operate for long periods of time with a reproducible response to reducing gases. If the films undergo significant restructuring when reduced, this is an indication they will be unstable and unsuitable as sensor substrates. Film stability is evaluated through oxidation-reduction cycling. Potentially stable substrates are those whose reactivity is unchanged by repeated treatments.

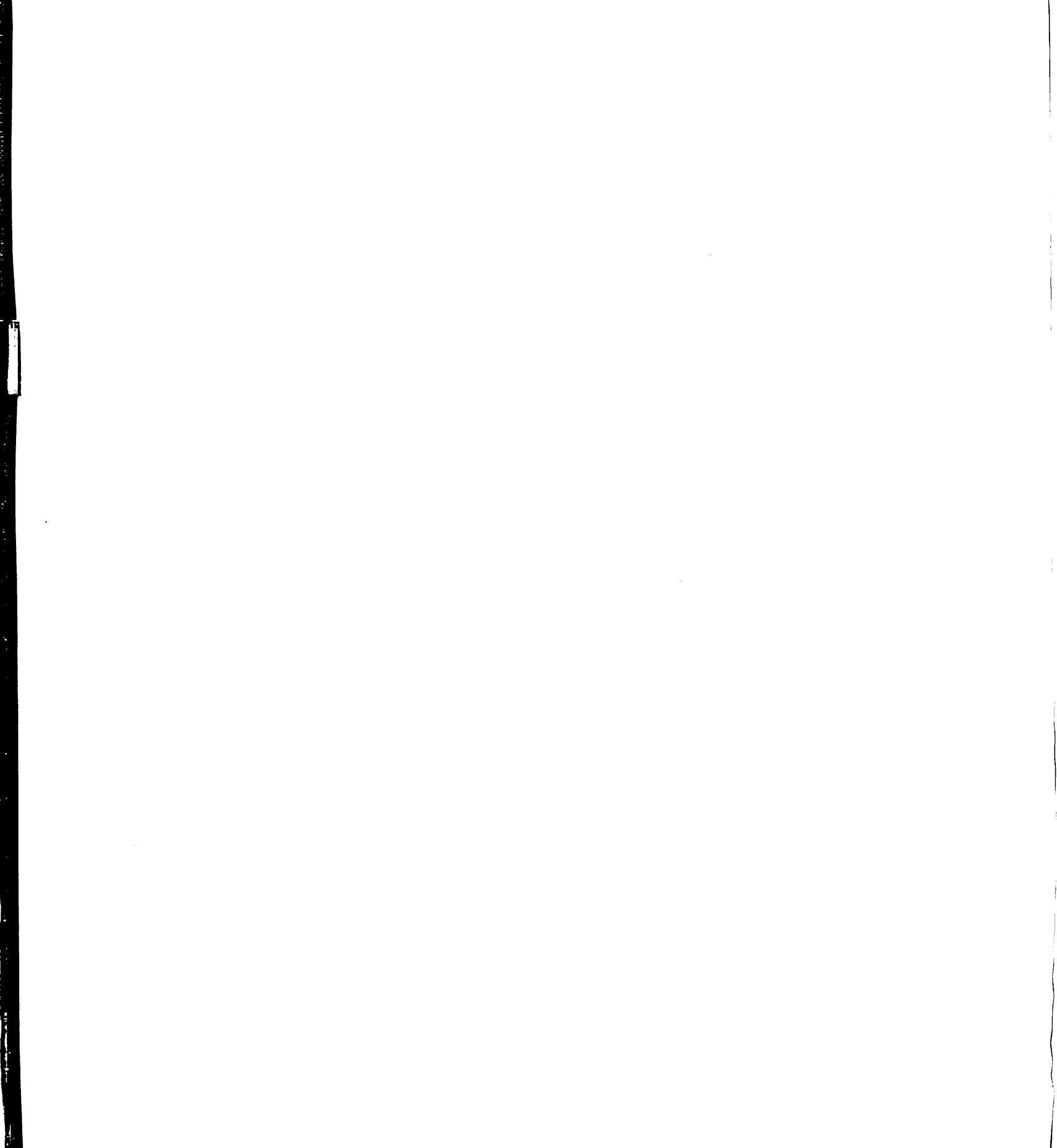
5.3 Experimental

Materials. Tin(IV) isopropoxide 10% w/v in isopropanol (Chemat Technologies), hydrogen peroxide, 30% (Baker analyzed reagent, J.T. Baker), and valeric acid (99+%, Aldrich Chemical Company) were used without further purification. Distilled, deionized water was used for all syntheses. Tin(IV) oxide (99.995+%, Aldrich Chemical Company) was pressed into pellets or suspended in absolute methanol (Photrex reagent, J.T. Baker) and spray coated with an airbrush onto quartz slides. Pellets and spray coated slides were calcined in dry air (80 cm³/min, medical grade, AGA Gas Co.) at 600°C for 4 h.

Film Preparation. The methods used to synthesize films were based on techniques developed previously [11, 23]. Films synthesized from $\text{Sn}(\text{OPr}^i)_4$ were prepared using mixtures of 40 isopropanol : 9 valeric acid : 1.5 water : 1 $\text{Sn}(\text{OPr}^i)_4$. Reactions were carried out at room temperature in capped vials in a N_2 purged glovebox. Valeric acid was added to the alkoxide followed by water. A vortex mixer was used to vigorously stir solutions following the addition of each reactant.

Freshly prepared solutions were dispersed on cleaned, acetone rinsed and dried quartz slides, spun for five minutes, and air-dried overnight. Films were oxidized using two different methods. Room temperature oxidation was accomplished by immersing “as cast” films in H_2O_2 for 4h, followed by rinsing with deionized water, and air-drying. Oxidation at temperatures between 200 °C and 600 °C was carried out by calcining films in a tube furnace under a flow of dry air (100 cm^3/min , medical grade, AGA Gas Co.) at the desired temperature for 24 h. Because a calcination temperature of at least 250 °C was necessary for removal of the organic components of the film [24], those films calcined at 200 °C were pretreated with H_2O_2 before calcination. Films were stored in a desiccator before analysis or further treatment. Unless otherwise noted, all films prepared in this study were visually transparent, colorless, and exhibited complete and uniform adhesion to quartz substrates.

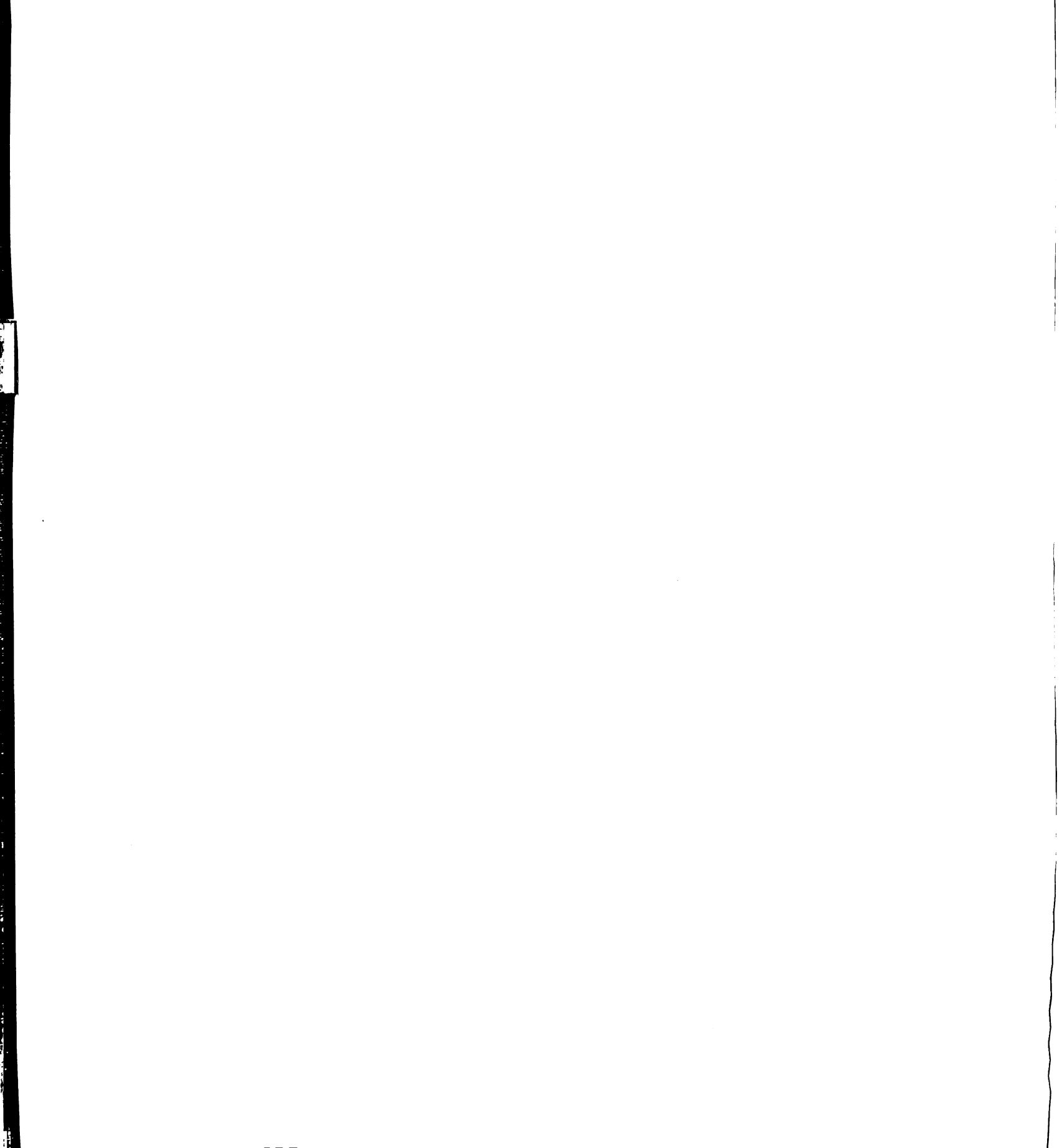
Films studied without further treatment are referred to as valerate or “as cast” films and designated with “Val” (i.e.: “as cast” film = SnVal). Films which were heated in air are referred to as calcined or tin oxide films and designated with a “C” followed by the



calcination temperature (i.e.: a film which has been calcined at 400 °C = SnC400). H₂O₂ treated SnVal films are designated as SnP films.

In Situ Heat Treatments. Oxidation and reduction of materials were carried out in a reactor attached to the surface science instrument. The reactor was equipped with a heater cartridge, a thermocouple, and temperature controller (Omega). Materials were heated for 1 h. under a flow (100 cm³/min) of the desired gas at atmospheric pressure. Unless otherwise noted, reactions were complete within 1 h. and heating for additional time did not cause further changes to samples. Reductions were carried out under pure H₂ (99.95%, AGA Gas Co.) which had been passed through water and oxygen filters. Unless otherwise specified, reductions were carried out sequentially with increasing temperature from 200 °C to 400 °C. Oxidation was performed under a dried mixture of 20% O₂ (U.H.P., Purity Gas Co.) in He (99.995%, AGA Gas Co.). Samples were allowed to cool to room temperature before the reactor was evacuated. The sample was then transferred to the main chamber for XPS analysis without intervening exposure to ambient air. XRD measurements were made within 24 h. of treatment.

X-ray Photoelectron Spectroscopy (XPS). Materials were analyzed with a VG Microtech spectrometer using a Clam2 hemispherical analyzer. All XPS spectra were collected using a Mg anode (1253.6 eV) operated at a power of 300 W (15 kV and 20 mA emission current) with an analyzer pass energy of 50 eV. Four regions were scanned for each film: C 1s, O 1s, Sn 3d, and the valence band. Binding energies were referenced to adventitious carbon (C 1s = 284.6 eV) and were measured with a precision of ± 0.1 eV. Quantitative XPS calculations were performed using empirically derived sensitivity factors



previously determined in this laboratory [11,23]. XPS peaks were fitted with 20% Lorentzian-Gaussian mix Voigt functions using a non-linear least squares curve fitting program [25]. Values reported have a standard deviation of < 10%.

X-ray Diffraction (XRD). XRD patterns of calcined films on quartz slides and tin oxide spray coated on quartz were obtained with a Rigaku XRD diffractometer employing Cu K α radiation ($\lambda = 1.541838 \text{ \AA}$). The X-ray was operated at 45 kV and 100 mA. Diffraction patterns were collected using DD and DS slit widths of 1°. Peak widths and locations were determined using a non-linear least squares curve fitting program [25] and assuming Gaussian line shapes. Particle sizes were calculated using the Scherrer equation [26] assuming no line broadening due to stress.

5.4 Results and Discussion

5.4.1 H₂ Reduction of Polycrystalline Tin Oxide.

The XPS spectrum of the polycrystalline tin oxide powder contains a single Sn 3d_{5/2} peak at 486.6 eV and O 1s peaks due to lattice oxygen (530.5 eV) and hydroxyl oxygen (532.2 eV). These binding energies are typical for tin oxides [15-22]. The surface of the powder is slightly hydroxylated with approximately 1.85 lattice oxygen (oxide) and 0.30 hydroxyl groups per tin. The valence band spectrum (Figure 5.1a) collected for this powder is characteristic of a Sn⁴⁺ oxide [15, 19 - 22]. The XRD pattern indicates that the powder consists of cassiterite crystallites [27] with an average particle size of approximately 200 nm (Figure 5.2a). Results of all analyses (including reduction studies) were similar for tin oxide pellets and tin oxide spray coated onto quartz slides.

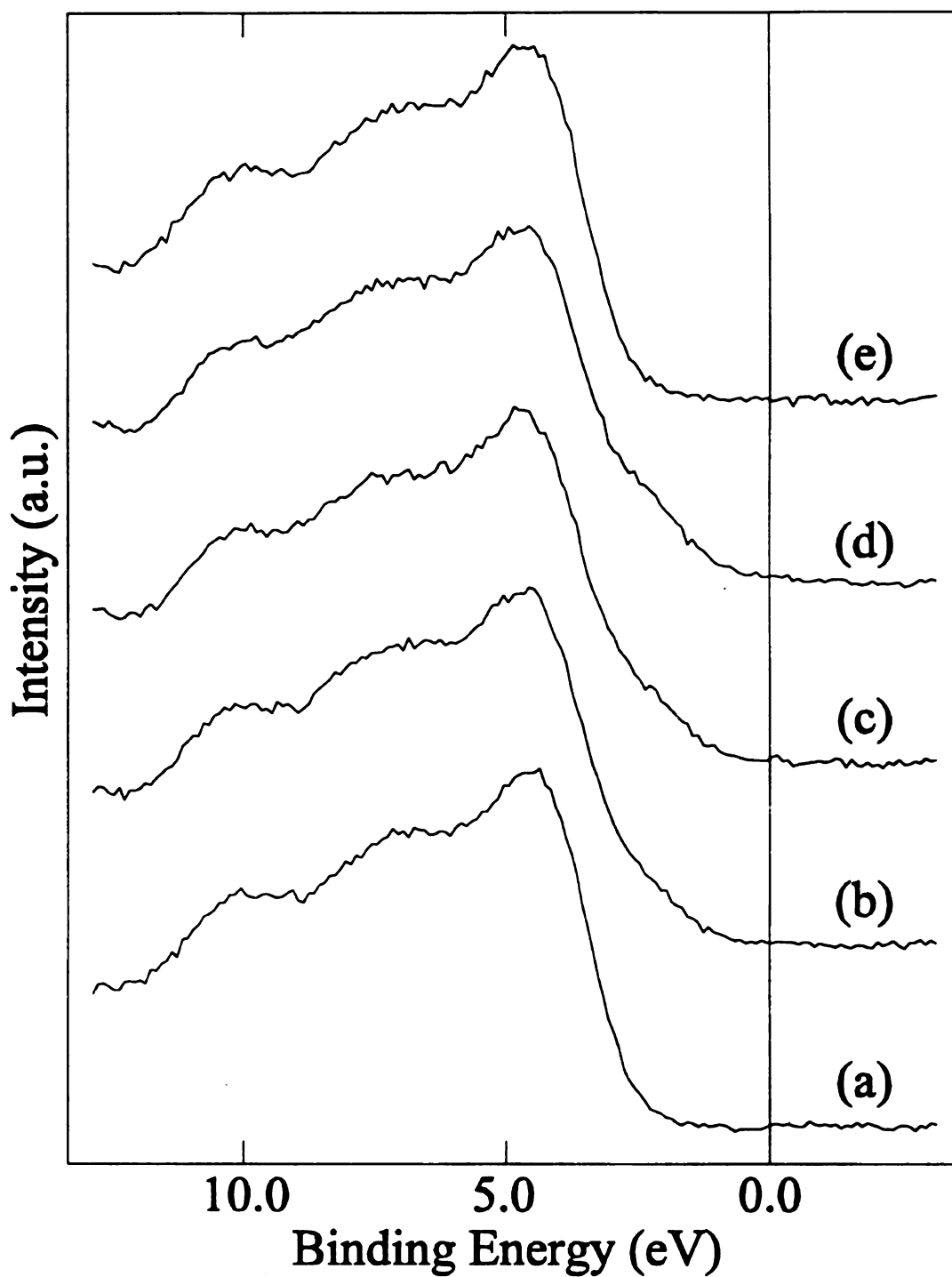


Figure 5.1 XPS valence band spectra of polycrystalline tin oxide pellet (a) initially; after sequential H₂ reductions for 1 h. each at (b) 200 °C, (c) 250 °C, and (d) 300 °C; and (e) after reoxidation in 20% O₂ (He) for 1 h. at 200 °C.

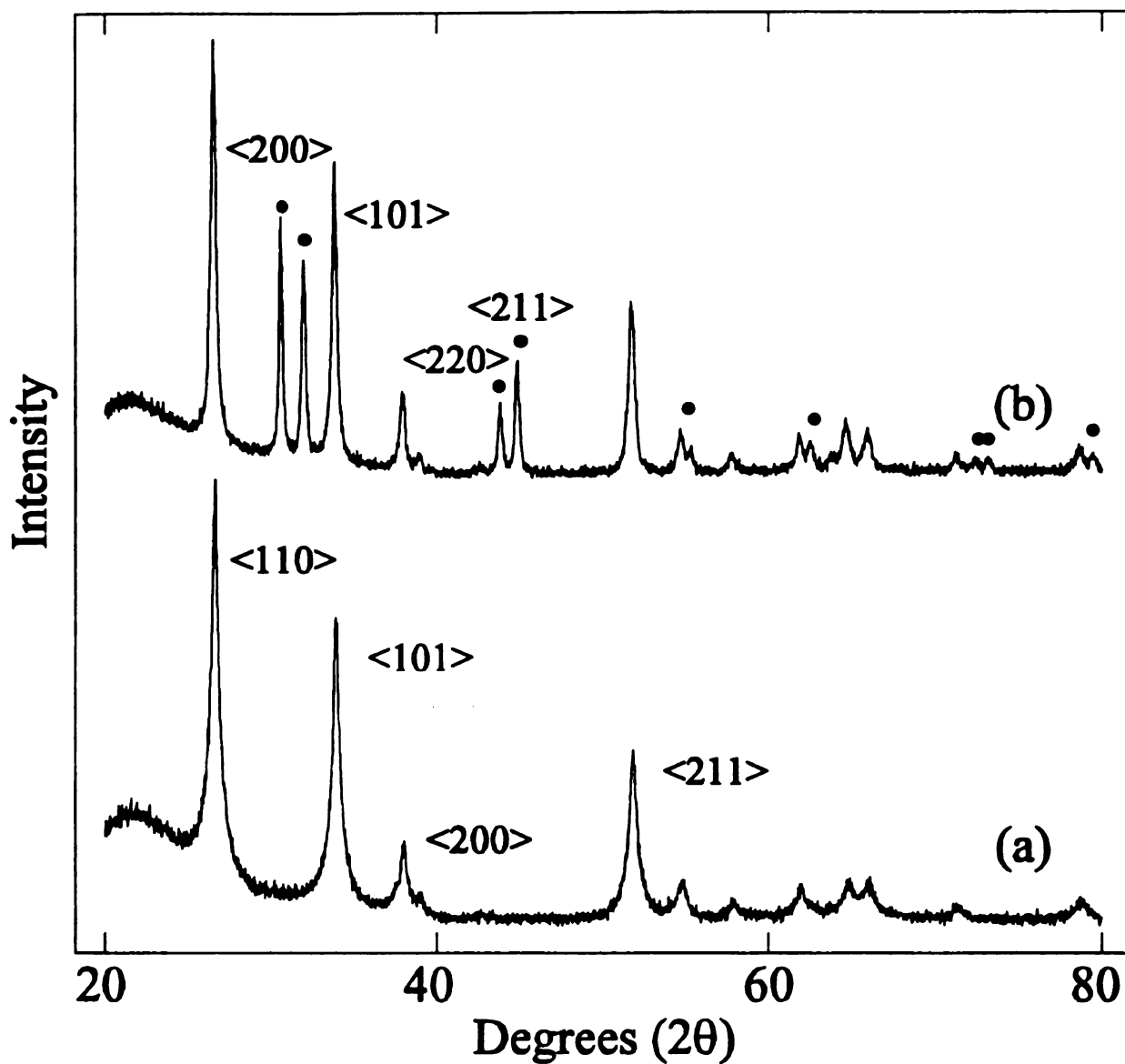


Figure 5.2 XRD pattern of polycrystalline SnO₂ (a) initially, with most intense cassiterite peaks labelled, and (b) after H₂ reduction at 350 °C for 0.5 h. Peaks due to β-tin are designated with a dot (•) and major β-tin peaks are identified.

H₂ reduction of the tin oxide powder at 200 °C leads to a reduction in the lattice oxygen concentration to 1.6 per tin, a decrease of almost 15%. The hydroxyl concentration is decreased by one half. There is no evidence of tin metal in the reduced powder and XPS binding energies have not shifted significantly with reduction. The oxidation state of tin which is inferred from the oxide and hydroxyl concentrations using charge balance calculations [11] is approximately +3.35, suggesting that the surface has been partially reduced to a Sn²⁺ oxide. Approximately one third of the tin centers are in a +2 oxidation state. The valence band spectrum (Figure 5.1b) still resembles that of a Sn⁴⁺ oxide material, but there is peak present at 2 eV which can be attributed to electrons in antibonding Sn 5s - O 2p orbitals.

Subsequent reduction at 250 °C leads to a slight additional decrease in the oxide and hydroxyl concentrations to 1.55 and 0.10 per tin, respectively. Again, there is no change in the binding energies but there is an increase in the relative intensity of the peak at 2 eV due to the presence of Sn²⁺ oxide (Figure 5.1c). Additionally, it becomes apparent that there is an increase in the intensity of a feature at 9 eV which is due to electrons in bonding Sn 5s - O 2p orbitals [19].

Reduction at 300 °C causes a decrease in the oxide concentration to 1.5 per tin with no additional decrease in the hydroxyl concentration. The binding energies of the Sn 3d and O 1s peaks decrease by 0.15 eV. If the shift in the Sn 3d binding energy is due to the increase in the Sn²⁺ concentration, the O 1s peak associated with it is also decreasing in binding energy. It is commonly noted that the separation between the Sn 3d and O 1s peaks is the same for Sn²⁺ and Sn⁴⁺ oxides and is equal to 43.9 eV [15], as seen in this

study. The charge balance calculation indicates that the surface is comprised of a 50:50 mixture of the two oxides. The valence band spectrum reflects the increased Sn^{2+} concentration in the increased intensity of the peaks at 2 eV and 9 eV (Figure 5.2d).

After the polycrystalline tin oxide powder has been reduced under H_2 at 300 °C it can be reoxidized by exposure to atmospheric oxygen at room temperature. Heating under a 20% O_2 in He mixture at 200 °C for 1 h. also restores the material to its original composition as determined with XPS. The valence band of the reoxidized pellet is shown in Figure 5.1e and is indistinguishable from the initial valence band spectrum (Figure 5.1a). Initial concentrations of oxide and hydroxyl groups are also restored by this treatment.

Thermodynamic calculations indicate that SnO_2 can be reduced to Sn metal by H_2 at 200 °C provided that the partial pressure of water is less than $\sim 10^{-2}$ torr. The only sources of water are sample and reactor outgassing, and reaction products. Water is being continuously swept out of the reactor by the flow of H_2 gas and its partial pressure is undoubtedly maintained below this level. Despite this, only a fraction of the lattice oxygen at the surface of the polycrystalline tin oxide is susceptible to H_2 reduction at 200 °C and only slightly more is removed by a 300 °C reductive treatment. Additionally, no tin metal is formed. The reason that only a limited amount of the lattice oxygen is extractable under these conditions must be due to kinetic factors.

The mobility of lattice oxygen vacancies may limit the extent of reduction. In order for lattice oxygen to react with H_2 , it has to be available at the surface. If lattice oxygen vacancies are not highly mobile at these temperatures, the reduction rate would slow down as vacancies accumulate at the surface. Kohl [28] indicates that lattice oxygen

vacancies in single crystal SnO_2 are mobile at 275 °C. Fattore *et al.* [4] studied the oxidation of propene by polycrystalline SnO_2 in the absence of gaseous oxygen at temperatures between 450 °C and 550 °C. They found that oxygen at the surface rapidly oxidized propene but once this surface oxide was depleted, the reaction slowed down dramatically. The limiting factor was determined to be the rate of lattice oxygen migration to the surface (alternatively, lattice oxygen vacancy migration to the bulk). From these results, it is certainly possible that at our reduction temperatures, between 200 °C and 300 °C, migration of lattice oxygen vacancies could play a role in limiting the oxide accessible for H_2 reduction.

Alternatively, the activation energy may be too high for the reduction of bulk SnO_2 to Sn metal or even to SnO. In that case, the oxygen which reacts may not be normal lattice oxygen but oxygen associated with a defect or non-stoichiometric site, such as a coordinatively unsaturated surface site. Oxygen in these sites is known to be more reactive than bulk lattice oxygen [2]. Additionally, reduction studies of SnO_2 single crystal (110) surfaces by Cox *et al.* [29] demonstrated that there were two types of lattice oxygen at the surface: “bridging” and “in plane” oxygen. These were found to require dramatically different temperatures for their removal under vacuum. Therefore, limited reaction can also be explained in terms of lattice oxygen with different activation energy requirements for removal.

It should be noted that increasing the reaction time does not change the oxide concentration at the surface. A constant oxide concentration is only possible if vacancies are mobile enough to maintain this concentration as the reduction continues or completely

immobile so that reduction stops. In the former case, the lattice oxygen concentration which is maintained is activation energy limited. In the latter, the oxide concentration is vacancy mobility limited. These two possibilities could be distinguished by analysis for H_2O in the exhaust gas stream. This would determine if the reduction process is continuing or stops after this oxide concentration is attained.

H_2 reduction at temperatures above $300\text{ }^\circ\text{C}$ leads to the formation of crystalline tin metal (β -tin). The XRD pattern of the polycrystalline tin oxide powder after H_2 reduction at $350\text{ }^\circ\text{C}$ for 1/2 h. is shown in Figure 5.2b. Even after reduction, cassiterite crystallites are still evident. Peaks due to β -tin are also prominent and these crystallites have an average size of approximately 250 nm. There is no evidence of the presence of any other crystalline phases, however, the sample was exposed to air before and during the XRD analysis. The size of the β -tin crystallites suggests that lattice oxygen vacancy mobility is not a limiting factor at this temperature.

Like reduction at lower temperatures, additional reaction time does not lead to a significant change in the oxide/tin ratio of the polycrystalline tin oxide. A pellet reduced for 0.5 h at $325\text{ }^\circ\text{C}$ has an oxide/tin ratio of 1.45. Increasing the reduction temperature from $325\text{ }^\circ\text{C}$ up to $350\text{ }^\circ\text{C}$ does not change this ratio, nor does doubling the reaction time. The relative concentration of metal, however, does increase with either increased treatment time or temperature. Since the oxide/tin ratio does not change with increases in metal concentration, this suggests that either a disproportionation reaction is occurring or that lattice oxygen vacancies are migrating into the bulk, maintaining a constant oxide concentration at the surface as metal forms. As stated previously, a temperature of

approximately 275 °C is necessary for diffusion of oxygen vacancies into the bulk, so the temperature is high enough for this process to occur.

Egdell [30] studied reduction of single crystal SnO₂ (110) surfaces using Ar⁺ ion bombardment (2 eV) and electron beam reduction in an attempt to create controlled lattice oxygen vacancies. They found that ion bombardment led to a SnO material but it was difficult to achieve or control intermediate stoichiometries. Irradiation with an electron beam (160 eV) resulted in the formation of tin metal. We have found that with H₂ reduction, some control over the concentration of lattice oxygen vacancies can be exerted at temperatures ≤ 300 °C without the formation of metal. The minimum oxide/tin ratio obtainable is only 1.5, not 1, as achieved with ion bombardment. H₂ reduction may be a more effective method of introducing a limited number of lattice oxygen vacancies.

5.4.2 H₂ Reduction of Tin Oxide Films

Characteristics of tin oxide films have been extensively explored previously [11, 31] and findings relevant to this discussion are briefly reiterated here. As determined with XRD, SnP films and those calcined at temperatures <400 °C are amorphous. Films calcined at 400 °C and 600 °C contain traces of cassiterite. The concentration and average size of cassiterite crystallites is greater in the SnC600 films (8 nm) than in the SnC400 films (4 nm). Those calcined at 600 °C are slightly cracked. This is inferred from the presence of a low intensity Si 2p peak in the XPS spectrum of the SnC600 films. Like the polycrystalline tin oxide powder, the surfaces of all films are hydroxylated and results of charge balance calculations show that tin in all films is in a +4 oxidation state. Calcination at 250 °C is adequate to remove all organic components of the valerate films.

Films calcined at 250 °C or higher are fully densified (collapsed 21% from the valerate film) with thicknesses of ~240 nm, as determined with ellipsometry. Films prepared at room temperature through hydrogen peroxide treatment are partially collapsed (12%) with thicknesses of 286 nm. Subsequent heating in air at 200 °C causes complete collapse to the same thickness as the film calcined at higher temperatures.

These oxide films are similar in composition to polycrystalline tin oxide and, as indicated by their valence band spectra, are electronically similar as well (Figure 5.3). The valence band has the same general shape for all materials, though the peaks are broader in the less structured materials. With an increase in calcination temperature, the materials become more uniformly structured and as a result, the features in the spectrum become more well defined.

Reduction at Temperatures ≤ 300 °C. As with the tin oxide powder, changes due to H₂ reduction are completed within 1 h. Subsequent reduction at the same temperature does not lead to significant changes in film composition.

SnP Films. Reduction of SnP films at 200 °C leads to a decrease in the oxide concentration from 1.80 to 1.38 per tin (Figure 5.4). Like the powder, changes in the valence band spectra are consistent with the formation of a Sn²⁺ oxide. Increasing the reduction temperature to 250 °C decreases the oxide concentration to 1.28 per tin and reduction at 300 °C to a material with a oxide/tin ratio of 1.18. The valence band spectrum of an SnP film after reduction at 300 °C is shown in Figure 5.5a. It is similar to valence band spectra of tin oxides with high Sn²⁺ concentrations reported by other researchers [15, 19].

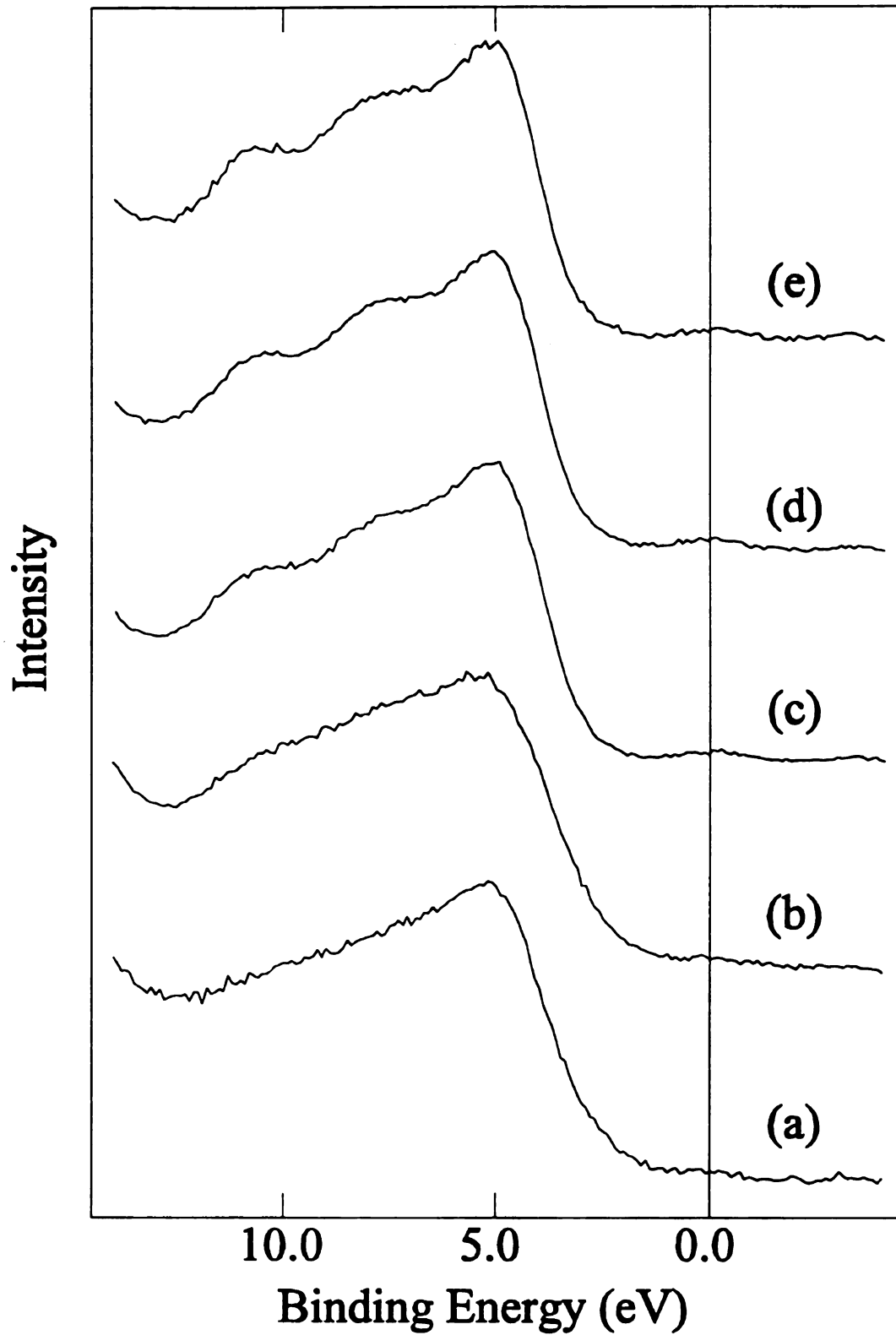


Figure 5.3 XPS valence band spectra of (a) SnP, (b) SnC200, (c) SnC250, (d) SnC400, and (e) SnC600 films.

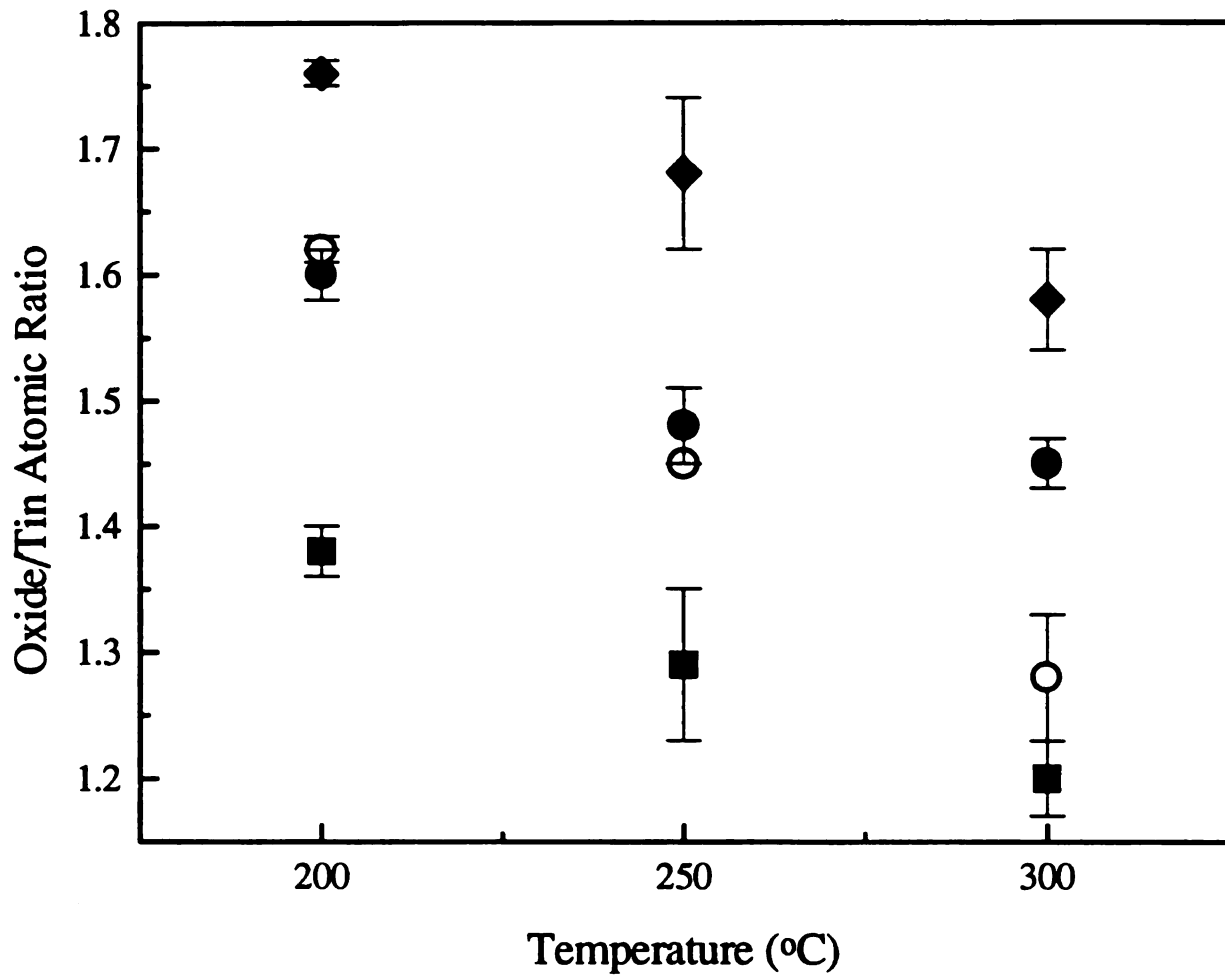


Figure 5.4 Changes in oxide concentration with reduction temperature as determined with XPS for ■SnP, ○SnC200, ●SnC400, and ◆SnC600 films.

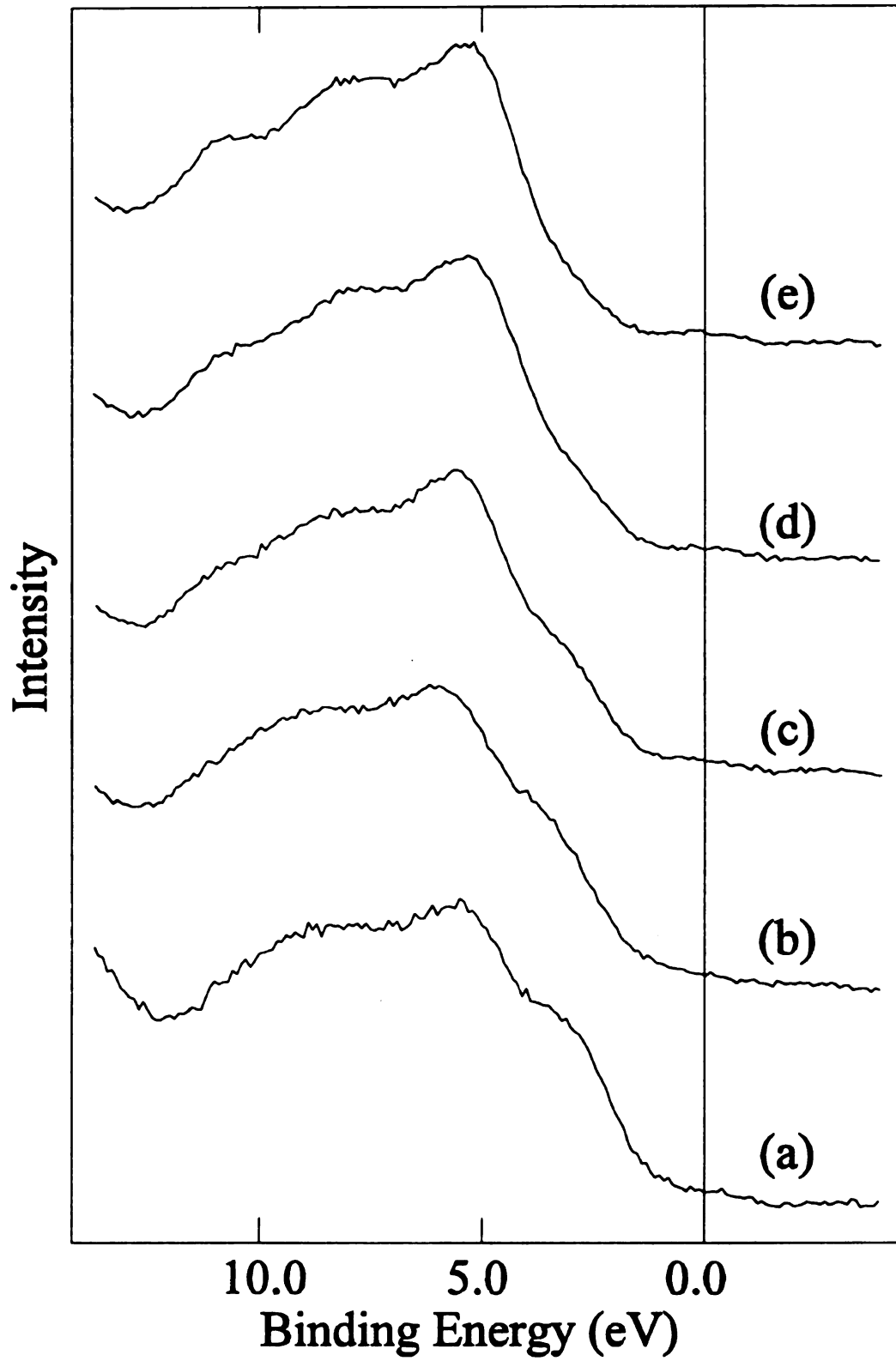


Figure 5.5 XPS valence band spectra of tin oxide materials after H_2 reduction at 300 $^\circ\text{C}$: (a) SnP, (b) SnC200, (c) SnC250, (d) SnC400, and (e) SnC600 films.

Changes in the oxide concentration with sequential reductive - oxidative treatments are shown in Figure 5.6. This study was undertaken to determine the amount of irreversible restructuring the films undergo when they are reduced at different temperatures. This is especially important for SnP films since they are being reduced at temperatures (up to 300 °C) much higher than used to prepare the film (room temperature).

Initially the film has an oxide/tin ratio of 1.75 and H₂ reduction at 200 °C decreases this ratio to 1.37 (Treatment 1 (T1) Figure 5.6). Reoxidation of the film at 200 °C for 1 h. (T2) restores the film stoichiometry and valence band spectrum to those characteristic of a Sn⁴⁺ oxide material, however, the oxide concentration has increased slightly. With reduction, the hydroxyl concentration decreases and when the film is reoxidized, some of the hydroxyl groups are replaced with lattice oxygen.

After reoxidation (T2), the H₂ reactivity of the film has been altered. Reduction at 200 °C only decreases the oxide/tin ratio to 1.63 (T3); a reduction temperature of 250 °C is necessary to obtain a 1.37 oxide/tin ratio (T4). This suggests that significant restructuring has occurred with the initial reductive and oxidative treatments at 200 °C. Though the film was at 200 °C for only 2h. it is possible that this was adequate to cause the film to collapse to the fully densified state found for SnC200 films. This may be responsible for the decreased reactivity.

The film was then reoxidized (T5) and reduced at 200 °C (T6) and 250 °C (T7) which resulted in oxide/tin ratios similar to those measured in the previous redox cycle. Reduction at 300 °C (T8) leads to additional loss of oxide and reoxidation (T9) to a Sn⁴⁺ oxide. Increased oxide concentration after these treatments (1.97 oxide/tin) is balanced

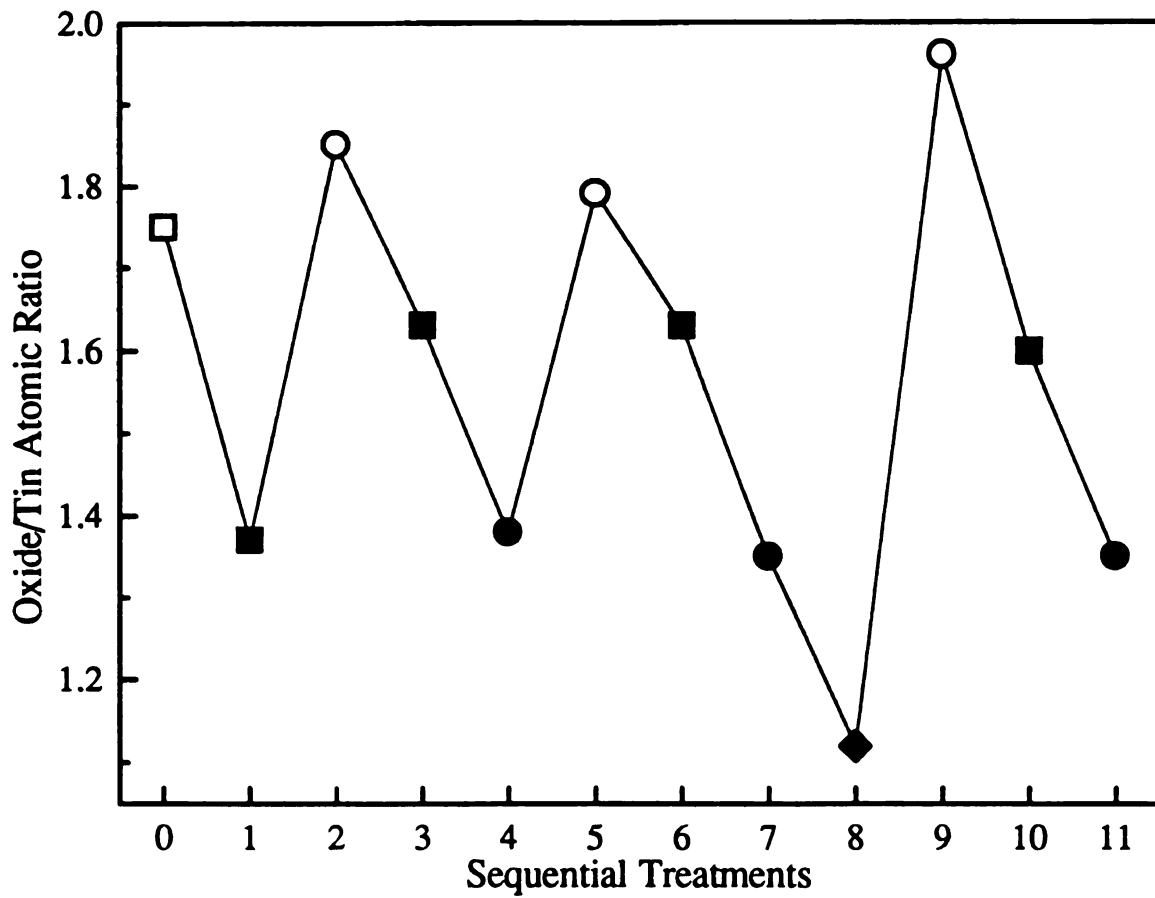


Figure 5.6 Oxidation - reduction cycling of SnP film: \square initial film; \blacksquare 200 °C, \bullet 250 °C, and \blacklozenge 300 °C H₂ reduction; and \circ 200 °C 20% O₂(He) oxidation. Oxide/tin atomic ratio is determined with XPS analysis after each sequential *in situ* treatment.

by a lower hydroxyl concentration. The calculated Sn oxidation state is approximately the same (+4.1) after all three reoxidations (T2, T5, and T9). The final two reductions at 200 °C (T10) and 250 °C (T11) result in oxide concentrations similar to those in the previous cycle (T6 and T7, respectively), despite the intervening, higher temperature reduction at 300 °C (T8). Overall, these results suggest that after the initial restructuring, the films are quite stable with respect to oxidation and reduction at these temperatures. The films behave as if the oxide can be removed and replaced without causing irreversible changes in the film structure.

SnC200 Films. These films are less reactive than the SnP films. As seen in Figure 5.4, reductive treatments at 200 °C, 250 °C, and 300 °C lead to oxide/tin ratios of approximately 1.6, 1.45, and 1.3, respectively. These oxide concentrations are significantly higher than those that remain in the SnP films after reduction at the same temperatures. The valence band spectrum of a SnC200 film after reduction at 300 °C (Figure 5.5b) is characteristic of a largely Sn²⁺ oxide material, as expected from the film stoichiometry.

Redox cycling was explored for these films and the results are presented in Figure 5.7. The film was subjected to four reduction cycles each consisting of H₂ reduction at 200 °C, 250 °C, and 300 °C and reoxidation at 200 °C. In Figure 5.7a the results are presented in terms of the oxide/tin ratio determined after each treatment. It can be seen that at reduction temperatures of 200 °C and 250 °C, approximately the same amount of oxide remains after each treatment in all four cycles. Unlike the SnP films, little restructuring occurs in the first cycle. Some of the scatter in the data can be accounted for

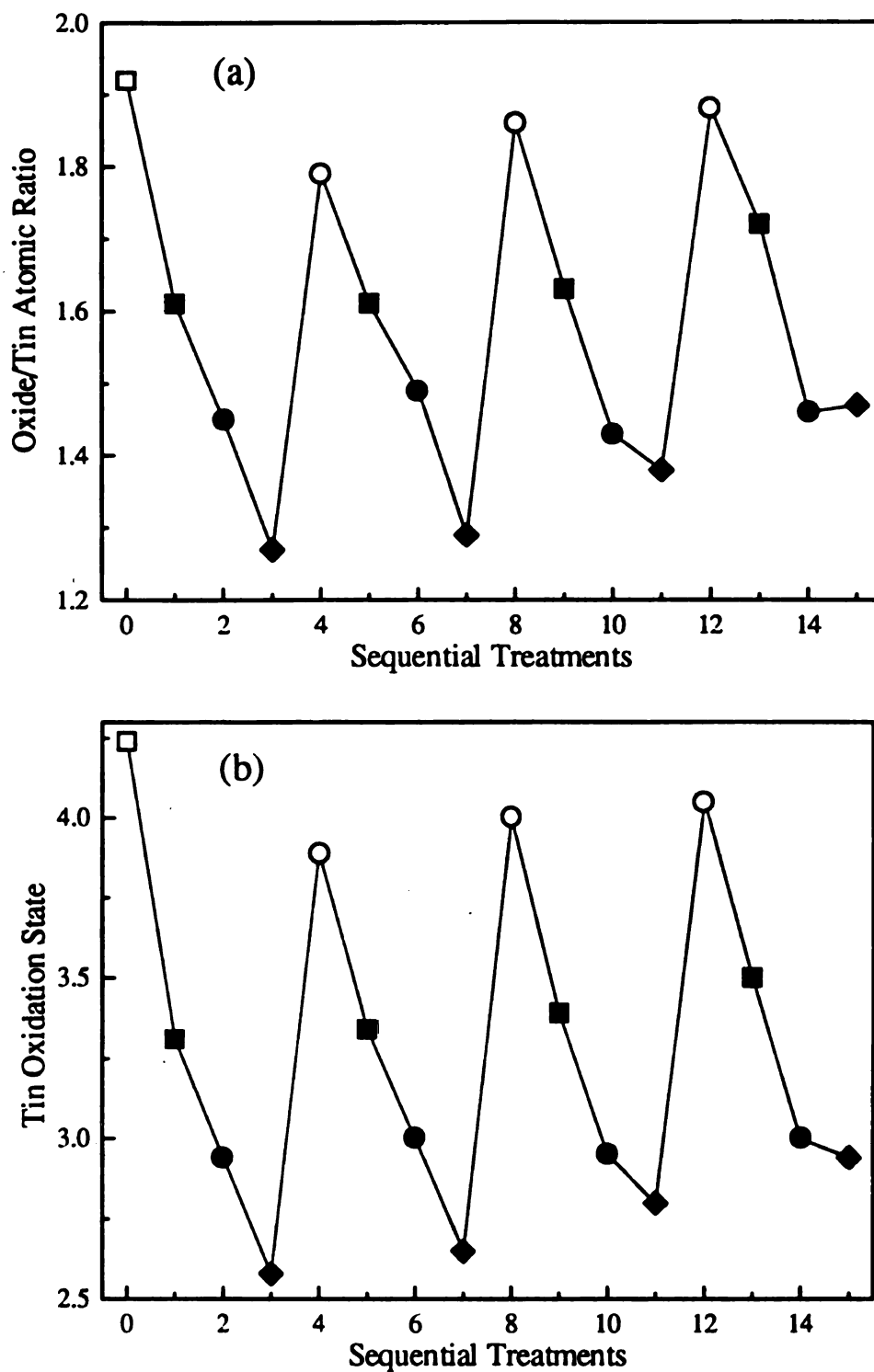


Figure 5.7 Oxidation - reduction cycling of SnC200 film: □ initial film; ■ 200 °C, ● 250 °C, and ◆ 300 °C H₂ reduction; and ○ 200 °C 20% O₂(He) oxidation. (a) Oxide concentration and (b) tin oxidation state as calculated using charge balance from XPS determined oxide and hydroxyl concentrations after sequential treatments.

by replacement of hydroxyl groups with oxide groups as the cycling progresses. This is evident from Figure 5.7b in which the calculated tin oxidation state is reported after each treatment. There is very little change in the oxidation state from cycle to cycle. The tin oxidation state is approximately +4 after oxidation and +3.3 and +3.0 after reductions at 200 °C and 250 °C, respectively.

There is a steady increase in the oxide concentration after reduction at 300 °C in each subsequent cycle. This indicates that there is restructuring occurring at this temperature. Interpretation can be based upon several assumptions. First, the oxide in the film can be in multiple bonding environments. These may include not only coordinatively unsaturated surface sites and bulk sites but also, because the film is amorphous, bond angles and bond lengths are variable. Second, these differences in local structure lead to lattice oxygen with different activation energy requirements for removal. It is possible that very little restructuring is needed to raise the activation energy enough to make oxide in some of these sites inaccessible to H₂ reduction at 300 °C.

SnC400 Films. The reduction behavior of these films is shown in Figure 5.4 and is very similar to that of polycrystalline tin oxide. Reduction at 200 °C results in an oxide/tin ratio of 1.6, subsequent reduction at 250 °C decreases this value to 1.48. Additional reduction at 300 °C results in little additional oxide loss (1.45). The valence band spectrum of the SnC400 film after reduction at 300 °C (Figure 5.5d) resembles that of the polycrystalline tin oxide after similar treatment (Figure 5.1d). Note that these results are also very similar to those of the SnC200 film after it has undergone several redox cycles.

Results of redox cycling of a SnC400 film are shown in Figure 5.8. While there is some scatter in the results, the oxide concentrations measured after the treatments are very similar in all of the cycles and suggest that little restructuring occurs with reduction.

SnC600 Films. These films are significantly less reactive than the SnC400 films and polycrystalline tin oxide (Figure 5.5). A treatment at 300 °C is need to achieve the same degree of reduction obtained with a 200 °C reduction of the other two materials. It is not surprising that these films are less reactive than the SnC400 films: they are significantly more structured as indicated by the higher degree of crystallinity in the SnC600 films. It seems plausible that a densified, partially crystalline thin film might have a lower reactivity than a polycrystalline powder. Differences may be related to differences in surface area. Recall that the SnP film became less reactive after densification. Lattice oxygen vacancies may also be more mobile in the powder.

Overall, reactivity of the films at temperatures ≤ 300 °C is related to the preparation temperature of the film. The SnP (after the initial restructuring), SnC400, and SnC600 have significantly different reactivities. Additionally, these films are subjected to very harsh treatment conditions and very little restructuring is occurring, other than the initial change in reactivity of the SnP films. This indicates that they are quite stable with respect to oxidation and reduction at these temperatures. Despite the densification, films are reactive and densification may contribute to the overall stability of these materials. There is also no evidence of cracks developing the in materials with oxidative and reductive treatments at these temperatures. This is another indication that these films do not undergo extensive restructuring.

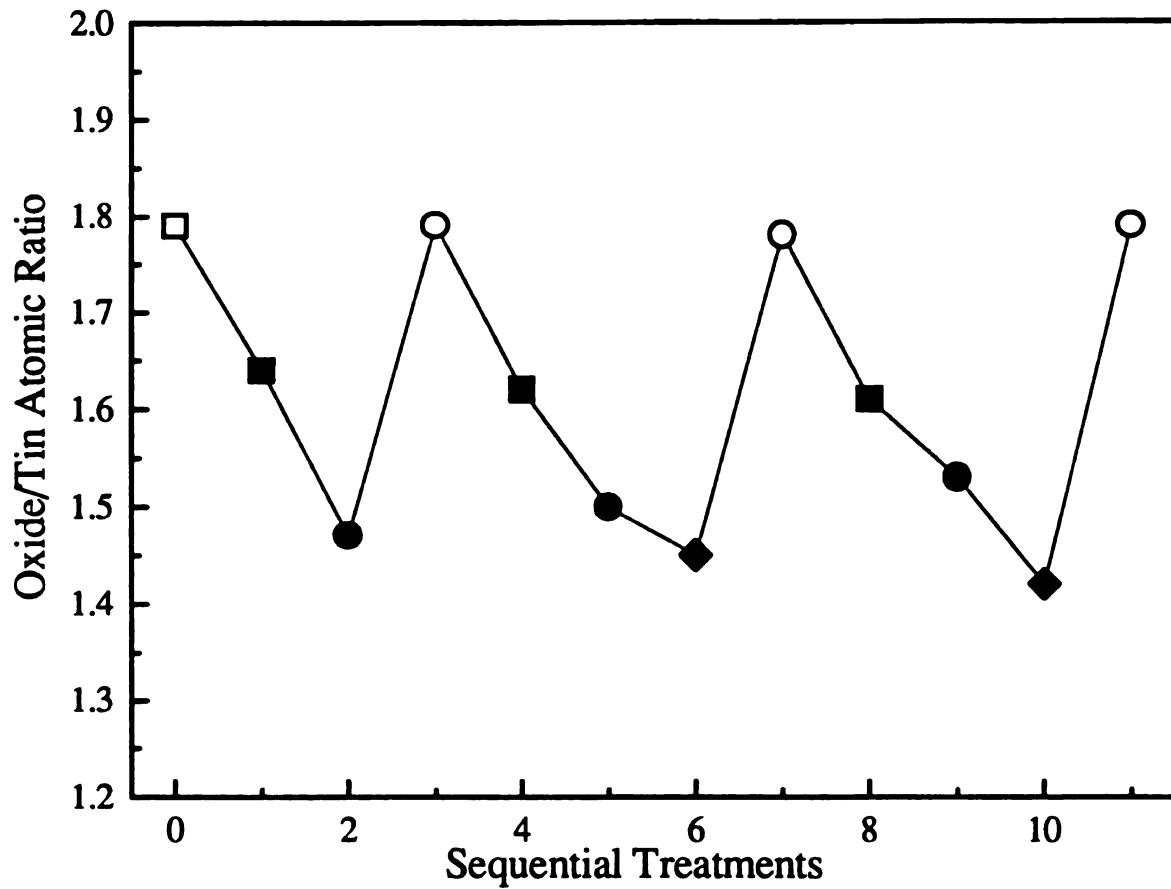


Figure 5.8 Oxidation - reduction cycling of SnC400 film. □initial film; ■200 °C, ●250 °C, and ◆300 °C H₂ reduction; and ○200 °C 20% O₂(He) oxidation. Oxide/tin atomic ratio is determined with XPS analysis after each sequential *in situ* treatment. Scale is adjusted to that of Figure 5.7a to avoid an artificial over emphasis of differences.

Reduction at Temperatures > 300 °C. As with the polycrystalline tin oxide, reduction for extensive periods of time at 300 °C does not lead to the formation of metal in any film, however, β -tin is present in all films after H₂ reduction at 325 °C. Once metal crystallites form, the films become discontinuous and the original structure cannot be restored by an oxidative treatment. The reduction mechanism for SnC400 and SnC600 films may be similar to that of the powder: in these films the oxide/tin concentration also remains at about 1.40 - 1.45 for reduction at 325 °C and 350 °C, despite an increase in metal concentration with reduction time.

5.5 Concluding Remarks

The reactivity of tin oxide films when exposed to pure H₂ at atmospheric pressure was found to be strongly correlated with degree of structure in these films. This would be expected thermodynamically since the driving force for crystallization must be an increase in the stability of the metal oxygen bonds. However, the reactivity was determined in a flow system where products are constantly removed. Therefore, the complete reduction of all films to Sn metal (and certainly to SnO) is thermodynamically allowed even at 200 °C. Films are not reduced to metal unless the temperature is above 300 °C even after extensive reaction times. The reduction must be limited by kinetic factors such as lattice oxygen vacancy mobility or high activation energies. Vacancy mobility alone does not account for the limited reactivity since it is expected to be greater in more structured materials and these have been shown to be less reactive than the amorphous films.

In this study, the reduced oxide is referred to as a Sn²⁺ oxide. It may be equally (or more) valid to view these materials as defective Sn⁴⁺ oxides since no new crystalline

phases are detected and the Sn^{4+} oxide structure and composition are apparently easily restored. A distinction between a defective Sn^{4+} oxide and a Sn^{2+} oxide is not often made and may account for the controversy over the magnitude of the chemical shift between Sn^{4+} and Sn^{2+} oxides.

One of the problems with determining the binding energy of Sn 3d peaks for SnO is that its surface is easily oxidized to SnO_2 . Commonly the surface is ion sputtered to remove the SnO_2 overlayer but this can alter the surface due to preferential sputtering of oxygen [19, 22]. It is therefore questionable whether the material being analyzed is in fact SnO at the surface. A second difficulty is created because materials may charge in the spectrometer and there is not a reliable binding energy reference. The separation between the O 1s and Sn $3d_{5/2}$ peaks is 43.9 eV for tin oxide in both forms [15], so the O 1s peak cannot be used as a reference.

The lack of a reliable binding energy standard made it impossible to conclusively determine the binding energy of the Sn $3d_{5/2}$ peak of the films reduced at temperatures ≤ 300 °C in this study. Films reduced at higher temperatures contain tin metal. Chemical shifts between the metal and oxide Sn $3d_{5/2}$ peaks can be measured and correlated with the oxide/tin ratios. If samples have dramatically different oxide/(tin oxide) ratios, this would provide a way of measuring the chemical shift between Sn^{4+} and Sn^{2+} (defective Sn^{4+}) oxides.

Angle resolved XPS, as described previously [31], was used to study the formation of metal on the surface of an SnC400 film after it was reduced at 350 °C. The measured metal concentration decreased with increasing sampling depth (Figure 5.9) indicating that

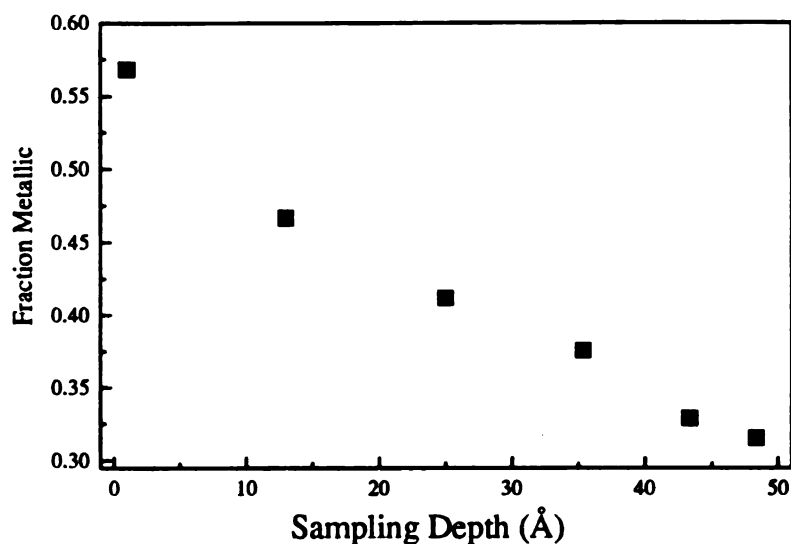


Figure 5.9 AR-XPS analysis of the formation of metal in an SnC400 film after H₂ reduction for 4h at 350 °C. the metal crystallites are forming at the surface of the film.

The oxide/(tin oxide) ratio was determined for all sampling depths (Figure 5.10). It was found that this ratio was approximately 1.25 at the surface and increased to approximately 1.7 over the maximum sampling depth. These concentrations suggest that tin is largely in a +2 oxidation state at the surface and in a +4 oxidation state in the bulk. This correlates with an increase in the separation between the metal and oxide Sn 3d_{5/2} peaks. At the surface, the chemical shift is 1.5 eV and it increases to a value of 2.0 eV as the sampling depth increases. This suggests that there is a separation between the the Sn⁴⁺ and Sn²⁺ oxide Sn 3d peaks of at least 0.5 eV. This result is consistent with Themlin *et al.* [19] who found that the chemical shift was approximately 0.7 eV.

Lau and Wertheim [15] found that there was no chemical shift between Sn²⁺ and Sn⁴⁺ oxides. Their SnO sample was deposited within the spectrometer prechamber and did not have an SnO₂ overlayer. They reason that there is no difference in binding energy

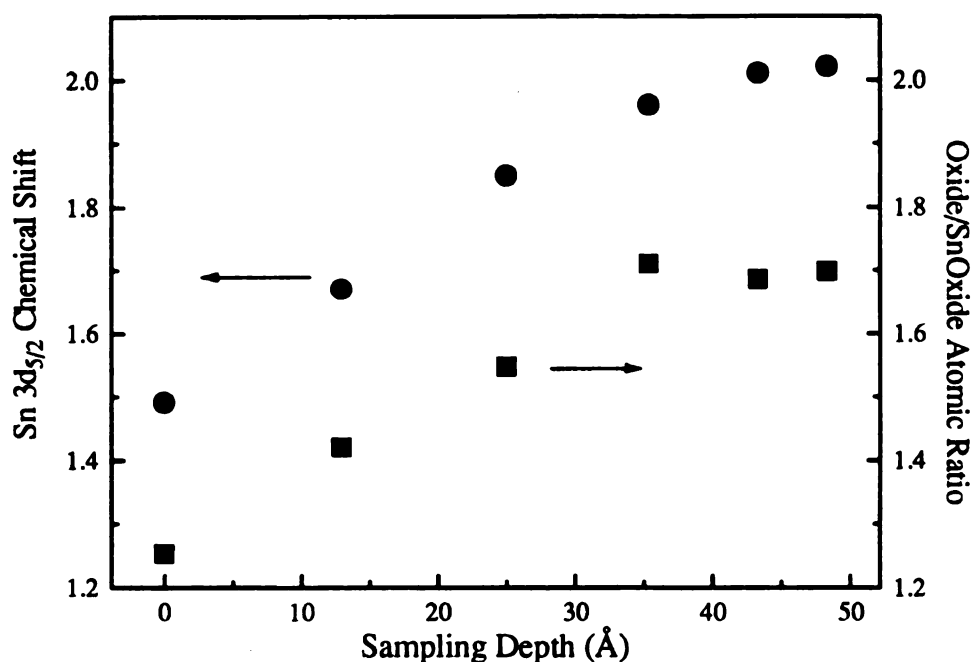


Figure 5.10 Chemical shift between Sn 3d_{5/2} metal and oxide peaks and the oxide/tin oxide atomic ratio as a function of sampling depth for SnC400 film after H₂ reduction for 4h at 350 °C.

because the difference in free ion potential between Sn²⁺ and Sn⁴⁺ is balanced by the difference in the Madelung potential between the SnO and SnO₂ lattices. While this may be true for crystalline SnO and SnO₂, the Madelung potential in an unrestructured defective Sn⁴⁺ oxide may be different than that in SnO. In a defective Sn⁴⁺ oxide material, the chemical shift may indeed be 0.7 eV from that of SnO₂.

5.6 References

1. Madou, M.J.; Morrison, S.R. *Chemical Sensing with Solid State Devices*; Academic Press, Inc.: San Diego, CA, 1989.
2. Kung, H.H. *Transition Metal Oxides: Surface Chemistry and Catalysis*; Elsevier: Amsterdam, 1989.
3. Aso, I.; Nakao, M.; Yamazoe, N.; Seiyama, T. *J. Catal.* **1979**, *57*, 287.
4. Fattore, V.; Fuhrman, Z.A.; Manara, G.; Notari, B. *J. Catal.* **1975**, *37*, 215.
5. Yamazoe, N.; Kurokawa, Y.; Seiyama, T. *Sens. Actuators* **1983**, *4*, 283.
6. Ippommatsu, M.; Sasaki, H. *J. Electrochem. Soc.* **1989**, *136(7)*, 2123. Capehart, T.W.; Chang, S.C. *J. Vac. Sci. Technol.*, **1981**, *18(2)*, 393.
7. Mokwa, W.; Kohl, D.; Heiland, G. *Sens. Actuators* **1985**, *8*, 101.
8. Pink, H.; Treitinger, L. Vite, L. *Japan. J. Appl. Phys.* **1980**, *19(3)*, 513. Tomar, M.S.; Garcia, F.J. *Prog. Cryst. Growth Charact.* **1981**, *4*, 221.
9. Lalauze, R.; Pijolat, C.; Vincent, S.; Bruno, L. *Sens. Actuators* **1992**, *8*, 237. Kim, K.; Finstad, T.G.; Chu, W.K.; Cox, X.B.; Linton, R.W. *Solar Cells* **1985**, *13*, 301.
10. Park, S.-S.; Mackenzie, J. D. *Thin Solid Films* **1996**, *274*, 154. Hampden-Smith, M.J.; Wark, T.A.; Brinker, C.J. *Coor. Chem. Rev.* **1992**, *112*, 81. Takahashi, Y.; Wada, Y. *J. Electrochem. Soc.* **1990**, *137*, 267.
11. Severin, K.G.; Ledford, J.S. *Langmuir* **1995**, *11(6)*, 2156.
12. Brinker, C.J.; Scherer, G. *Sol-Gel Science*; Academic Press: San Diego, 1990.
13. Roger, C.; Hampden Smith, M.J.; Brinker, C.J. In *Better Ceramics Through Chemistry V*, Hampden Smith, M.J., Klemperer, W.G., Brinker, C.J., Eds.; Mater. Res. Soc. Symp. Proc. 271; MRS: Pittsburgh, PA, 1992; 51.
14. Jones, A.; McNicol, B.D. *Temperature-Programmed Reduction for Solid Materials Characterization*; Marcel Dekker, Inc.: New York, 1986. LeMaitre, J. L. in *Characterization of Heterogeneous Catalysts*, Delanney, F., Ed.; Marcel Dekker, Inc.: New York, 1984.
15. Lau, C.L.; Wertheim, G.K. *J. Vac. Sci. Technol.* **1978**, *15(2)*, 622.

16. Morgan, W. E.; Van Wazer, J. R.; *J. Phys. Chem.* **1973**, *77*, 964.
17. Hoflund, G. B. *Chem. Mater.* **1994**, *6*, 562.
18. Paparazzo, E.; Fierro, G.; Ingo, G. M.; Zacchetti, N. *Surf. Interface Anal.* **1988**, *12*, 438.
19. Themlin, J.M.; Chtaib, M.; Henrard, L.; Lambin, P.; Darville, J.; Gilles, J.-M. *Phys. Rev. B* **1992**, *46(4)*, 2460.
20. Kover, L.; Moretti, G.; Kovacs, Zs.; Sanjines, R.; Cserny, I.; Margaritondo, G.; Palinkas, J.; Adachi, H. *J. Vac. Sci. Technol. A* **1995**, *13(3)*, 1382.
21. Sherwood, P.M.A. *Phys. Rev. B* **1990**, *41(14)*, 10 151.
22. Sanjinés, R.; Coluzza, C.; Rosenfeld, F.; Gozzo, F.; Alméras, Ph.; Lévy, F.; Margaritondo, G. *J. Appl. Phys.* **1993**, *73(8)*, 3997.
23. Severin, K. G.; Ledford, J. S.; Torgerson, B. A.; Berglund, K. A. *Chem. Mater.* **1994**, *6*, 890.
24. Severin, K. G.; Ledford, J. S. unpublished results
25. Software provided by Dr. Andrew Proctor, University of Pittsburgh, Pittsburgh, PA.
26. Scherrer, P. *Gött. Nachr.* **1918**, *2*, 98.
27. Swanson; Tatge NBS Circular 539(1), **1953**, 54.
28. Kohl, D. *Sens. Actuators* **1989**, *18*, 71.
29. Cox, D. F.; Fryberger, T. B.; Semancik, S. *Phys. Rev. B* **1988**, *38(3)*, 2072.
30. Egdell, R. G.; Eriksen, S.; Flavel, W.R. *Surf. Sci.* **1987**, *192*, 265.
31. Severin, K. G.; Ledford, J. S. to be submitted to *Langmuir*

Chapter 6

Conclusions

6.1 Project Summary

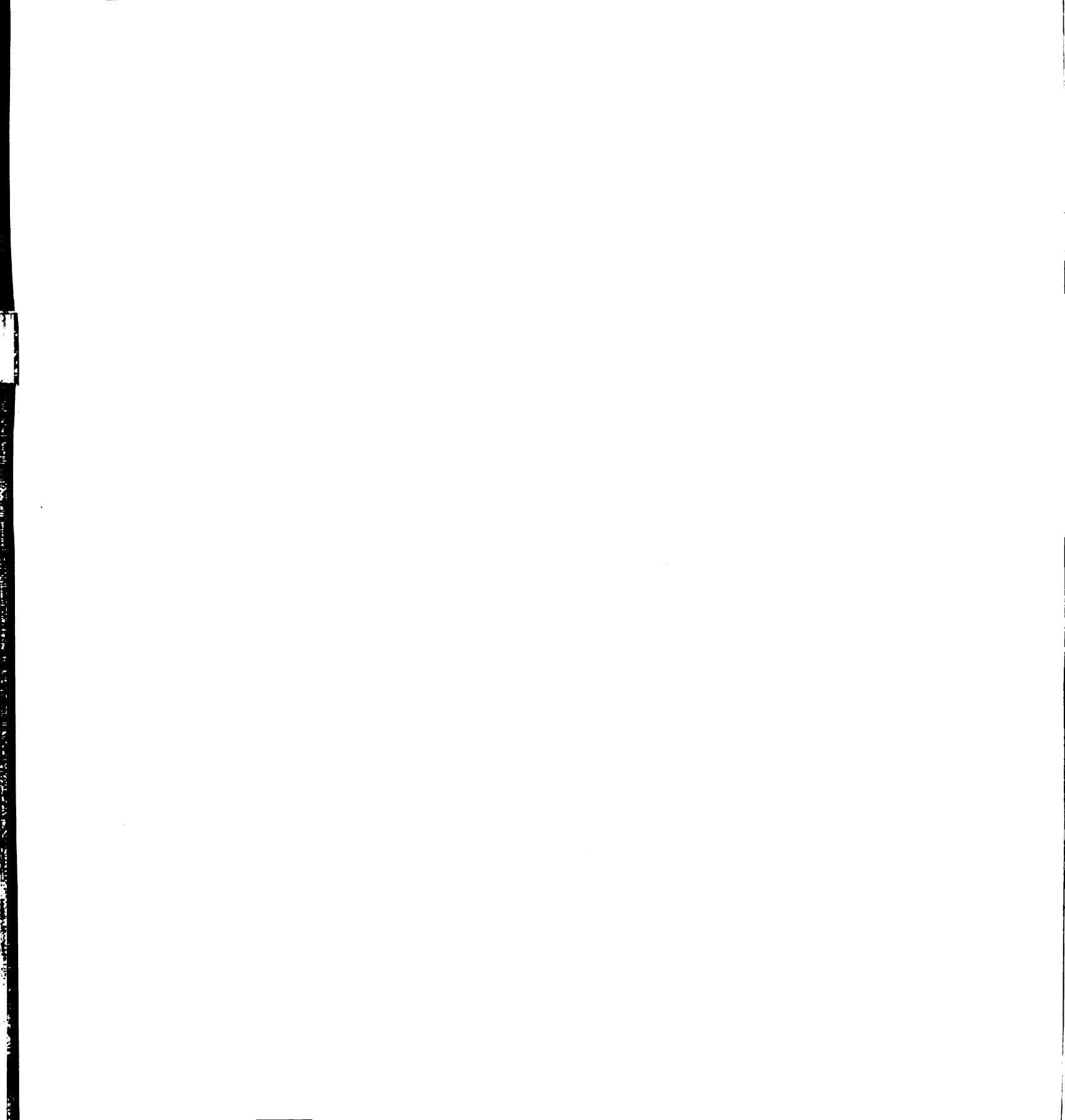
Tin, titanium, and zirconium valerate thin films have been prepared by spin casting solutions produced from the hydrolysis of metal alkoxides in excess valeric acid at room temperature. These films are amorphous, visually transparent, uniform in thickness and composition, adhere well to quartz substrates, are stable and crackfree. Film thicknesses are ~300 nm for SnVal films and ~400 nm for TiVal and ZrVal films. All films consist of a network of metal oxygen backbones coordinated with valerate ligands. Significant concentrations of hydroxyl ligands were found only in the tin valerate films. In no film was there any evidence of unreacted alkoxide ligands.

Titanium valerate (TiVal) films which are spin cast from aged solutions have higher valerate levels (1.4/Ti) than films made from freshly prepared solutions (1.2/Ti). FTIR analysis showed that alkoxide ligands are present in freshly prepared solutions but absent in 24 h. old solutions. Apparently, as the solutions age valerate ligands replace alkoxide ligands. FTIR spectra indicate that the additional valerates may be bidentate bridging ligands. Bridging ligands probably contribute significantly to structural integrity of the films. This would account for the observations that aged solutions make higher quality films and that TiVal films dissolve in H_2O_2 . Hydrolysis and condensation reactions must be completed during the spin casting and drying processes, since no alkoxide or hydroxyl ligands are present in valerate films.

The concentration of valerate ligands in the zirconium valerate (ZrVal) films is $\sim 1.9/\text{Zr}$ regardless of the solution age. Hydrolysis must occur more rapidly than in the TiVal solutions since no alkoxide ligands are evident in the FTIR spectra of freshly prepared ZrVal solutions. More rapid carboxylation and hydrolysis rates are consistent with a nucleophilic substitution reaction mechanism since Zr is more electropositive than Ti and is coordinated with less bulky alkoxide groups.

Tin valerate (SnVal) films have much lower valerate concentrations ($0.26/\text{Sn}$) than either the TiVal or ZrVal films and solution aging does not increase it. Unlike the TiVal and ZrVal solutions, alcohol not valeric acid, is the major component of these film solutions. It was found that if an equivalent concentration of isopropanol was added to a TiVal film solution, the valerate concentration in the films was also $0.3/\text{metal}$. Therefore, the low valerate concentration in these films is a result of the high alcohol level. Both bidentate and monodentate valerate ligands are present in SnVal solutions and films. The monodentate ligands are stabilized by H-bonding to water adsorbed in the films. The hydroxyl concentration in the SnVal films is $0.55/\text{metal}$.

Tin oxide and titanium oxide films were made from TiVal and SnVal films by calcination in air at temperatures up to $1000\text{ }^{\circ}\text{C}$. Calcination at $250\text{ }^{\circ}\text{C}$ was found to be adequate to remove the organic components of the films. SnVal films are fully collapsed (20%) by calcination at this temperature. A temperature of $400\text{ }^{\circ}\text{C}$ is required for complete compaction of TiVal films (50%). The higher percent compaction is consistent with the higher concentration of valerate ligands in the TiVal films than in the SnVal films.

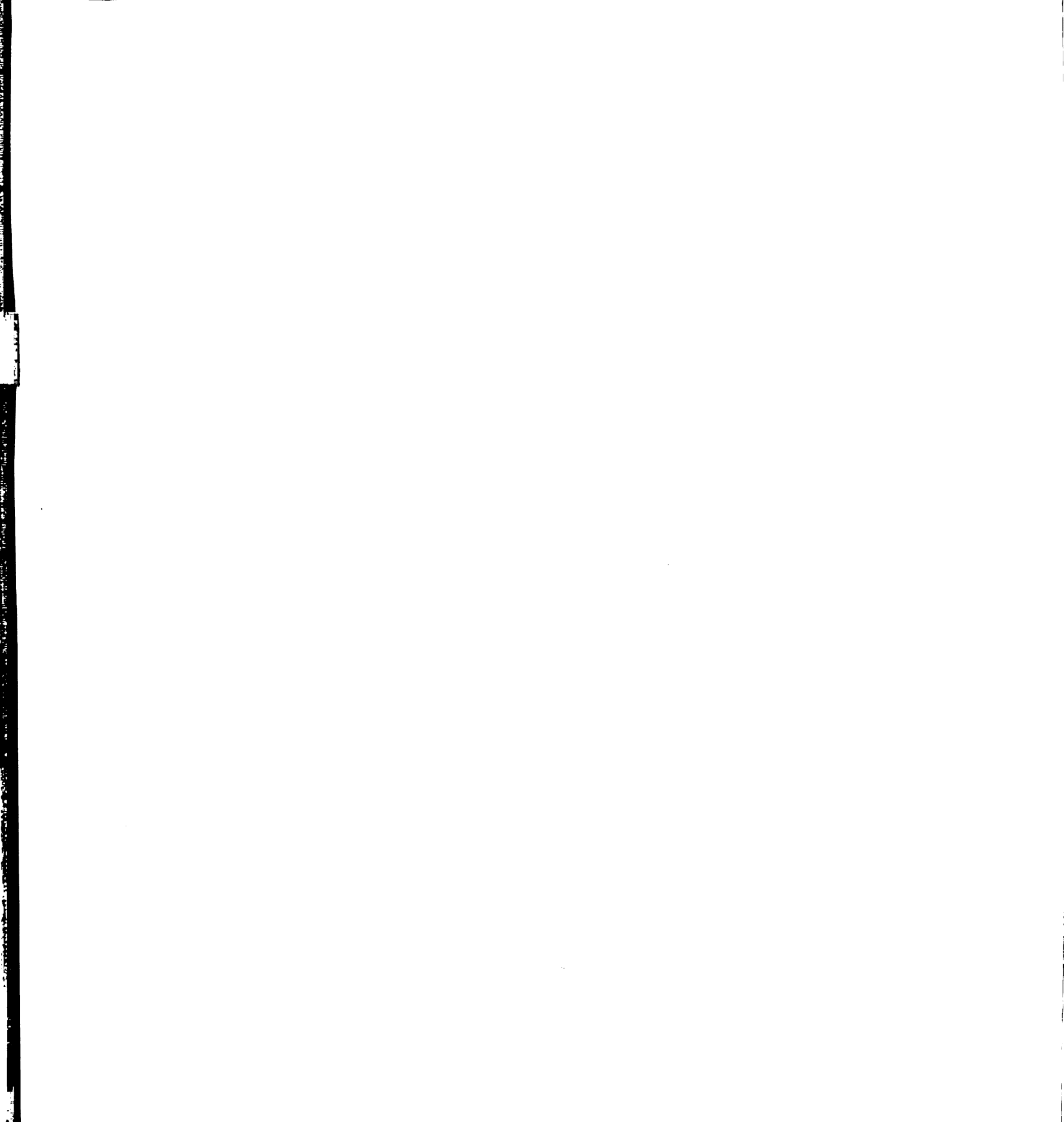


As determined with XPS, the composition of all calcined TiVal and SnVal films is similar to that of polycrystalline TiO₂ and SnO₂ powders, respectively.

Crystallization occurs with calcination at 400 °C and TiC400 and SnC400 films contain traces of anatase and cassiterite, respectively. Particle sizes and crystallite concentrations increase with calcination temperature. Rutile crystallites are present in the Ti films calcined at 600 °C or above and are the predominant crystalline phase in the TiC1000 films. All films calcined at 600 °C are slightly cracked, as indicated by the presence of a Si 2p peak in the XPS spectrum. The films become more fractured as the calcination temperature increases.

A room temperature hydrogen peroxide treatment was used to remove the valerate ligands from SnVal films while leaving the tin oxygen backbone relatively untouched. It was found that the films collapsed only 12% with this method compared with 20% for calcination. As with the calcined films, their composition and XPS valence band spectra are consistent with an Sn⁴⁺ oxide.

Mixed metal valerate films were prepared from Ti(OPrⁱ)₄ and Sn(OPrⁱ)₄. AR-XPS analysis suggests that these films are well mixed if the alkoxides are combined before the addition of valeric acid. As with the single metal films, all mixed films are transparent, stable, and exhibit uniform adhesion to quartz. Crystallization is inhibited by mixing: no crystallites are apparent in the XRD patterns of mixed films calcined at 400 °C. All mixed films calcined at this temperature are also crackfree and homogeneously mixed. Refractive indices were found to be related to film composition.



Mixed oxide films calcined at 600 °C and higher are heterogeneous due to the formation of crystallites. These crystallites are of mixed rutile phases only, no single metal oxide crystalline phases are evident. Concentration of crystallites and crystallite size increases with increasing calcination temperature. Mixed films range from the highly inhomogeneous 75:25 Sn:Ti films which have a strong surface enhancement of Ti after crystallization to the 25:75 Sn:Ti film whose surface composition changes little with calcination and crystallization.

The reactivity of tin oxide films when exposed to pure H₂ at atmospheric pressure was found to be strongly correlated with degree of structure in these films. Amorphous SnP films are highly reactive and are reduced to largely Sn²⁺ oxide materials by a 300 °C H₂ treatment, as indicated by surface stoichiometry and XPS valence band spectra. At the other extreme SnC600 films, which contain cassiterite crystallites, are less reactive than polycrystalline tin oxide powder. This latter result may be due to differences in surface area and lattice oxygen mobility. Reduction at temperatures >300 °C results in the formation of tin metal (β -tin) in all films and the powder. Reoxidation at 200 °C for 1 h. restores the original composition and reactivity of all materials except the SnP films, provided they have not been reduced to metal. Once metallic tin is formed, the films are irreversibly modified.

6.2 Future Work

Technology is currently available for the production of semiconductor gas sensors from these sol-gel derived films. Films can either be coated onto an electrode array or electrodes can be attached to the surface of the film. Several of the films are promising as

sensor materials. Calcined SnVal films are conductive at room temperature and can be prepared with a range of reactivities. The selectivity of these films should be investigated to see if there is indeed a correlation between reactivity and selectivity, as suggested by catalyst research. Additionally, sensors using highly reactive amorphous films (i.e. SnC250) may operate at lower temperatures than conventional polycrystalline tin oxide sensors.

Titanium oxide films and mixed $\text{TiO}_2\text{-SnO}_2$ films are potentially useful sensing materials. While they are not conductive at room temperature they may be at elevated temperatures. More importantly, the titanium oxide films become conductive at room temperature after they are reduced at temperatures as low as 200 °C. *In situ* H_2 reduction studies were carried out on these materials. It was found that TiC400 films were largely inert with respect to H_2 reduction and that no significant change in oxide concentration (1.80 - 1.85 oxide/titanium) was measured even after reduction at 400 °C. The stability of these films with respect to reduction suggests that they may have different sensing properties than tin oxide films.

As seen in Figure 6.1, mixed $\text{TiO}_2\text{-SnO}_2$ films have intermediate reactivities. These results suggest that the oxide reactivity of the thin films can be tailored by making mixed metal oxide films. However, it is possible that these films are composed of islands of the two individual oxides and that only the tin oxide is being reduced. Sensor measurements would indicate if the selectivity of mixed films is different than that of tin oxide films. Ideally, these films are homogeneous and contain a high concentration of Ti-O-Sn

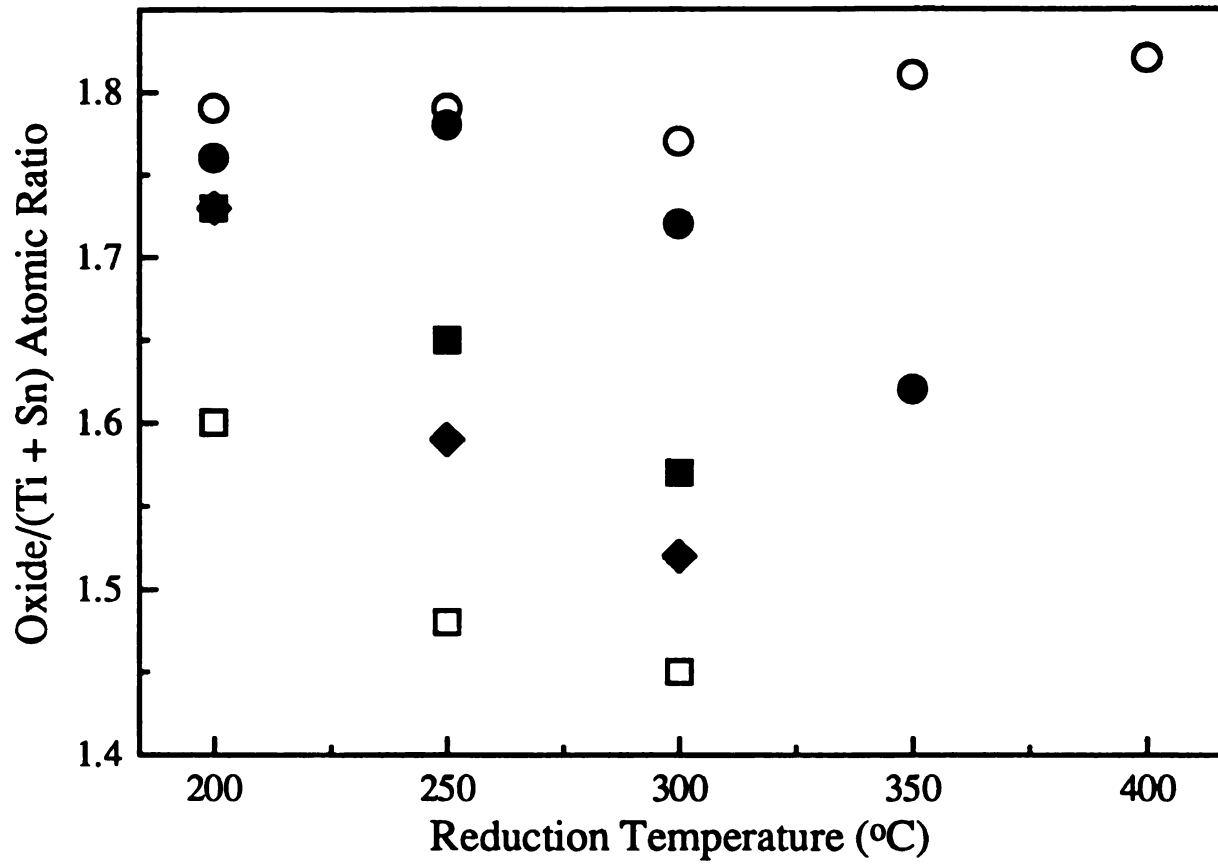


Figure 6.1 Oxide concentration as a function of reduction temperature for \circ TiC400, \square SnC400, \bullet TSC400, \blacksquare EMC400, and \blacklozenge STC400 films. The standard deviation in the reported atomic ratios is ± 0.05 .

moieties. If this is true, then mixed materials may have unique sensitivities and selectivities when used as sensors.

Finally, Sn metal is not evident in the XPS spectrum of TSC400 film after reduction at 350 °C for 1 h. The tin may be dispersed well enough in the TSC400 films to prevent the formation of metal at this temperature. A sensor made from this material may be more stable at high temperatures than one which uses a pure tin oxide film.

MICHIGAN STATE UNIVERSITY LIBRARIES



3 1293 01762 6239

